F.ETISH: FAST ELEMENTARY THERMOMECHANICAL ICE SHEET MODEL

USERS GUIDE

FRANK PATTYN
Contributors: K. Bulthuis, V. Coulon, E. Kazmierczak, S. Sun, L. Zipf
Laboratoire de Glaciologie, Université libre de Bruxelles,
Avenue F.D. Roosevelt 50, B-1050 Brussels, Belgium (Frank.Pattyn@ulb.be)

f.ETISh v1.9 — April 22, 2022

fetish *(noun)*:

1. an object believed to have magical power to protect or aid its owner.
2. a material object regarded with superstitious or extravagant trust or reverence.
3. an ice sheet model of intermediate complexity.

free after Merriam-Webster dictionary

TERMS AND CONDITIONS

```
f.ETISh (Fast Elementary Thermomechanical Ice Sheet model) is a
two-dimensional finite difference numerical ice sheet model of
intermediate complexity.

Copyright (C) 2022 Frank Pattyn

This program is free software: you can redistribute it and/or modify
it under the terms of the GNU General Public License as published by
the Free Software Foundation, either version 3 of the License, or
(at your option) any later version.

This program is distributed in the hope that it will be useful, but
WITHOUT ANY WARRANTY; without even the implied warranty of
MERCHANTABILITY or FITNESS FOR A PARTICULAR PURPOSE.  See the GNU
General Public License for more details.

You should have received a copy of the GNU General Public License
along with this program.  If not, see <https://www.gnu.org/licenses/>.
```

Contents

1 f.ETISh model description

1.1 Introduction

1.1.1 Changes with f.ETISh v1.0

f.ETISh (fast Elementary Thermomechanical Ice Sheet model) is an ice sheet model applicable to major ice sheets on Earth (both land-terminating and marine ice sheets) as well as on other planets (such as the Martian North Pole Layered Deposits). It reduces the three-dimensional nature of ice sheet flow and its dynamics to a two-dimensional problem, while keeping the essential (or elementary) characteristics of ice sheet and ice stream flow. Processes controlling grounding line motion are adapted in such a way that they can be represented at coarser resolutions. This way, the model can more easily be integrated within computational-demanding Earth-system models. An initial description of the f.ETISh model (v1.0) is given in Pattyn [2017]. Since then several improvements have been made and extensions have been implemented, the most important are listed below:

1. To facilitate the integration of the Earth-system model output with ice sheet models, several sub-shelf melt models have been implemented, such as PICO [Potsdam Ice-shelf Cavity mOdel; Reese et al., 2018a] that links far-field ocean temperature and salinity to sub-shelf melting via a box model of overturning circulation within ice-shelf cavities [Olbers and Hellmer, 2010]. Furthermore, the plume parametrization [Lazeroms et al., 2018] has been implemented as well as its combination with PICO, called PICOP [Pelle et al., 2019].

2. Basal sliding has been significantly improved through the implementation of a general sliding law [Zoet and Iverson, 2020], based on regularized Coulomb friction [Joughin et al., 2019]. This allows to control a higher plasticity of the fast-flowing outlet glaciers, while keeping a power-law relationship (Weertman-type sliding law) for slower-moving ice.

3. Subglacial hydrology has been implemented through subglacial water flow based on a thin water film and a porous water model in subglacial till.

4. Calving and hydrofracturing results in a dynamic boundary for floating ice shelves in contact with the ocean.

5. Changes in the geoid due to mass changes of ice sheets have are now taken into account, leading to non-uniform sea level changes that may impact grounding-line stability. The standard bedrock adjustment based on an elastic lithosphere and relaxed asthenosphere (ELRA-model) has been extended to spatially varying characteristics of both lithosphere effective thickness and mantle viscosity [Coulon et al., 2021].

6. Ice sheet model initialization has been improved with a two-step method, allowing to optimize basal melt rates underneath ice shelves to keep the ice sheet in steady-state [Bernales et al., 2017].

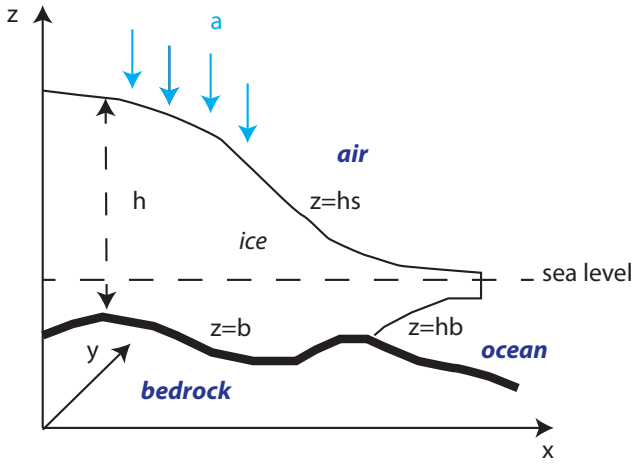

Figure 1: General Cartesian geometry of the f.ETISh model.

1.1.2 Basic equations

The model consists of diagnostic equations for ice velocities, and three prognostic equations for the temporal evolution of ice thickness, ice temperature, and bedrock deformation beneath the ice. Prescribed boundary fields are equilibrium bedrock topography, basal sliding coefficients, geothermal heat flux, and sea level. Present-day mean surface air temperatures and precipitation are derived from data assimilation within climate models. Optionally, ablation is determined from a Positive Degree-Day model and sub-shelf melt through simplified ocean circulation models. A list of model symbols is provided in the Appendix A (Tables 4–6). A general overview of the Cartesian geometry used is given in Fig. 1. For the coupled ice sheet/ice shelf system the surface elevation h_s is defined as

$$h_s = \max \left[b + h, \left(1 - \frac{\rho_i}{\rho_s} \right) h + z_{\mathrm{sl}} \right] , \tag{1}$$

where h is the ice thickness, b is the bedrock elevation, z_{sl} is the sea-level height with respect to the chosen datum, ρ_i and ρ_s are the ice and seawater density, respectively. It follows that the bottom of the ice sheet equals $h_b = h_s - h$, and that $h_b = b$ holds for the grounded ice sheet.

1.2 Ice velocities

1.2.1 Approximations

The ice sheet model has several modes of operation, depending on the boundary conditions that are applied. The most elementary flow regime of the grounded ice sheet is according to the Shallow-Ice approximation [SIA; Hutter, 1983], extended with either a Weertman-type (or regularized Coulomb friction) law for basal sliding. A more appropriate mode of operation for most applications is the hybrid mode, in which the flow regime of the grounded ice sheet is governed by a combination of SIA, responsible for ice-deformational flow, and the Shallow-Shelf approximation [SSA; Morland, 1987, MacAyeal, 1989] for basal sliding, which exerts a given friction at the ice sheet base [Bueler and Brown, 2009, Martin et al.,

2011, Winkelmann et al., 2011]. Ice shelf flow is governed by the SSA, defined by zero basal drag and extended by a water-pressure condition at the seaward edge. Depending on the spatial resolution used, the transition between both systems (ie sheet and ice shelf) can be given by a flux-condition at the grounding line [Pollard and DeConto, 2009, 2012a], derived from boundary layer theory based on SSA [SGL; Schoof, 2007a] for a Weertman sliding law.

1.2.2 Shallow-Ice Approximation (SIA)

The Shallow-Ice approximation [SIA; Hutter, 1983] is commonly used in ice sheet modelling. This approximation is valid for ice sheets of small aspect ratios $h \ll L$, where L is the horizontal length scale of the ice sheet domain, and further characterized by a low curvature and low sliding velocities. The approximation is, however, not valid near grounding lines nor for ice shelf flow, for which other approximations are applied (see below). According to SIA, the vertical mean horizontal velocity in an ice sheet is given by

$$\vec{v}_{\mathrm{SIA}} = \vec{v}_b + \frac{2A}{n+2} h \left|\tau_d\right|^{n-1} \tau_d \,, \tag{2}$$

where $\tau_d = -\rho_i g h \nabla h_s$ is the driving stress, A is the flow parameter in Glen's flow law (with $n = 3$), $\vec{v}_b = (u_b, v_b)$ is the basal sliding velocity and $\vec{v}_{\mathrm{SIA}} = (u, v)$ is the vertical mean horizontal velocity according to SIA. The flow parameter A is a function of ice temperature (see Sect. 1.8). For the thermomechanically-coupled case, n in Eq. (2) is replaced by p_r (see Sect. 1.8 for more details).

1.2.3 Hybrid Shallow-Shelf/Shallow-Ice approximation (HySSA)

The flow velocity in an ice shelf or an ice stream characterized by low drag is derived from the Stokes equations [Stokes, 1845] by neglecting vertical shear terms and by integrating the force balance over the vertical [Morland, 1987, MacAyeal, 1989]. The hybrid (HySSA) model considers that inland ice flow is governed by both deformational velocity (represented by Eq. (2)) and membrane stresses incorporated in basal sliding $\vec{v}_b = \vec{v}_{\mathrm{SSA}}$. Bueler and Brown [2009] use a weighing function to ensure a continuous solution of the velocity from the interior of the ice sheet across the grounding line to the ice shelf. However, Winkelmann et al. [2011] have demonstrated that a simple addition (for the grounded ice sheet velocities) still guarantees a smooth transition for ice-stream flow, i.e., $\vec{v} = \vec{v}_{\mathrm{SIA}} + \vec{v}_{\mathrm{SSA}}$. Here, we incorporate both into one equation, which leads to the following set of equations for both horizontal components of the ice velocity $\vec{v} = (u, v)$,

$$2\frac{\partial}{\partial x}\left(2\eta h\frac{\partial u}{\partial x} + \eta h\frac{\partial v}{\partial y}\right) + \frac{\partial}{\partial y}\left(\eta h\frac{\partial u}{\partial y} + \eta h\frac{\partial v}{\partial x}\right) - \beta^2 u = -\tau_{d_x} - \beta^2 u_{\mathrm{SIA}} \,, \tag{3}$$

$$2\frac{\partial}{\partial y}\left(2\eta h\frac{\partial v}{\partial y} + \eta h\frac{\partial u}{\partial x}\right) + \frac{\partial}{\partial x}\left(\eta h\frac{\partial v}{\partial x} + \eta h\frac{\partial u}{\partial y}\right) - \beta^2 v = -\tau_{d_y} - \beta^2 v_{\mathrm{SIA}} \,, \tag{4}$$

where

$$\eta = \frac{A^{-1/n}}{2}\left[\left(\frac{\partial u}{\partial x}\right)^2 + \left(\frac{\partial v}{\partial y}\right)^2 + \frac{\partial u}{\partial x}\frac{\partial v}{\partial y} + \frac{1}{4}\left(\frac{\partial u}{\partial y} + \frac{\partial v}{\partial x}\right)^2 + \dot{\varepsilon}_0{}^2\right]^{(1-n)/2n} , \tag{5}$$

and where $\tau_{d_x} = \rho_i g h(\partial h_s/\partial x)$ (similar for τ_{d_y}). $\dot{\varepsilon}_0 = 10^{-20}$ a^{-1} is a small factor to keep η finite, hence to prevent singularities when velocity gradients are zero. For the ice shelf, $\beta^2 = 0$. The SSA stress-equilibrium equations (3) and (4) require boundary conditions to be specified along the contour which defines the boundary to the ice-shelf domain, which is taken as the edge of the computational domain, irrespective of whether or not calving is considered. Dynamic conditions (specification of stress) are applied at this seaward edge, so that the vertically-integrated pressure balance then reads

$$2\eta h\left[\left(2\frac{\partial u}{\partial x}+\frac{\partial v}{\partial y}\right)n_x+\frac{1}{2}\left(\frac{\partial u}{\partial y}+\frac{\partial v}{\partial x}\right)n_y\right] = n_x\frac{1}{2}\rho_i g h^2\left(1-\frac{\rho_i}{\rho_s}\right), \quad (6)$$

$$2\eta h\left[\left(2\frac{\partial v}{\partial y}+\frac{\partial u}{\partial x}\right)n_y+\frac{1}{2}\left(\frac{\partial u}{\partial y}+\frac{\partial v}{\partial x}\right)n_x\right] = n_y\frac{1}{2}\rho_i g h^2\left(1-\frac{\rho_i}{\rho_s}\right), \quad (7)$$

where n_x, n_y are the outward-pointing normal vectors in the x and y direction, respectively.

1.3 Ice thickness evolution

Ice sheet thickness evolution is based on mass conservation, leading to the continuity equation. For the general ice sheet/ice shelf system (HySSA), this is either written as:

$$\frac{\partial h}{\partial t} = -\frac{\partial(uh)}{\partial x}-\frac{\partial(vh)}{\partial y}+\dot{a}-M\,, \quad (8)$$

or

$$\frac{\partial h}{\partial t} = -\frac{\partial(u_b h)}{\partial x}-\frac{\partial(v_b h)}{\partial y}+\frac{\partial}{\partial x}\left(d_d\frac{\partial(h+h_b)}{\partial x}\right)+\frac{\partial}{\partial y}\left(d_d\frac{\partial(h+h_b)}{\partial y}\right)+\dot{a}-M\,, \quad (9)$$

where $\dot{a}$ is the surface mass balance (accumulation minus surface ablation), M is the basal melt rate (i.e., sub-shelf melting as well as basal melting underneath the grounded ice sheet), and d_d diffusion coefficients for the deformational velocity according to SIA. The latter are defined as

$$d_d = \frac{2}{n+2}Ah^{n+2}(\rho_i g)^n|\nabla(h+h_b)|^{n-1} \quad (10)$$

The treatments of the various local ice gains or losses (surface mass balance, etc.) are described in later sections. For the SIA model in the grounded ice sheet, Eq. (8) is written as a diffusion equation for ice thickness:

$$\frac{\partial h}{\partial t} = \frac{\partial}{\partial x}\left(d\frac{\partial(h+h_b)}{\partial x}\right)+\frac{\partial}{\partial y}\left(d\frac{\partial(h+h_b)}{\partial y}\right)+\dot{a}-M\,, \quad (11)$$

where h_b is the bottom of the ice sheet (or the bedrock elevation b for the grounded ice sheet) and d contains both the deformational and sliding contributions [Huybrechts, 1992].

1.4 Basal sliding

We use a generalized slip law, or regularized Coulomb friction law, that reconciles both Weertman/Budd and Coulomb slip laws [Schoof, 2005, Gagliardini et al., 2007, Joughin et al., 2019, Zoet and Iverson, 2020, Helanow et al., 2021]:

$$\tau_b = CN \left(\frac{|\vec{v}_b|}{|\vec{v}_b| + u_0} \right)^{1/m} \frac{\vec{v}_b}{|\vec{v}_b|} = CN \left(\frac{|\vec{v}_b|}{|\vec{v}_b| + A'_b C^m N^m} \right)^{1/m} \frac{\vec{v}_b}{|\vec{v}_b|} \tag{12}$$

where, $A'_b = u_0 (CN)^{-m}$ is a sliding coefficient, often used when a friction law is written as a sliding law. Low speeds and high effective stresses result in viscous Weertman-style sliding; high sliding speeds and low effective stresses – conditions commonly present at the bases of ice streams – promote shallow deformation of the bed at its Coulomb strength. The main advantage of this description is that the transition from power-law slip to plastic Coulomb occurs smoothly.

In the f.ETISh model, we formulate the slip law as a function of $f(A'_b, u_0)$, instead of $f(C, u_0)$ in Joughin et al. [2019] or $f(A'_b, C)$ in Helanow et al. [2021]. Since $A'_b = u_0 (CN)^{-m}$, we can write Eq. (11) as

$$\tau_b = {A'}_b^{-1/m} \left(\frac{u_0}{|\vec{v}_b| + u_0} \right)^{1/m} |\vec{v}_b|^{1/m-1} \vec{v}_b \tag{13}$$

where the term between brackets varies between 0 (plastic) and 1 (viscous). This general slip law can be related to other existing laws by:

- Budd law: $u_0 \gg |\vec{v}_b|$,
- Weertman law: $u_0 \gg |\vec{v}_b|$ and N is a constant value,
- Plastic Coulomb: $u_0 \approx 0$, so that $\tau_b \approx CN$.

Through the definition of $A'_b = u_0 (CN)^{-m}$, the general slip law can in principle be expressed as a sliding law so that it fits in with the SIA description, i.e.,

$$\vec{v}_b = \frac{1}{\alpha} A'_b |\tau_b|^{m-1} \tau_b \tag{14}$$

where

$$\alpha = 1 - \frac{A'_b}{u_0} |\tau_b|^m \tag{15}$$

Note that the limiting condition is that $0 < \alpha \leq 1$. This means that the sliding law can never be pure plastic ($\alpha = 0$), but comes very close to plasticity for high sliding velocities. For $\alpha = 1$, the sliding law takes the form of the Budd/Weertman sliding law and corresponds to $u_0 \to +\infty$. The basal sliding factor A'_b implicitly incorporates u_0, is a function of the effective pressure N and is also temperature dependent. The latter allows for sliding within a basal temperature range between -3 and 0°C. It further takes into account sub-grid sliding across mountainous terrain [Pollard et al., 2015]:

$$A'_b = N^{-p} \left[(1 - r) A_{\text{froz}} + r A_b \right] , \tag{16}$$

where $r = \max[0, \min[1, (T^\star - T_r)/(-T_r)]]$, A_{froz} is the sliding coefficient in case of frozen bedrock (chosen to be very small but different from zero to avoid singularities in the basal friction calculation), $T^\star$ is the temperature corrected for the dependence on pressure (see Sect. 1.8.3) and $T_r = \min[-3 - 0.02\sigma_b]$, where σ_b is the standard deviation of bedrock elevation within the grid cell [Pollard et al., 2015]. Basal sliding factors A_b are either considered constant in space/time or are spatially varying and obtained through optimization methods (see Sect. 2.3). The exponent p equals m of the sliding law when effective pressure is calculated, and takes the value $p = 0$ otherwise.

1.5 Grounding-line flux condition for power-law sliding (SGL)

Previous studies have indicated that it is necessary to resolve the transition zone/boundary layer at sufficiently fine resolution in order to capture grounding-line migration accurately [Durand et al., 2009, Pattyn et al., 2012, 2013, Pattyn and Durand, 2013, Durand and Pattyn, 2015]. In large-scale models, this can lead to unacceptably small time-steps and costly integrations. Pollard and DeConto [2009, 2012a] incorporated the boundary layer solution of Schoof [2007a] directly in a numerical ice-sheet model at coarse grid resolution, so the flux, q_g, across model grounding lines is given by

$$q_g = \left[\frac{A(\rho_i g)^{n+1}(1-\rho_i/\rho_s)^n A_b'^{1/m}}{4^n} \right]^{\frac{m}{m+1}} \Theta^{\frac{nm}{m+1}} h_g^{\frac{m(n+3)+1}{m+1}} . \tag{17}$$

This yields the vertically averaged velocity $u_g = q_g/h_g$ where h_g is the ice thickness at the grounding line. Θ in Eq. (16) accounts for back stress at the grounding line due to buttressing by pinning points or lateral shear, and is defined as

$$\Theta = \frac{b_f \tau_{xx} + (1-b_f)\tau_f}{\tau_f} , \tag{18}$$

where τ_{xx} is the longitudinal stress just downstream of the grounding line, calculated from the viscosity and strains in a preliminary SSA solution without constraints given by Eq. (16), and τ_f the free-water tensile stress defined by

$$\tau_f = \frac{1}{2}\rho_i g h \left(1 - \frac{\rho_i}{\rho_s}\right) . \tag{19}$$

The parameter b_f is an additional buttressing factor to control the buttressing strength of ice shelves and may be varied between 0 (no buttressing) and 1 (full buttressing). All experiments in this paper use $b_f = 1$, except the sensitivity experiments on ice-shelf de-buttressing where b_f is set to zero. Grounding-line ice thickness h_g is linearly interpolated in space by estimating the sub-grid position of the grounding line between the two surrounding floating and grounded h-grid points. Therefore, the height above floatation is linearly interpolated on the Arakawa C-grid between those two points to where it is zero. Subsequently, the bedrock elevation is linearly interpolated to that location, and the floatation thickness of ice for that bedrock elevation and current sea level is obtained [Pattyn et al., 2006, Gladstone et al., 2010, Pollard and DeConto, 2012a]. The velocity u_g is then calculated at the grounding-line points and imposed as an internal boundary condition for the flow equations, hence overriding the large-scale velocity solution at the grounding line. $u_g = q_g/h_g$ is imposed exactly

at the u-grid grounding line point when the flux q_g is greater than the large-scale sheet-shelf equation's flux at the grounding line.

Equation (16) applies equally to the y direction, with v_g and τ_{yy} instead of u_g and τ_{xx}. Note that spatial gradients of quantities parallel to the grounding line, which are not included in Schoof's flow-line derivation of Eq. (16), are neglected here [Katz and Worster, 2010, Gudmundsson et al., 2012, Pattyn et al., 2013]. This parametrization was also found to yield results comparable to SSA models solving transient grounding line migration at high spatial resolution of the order of hundreds of meters [Pattyn and Durand, 2013, Durand and Pattyn, 2015], despite the fact that Eq. (16) applies to steady-state conditions.

The use of the above-described flux condition has been analysed and criticised by Reese et al. [2018b], claiming non-physical behaviour of the buttressing factor in the flux condition. However, Reese et al. [2018b] only considered ice-sheet diagnostics, as negative values of buttressing vanish when the ice sheet is allowed to change over time. As a precaution, we limit anyway $0 \leq \Theta \leq 1$.

The ice sheet model f.ETISh also allows for modelling separate drainage basins at high resolution. In this case the SGL condition is not needed.

1.6 Effective pressure at the ice sheet base

There are different ways of representing the effective pressure at the base of an ice sheet generally done in ice sheet models. In theory, the effective pressure N represents the ice overburden pressure p_o, i.e., the downward force due to the weight of overlying ice and till, minus the subglacial water pressure (p_w):

$$N = p_o - p_w = \rho_i g h - p_w \tag{20}$$

In the following sections, we describe in more detail on how either subglacial water pressure p_w or effective pressure N is determined.

1.6.1 Height above buoyancy

Subglacial water pressure is often neglected in ice sheet models and therefore its relationship with the effective pressure and the basal sliding is often neglected too. A simple way is to link p_w to the depth of the bed below sea level. Near grounding lines in direct contact with the ocean, subglacial water pressure of saturated till may be approximated by [Tsai et al., 2015]:

$$p_w = -P_w \rho_s g \left(b - z_{sl}\right) , \tag{21}$$

where P_w is a fixed fraction of the overburden pressure. Eq. (20) is valid for $b - z_{sl} < 0$, otherwise $p_w = 0$. By definition, $p_w = \rho_i g h$ at the grounding line and underneath floating ice shelves, so that the effective pressure becomes zero (or close to zero when modulated by the value of P_w). This means that only marine terminated parts of the ice sheet are impacted by the subglacial water. According to Lüthi et al. [2002], the pore water pressure, i.e., the pressure of the subglacial water mixed with the solid part of the till, represents a fraction slightly smaller than 100% of the ice overburden pressure. Bueler and Brown [2009] consider the pore water pressure locally as at most a fixed fraction (P_w = 95%) of the ice overburden pressure $\rho_i g h$. The fraction varies among different studies, i.e., 96% [Winkelmann et al.,

2011], 97% [Van Pelt and Oerlemans, 2012], and 99% [Gandy et al., 2019]. This is probably the most common representation of subglacial water pressure in large-scale Antarctic ice sheet models.

1.6.2 Subglacial water film

Subglacial water flow can be introduced following the method of Le Brocq et al. [2009] based on a single element type to describe the morphology of the drainage system, i.e., a Weertman-type water film [Flowers, 2015]. The model assumes that water flows in a thin film of water of the order of 10^{-3} m thickness. The evolution of the water film depth d_w is given by

$$\frac{\partial d_w}{\partial t} = M - \nabla \cdot (\mathbf{u}_w d_w) \tag{22}$$

where M is the basal melt rate (positive for melting) underneath the grounded ice sheet, and $\mathbf{u}_w$ is the depth-averaged water film velocity, calculated using a theoretical treatment of laminar flow between two parallel plates, driven by differences in the water pressure [Weertman, 1966]:

$$\mathbf{u}_w = \frac{d_w^2}{12\mu} \nabla \Phi \tag{23}$$

where μ is the viscosity of water and Φ is the hydraulic potential. The hydraulic potential represents the total mechanical energy per unit volume of water required to move the water from one state to another [Flowers, 2015], and is a function of the elevation potential and the water pressure, i.e.,

$$\Phi = \rho_w g b + p_w = \rho_w g b + \rho_i g h - N \tag{24}$$

The water pressure, p_w, is a function of the ice overburden pressure and the effective pressure N. In a distributed system, however, the water pressure will be close to, if not at, the overburden pressure. As a result, a simplification can be made to Eq. (23), assuming N to be zero (see, e.g., Budd and Jenssen, 1987; Alley, 1996). The assumption that N is zero simplifies the calculation of the hydraulic potential surface by removing the need to calculate the water pressure. With this simplification, the gradient of the potential surface is written as

$$\nabla \Phi = \rho_i g \nabla h_s + (\rho_w - \rho_i) g \nabla b \tag{25}$$

Taking $\partial d_w / \partial t = 0$ in Eq. (21) (steady-state approach), it is possible to use a flux balance approach to calculate the steady-state water depth (in a similar way to balance velocity calculations; see, e.g., Budd and Warner (1996) or Le Brocq and others (2006), for more details). The balance approach requires the outgoing flux in any given grid cell to be equal to the incoming water flux plus the local melt rate within the cell. The routing direction of the subglacial water is given by the hydraulic potential gradient $\nabla \Phi$. The water depth is then obtained from the outgoing water flux Q_l, i.e.,

$$d_w = \left(\frac{12 \mu Q_l}{|\nabla \Phi|} \right)^{\frac{1}{3}} \tag{26}$$

Subglacial water thickness is then related to subglacial water pressure through

$$p_w = P_w \rho g h \left(\frac{d_w}{d_w^0} \right) , \tag{27}$$

where d_w^0 = 0.0015 m is a limit value to the subglacial water thickness.

1.6.3 Sliding related to water flux

Alternatively, Goeller et al. [2013] propose to introduce a simple physically plausible correlation of the sliding rate factor and the subglacial water flux:

$$A_b = A_o \exp \left(\frac{\Phi}{\Phi_0} \right) , \tag{28}$$

where Φ_0 is a limit factor on the subglacial water flux, taken as 10^5 [Goeller et al., 2013], and A_o the initial value of A_b. A similar approach has been followed by Pattyn et al. [2005]. The approach is rather intuitive than physical and just considers that basal sliding increases when the water flux beneath the ice sheet increases.

1.6.4 Effective pressure in till

Bueler and Brown [2009] employ an effective thickness of stored liquid water at the base of the ice column. This layer of thickness W is used to estimate the subglacial water pressure reduced to the pore water pressure according to

$$p_w = P_w \rho_i g h \frac{W}{W_{\max}} , \tag{29}$$

where $W_{\max}$ is the maximum saturated till thickness, fixed at 2 m, which has an impact on the till weakening by pressurized water. A fixed fraction of ice overburden equal to one will imply that the yield stress becomes zero in the case of full till saturation [Van Pelt and Oerlemans, 2012]. An alternative way, which has been used here, to derive the effective pressure in the case of a deformable bed composed by a permeable till is to express the effective pressure, N, in Eq. (19) as a function of the sediment void ratio, e, due to the changing water content in the till [van der Wel et al., 2013, Bougamont et al., 2014], i.e.,

$$N = N_0 \times 10^{-(e-e_0)/C_c} , \tag{30}$$

where e_0 is the void ratio at a reference effective pressure N_0 and C_c is the till compressibility. Bueler and van Pelt [2015] propose to employ Eq. (29) in a hydrological model of subglacial water drainage within an active layer of the till, W. As the water in till pore spaces is much less mobile than that in the linked-cavity system because of the very low hydraulic conductivity of till, an evolution equation for W_{til} without horizontal transport can be written [Bueler and van Pelt, 2015]

$$\frac{\partial W}{\partial t} = M - C_t \tag{31}$$

Here C_t is a fixed rate that makes the till gradually drain in the absence of water input; we choose C_t to be 1 mm a^{-1}, which is small compared to typical values of subglacial melt. We constrain the layer thickness by

$$0 \leq W \leq W_{\max} \tag{32}$$

The effective pressure N is then written as the following function of W [Bueler and van Pelt, 2015],

$$N = N_0 \left(\frac{\delta P_o}{N_0} \right)^s 10^{\left(\frac{e_0}{C_c}\right)(1-s)} \tag{33}$$

where $s = W/W_{\max}$ and bounded by $N = \min\{p_o, N\}$ and δp_o is the lower bound on N, taken as a fraction of the ice overburden pressure.

1.7 Calving, hydrofracturing and sub-shelf pinning

Ice-front calving is obtained from the large scale stress field [Pollard et al., 2015], based on the horizontal divergence of the ice-shelf velocities and which is similar to parametrizations used elsewhere [Martin et al., 2011, Winkelmann et al., 2011, Levermann et al., 2012]. Extensional stress is obtained via strain rate and the model SSA rheology. No distinction is made here between along-flow and transverse strains, whose combined effect is represented by ice divergence.

$$d_s = \frac{2}{\rho_i g} \left(\frac{\dot{\varepsilon}}{A} \right)^{1/n} \tag{34}$$

$$d_b = \left(\frac{\rho_i}{\rho_w - \rho_i} \right) \frac{2}{\rho_i g} \left(\frac{\dot{\varepsilon}}{A} \right)^{1/n} \tag{35}$$

where d_s and d_b are depths of dry-surface and basal crevasses respectively, and $\dot{\varepsilon}$ is ice divergence. Calving is potentially applied to all points within the ice shelf, but the setting of divergence $\dot{\varepsilon}$ depends on whether the floating ice covers all or a fraction of the cell area. A sub-grid parametrization of fractional ice area is used to set an adjusted ice thickness h and fractional cover f_i. At the ice-shelf edge adjacent to open ocean, the adjusted thickness h is the average of adjacent interior shelf thicknesses, each multiplied by a "downstream thinning" factor $1-w[1-\exp(\Delta x/100)]$, where the weight $w = \min[1, h_u/(h_a \exp(-\Delta x/100)]$, where Δx is the grid size in km, h_u is the unadjusted (grid-mean) ice thickness of the edge point, and h_a is the thickness of the adjacent interior point. The weight w is used to force $h \approx h_a$ for small amounts of ice ($h_u \ll h_a$), and to apply more downstream thinning when the edge cell has substantial ice cover. As in Pollard and DeConto [2012b], the fractional ice cover of the edge point is set to $f_i = h_u/h$, conserving ice mass.

For interior points (with $f_i = 1$), $\dot{\varepsilon}$ in Eqs. (33–34) is set to the grid-scale divergence of ice velocity $\partial u/\partial x + \partial v/\partial y$. For edge points (with $f_i < 1$), it is set to the longitudinal spreading value for a freely floating unconfined ice face, using the adjusted ice thickness h as described above.

$$\dot{\varepsilon} = \left(\frac{\partial u}{\partial x} + \frac{\partial v}{\partial y} \right) \qquad \text{for} \qquad f_i = 1 \tag{36}$$

$$\dot{\varepsilon} = A \left(\frac{\rho_i g h}{4} \right)^n \qquad \text{for} \qquad f_i < 1 \tag{37}$$

An additional calving rate due to accumulated strain (valid for large ice shelves), is parametrized as

$$d_a = h \max[0, \ln(u/1600)]/\ln(1.2) \tag{38}$$

where h is ice thickness (adjusted as above if at the shelf edge) and u is local ice speed. d_a is zero for speeds up to 1600 m a^{-1}, and approaches h as speeds increase to $\sim$1900 m a^{-1} and above, as they do in the outer regions of the Ross and Ronne shelves.

A pragmatic constraint is imposed for thin floating ice,

$$d_t = h \max[0, \min[1, (150 - h)/50]] \tag{39}$$

where again h is ice thickness (adjusted as above if at the shelf edge), and d_t is an additional crevasse depth. This simply has the effect of removing floating ice thinner than $\sim$100 to 150 m, and reduces unrealistic areas of thin ice extending seaward of the modern Ross and Filchner–Ronne calving fronts, where they are not limited by Eq. (37). It has the side-effect of not allowing thin ice shelves to grow from small ($\sim$100 m) tidewater glaciers, which may be unrealistic in some cases but does not noticeably affect the large-scale modern and "retreat" simulations.

Surface crevasses containing water are deepened due to the additional opening stress of the liquid by an amount d_{wa}, where d_{wa} is (ρ_w/ρ_i) times the depth of water drained into the crevasse from mobile surface melt and/or rainfall. d_{wa} (m) is simply set to

$$d_{wa} = 100R^2 \tag{40}$$

where R is the annual surface melt + rainfall available after refreezing in the model's surface mass balance scheme.

The overall calving rate C_r is expressed as a horizontal wastage rate (m a^{-1}):

$$C_r = 3000 \max[0, \min[1, (r - r_c)/(1 - r_c)]] \tag{41}$$

where r is the ratio of the combined crevasse depths to ice thickness $[d_s + d_b + d_a + d_t + d_{wa}]/h$, and r_c is a critical value for calving onset, set to 0.75 [Pollard et al., 2015].

Alternatively, the calving rate can also be defined as in Pollard and DeConto [2012b], i.e.,

$$C_r = 30(1 - w_c) + 3 \times 10^5 \max\left(\frac{\partial u}{\partial x} + \frac{\partial v}{\partial y}, 0\right) \frac{w_c h_e}{\Delta} \tag{42}$$

where $w_c = \min(1, h_e/200)$ is a weight factor and h_e is the subgrid ice thickness within a fraction of the ice edge grid cell that is occupied by ice [Pollard and DeConto, 2012a], defined by

$$h_e = \max\left[h_{\max} \times \max\left(0.25, e^{-h_{\max}/100}\right), 30, h\right] \tag{43}$$

where a minimum ice thickness of 30 m avoids too thin ice shelves. The value of $h_{\max}$ is defined as the maximum ice thickness of the surrounding grid cells (grounded or floating) that are not adjacent to the ocean [Pollard and DeConto, 2012a].The calving rate C_r is then subtracted from the basal melt rate M in Eq. (8).

Given the relatively low spatial resolution of a large-scale ice-sheet model, small pinning points underneath ice shelves due to small bathymetric rises scraping the bottom of the ice

and exerting an extra back pressure on the ice shelf [Berger et al., 2016, Favier et al., 2016] are not taken into account. To overcome this a simple parametrization based on the standard deviation of observed bathymetry within each model cell was accounted for to introduce a given amount of basal friction of the ice shelf [Pollard and DeConto, 2012a]. The fractional area f_g of ice in contact with sub-grid bathymetric high is defined as [modified from Pollard and DeConto, 2012a]:

$$f_g = \max\left[0, 1 - \frac{h_w}{\sigma_b}\right] \tag{44}$$

where h_w is the thickness of the water column underneath the ice shelf and σ_b is the standard deviation of the bedrock variability (see above). This factor f_g is multiplied with β^2 in the basal friction. For the grounded ice sheet, $f_g = 1$; for the floating ice shelf in deeper waters, $f_g = 0$, so that the ice shelf does not experience any friction.

1.8 Ice temperature and rheology

1.8.1 Ice-sheet temperature

The diffusion–advection equation for an ice sheet is given by [Huybrechts, 1992]:

$$\frac{\partial\theta}{\partial t} = \kappa\frac{\partial^2\theta}{\partial z^2} - u\frac{\partial\theta}{\partial x} - v\frac{\partial\theta}{\partial y} - w\frac{\partial\theta}{\partial z} + \frac{\Phi_d}{\rho_i c_p}\,, \tag{45}$$

where $\kappa = K/\rho_i c_p$ is the thermal diffusivity of ice, K is the thermal conductivity, c_p is the heat capacity of ice, θ is the ice temperature, and $\Phi_d = -\rho_i g(h_s - z)\nabla h_s \partial\vec{v}_d/\partial z$ represents deformational heating, where $\vec{v}_d$ is the deformational velocity component ($\vec{v}_d = \vec{v} - \vec{v}_b$). The basal boundary condition is given by

$$\frac{\partial\theta_b}{\partial z} = \frac{G + \tau_d\vec{v}_b}{K}\,, \tag{46}$$

where G is the geothermal heat flux and the second term represents frictional heating at the base. The last term in Eq. (45) represents strain heating. Phase changes at the base are incorporated in the model by keeping the the basal temperature at the pressure melting point whenever it is reached or basal melt water is present. The basal melt rate $\dot{b}$ (positive when melting) is calculated from the difference between the basal temperature gradient in Eq. (45) and the gradient corrected for pressure melting,

$$\dot{b} = \frac{K}{\rho L}\left[\left(\frac{\partial\theta_b}{\partial z}\right)_c - \frac{G + \tau_d\vec{v}_b}{K}\right] \tag{47}$$

where the subscript c denotes the gradient corrected for pressure melting, and L is the specific latent heat for fusion. Given the two-dimensional nature of the model, the temperature field employs shape functions for vertical profiles of deformational velocity $\vec{v}_d$, its vertical gradient, and the vertical velocity, based on SIA [Hindmarsh, 1999]. Eq. 44 is then solved in scaled vertical coordinates $\zeta = (h_s - z)/h$, with $\zeta = 0$ at the surface and $\zeta = 1$ at the bottom of the ice sheet. The use of shape functions for horizontal and vertical velocities allows for a faster calculation of the thermodynamic model. We follow the approach by Lliboutry [1979] and Ritz [1992] that take into account a higher power of the horizontal velocity profile due to softer ice at the bed, hence higher shear strain rates, i.e.,

$$\vec{v} = \frac{\dot{\gamma}_b h}{p_r + 2} \tag{48}$$

where

$$\dot{\gamma}_b = B_0 \tau_d^n \exp\left[\frac{Q}{R}\left(\frac{1}{\theta_{mb}} - \frac{1}{\theta_b}\right)\right] \tag{49}$$

and

$$p_r = n - 1 + KGh \tag{50}$$

so that,

$$\vec{v}(\zeta) = \vec{v}_b + \frac{p_r + 2}{p_r + 1}\left(1 - \zeta^{p_r+1}\right)\vec{v} \tag{51}$$

and

$$w(\zeta) = -\dot{a}\left(1 - \frac{p_r + 2}{p_r + 1}(1 - \zeta) + \frac{1}{p_r + 1}(1 - \zeta)^{p_r+2}\right) \tag{52}$$

For an isothermal ice sheet, $p_r = n$. However, since this is an approximation compared to fully solving Eq. 44, the EISMINT-I benchmark experiments [Huybrechts et al., 1996] were performed successfully and results are given in Section 3.1.

Update table with Ritz model results for EISMINT-2.

1.8.2 Ice-shelf temperature

In ice shelves, a simple temperature model is adopted, considering the accumulation at the surface balanced by basal melting underneath an ice shelf and with only vertical diffusion and advection into play [Holland and Jenkins, 1999]:

$$\theta(\zeta) = \frac{(T_s - \theta_b^s)\exp(\beta_1) + \theta_b^s - T_s\exp(\beta_2)}{1 - \exp(\beta_2)}\,, \tag{53}$$

where $\beta_1 = \dot{a}\zeta h/\kappa$, $\beta_2 = \dot{a}h/\kappa$, and θ_b^s is the ocean temperature at the base of the ice shelf, corrected for ice-shelf depth, i.e., $\theta_b^s = T_{oc} = T_{oc}(0) - 0.12 \times 10^{-3} h_b$ [Maris et al., 2014], where T_{oc} is the the ocean temperature near the surface corrected for depth.

1.8.3 Thermomechanical coupling

The flow parameter A and its temperature dependence on temperature are specified as in Ritz [1987, 1992]:

$$\begin{aligned} A \;=\; & \frac{E_f}{2} \times 1.66 \times 10^{-16} \exp\left[\frac{78.20 \times 10^3}{R}\left(\frac{1}{T_m} - \frac{1}{T^\star}\right)\right] \\ & \text{if} \quad T^\star \geq 266.65\text{K} \\ & \frac{E_f}{2} \times 2.00 \times 10^{-16} \exp\left[\frac{95.45 \times 10^3}{R}\left(\frac{1}{T_m} - \frac{1}{T^\star}\right)\right] \\ & \text{if} \quad T^\star < 266.65\text{K}\,, \end{aligned} \tag{54}$$

where $T^\star = T - T_m$ is the homologous temperature, with $T_m = -8.66 \times 10^{-4}(1-\zeta)h$ the pressure melting correction and R the gas constant. Units of A are Pa^{-3} yr^{-1} corresponding to $n = 3$. The enhancement factor E_f is set to 1 for the main ice sheet model, and to $E_f = 0.5$ for ice shelves. The ratio of enhancement factors represent differences in fabric anisotropy between grounded and ice shelf ice [Ma et al., 2010]. Verification of the thermomechanical coupling scheme using a vertical mean value of A follows the EISMINT-II benchmark experiments [Payne et al., 2000] and is detailed in Section 3.2.

1.9 Glacial Isostatic Adjustment (GIA)

As a first approximation, the equilibrium vertical displacement of the lithosphere in response to an ice loading is described as the equilibrium vertical displacement of a horizontal linear elastic plate subject to a transverse load. In order to represent the viscous asthenosphere underneath the lithosphere, it is also assumed that this plate lies on a viscous substratum. This representation of the lithosphere is considered for instance in the commonly used elastic lithosphere–relaxing asthenosphere (ELRA) model in glaciology.

1.9.1 Bedrock deformation for a plate with constant thickness

Consider a thin rectangular plate with constant thickness h (and infinite horizontal dimension). The mechanical properties of the plate are given by its Young's modulus E and its Poisson's ratio ν (both properties are assumed to be constant). The plate is subjected to a transverse load q_b. Let w_b be the normal displacement of the plate (also called the deflection). For a thin rectangular plate, it is assumed that the shear strains ϵ_{xz} and ϵ_{xy} and the normal strain ϵ_{xx} is negligible, where we denoted the strain tensor by ϵ. In this context and using a Hooke's law in linear elasticity (the plate is assumed to behave like a linear elastic material), the components σ_{xx}, σ_{yy} and σ_{xy} of the stress tensor are given by

$$\sigma_{xx} = \frac{E}{1-\nu^2}\left(\epsilon_{xx} + \nu\epsilon_{yy}\right) \tag{55}$$

$$\sigma_{yy} = \frac{E}{1-\nu^2}\left(\epsilon_{yy} + \nu\epsilon_{xx}\right) \tag{56}$$

$$\sigma_{xy} = \frac{1}{2}G\epsilon_{xy} \tag{57}$$

where $G = \frac{E}{2(1+\nu)}$ is the shear modulus. In the context of thin rectangular plates, these stress components can be written as:

$$\sigma_{xx} = -\frac{Ez}{1-\nu^2}\left(\frac{\partial^2 w_b}{\partial x^2} + \nu\frac{\partial^2 w_b}{\partial y^2}\right) \tag{58}$$

$$\sigma_{yy} = -\frac{Ez}{1-\nu^2}\left(\frac{\partial^2 w_b}{\partial y^2} + \nu\frac{\partial^2 w_b}{\partial x^2}\right) \tag{59}$$

$$\sigma_{xy} = -\frac{Ez}{1+\nu}\frac{\partial^2 w_b}{\partial x \partial y} \tag{60}$$

where the vertical coordinate z is measured from the middle surface of the plate. The resulting twisting (or torsion) moments M_{xx} and M_{yy} and bending moment M_{xy} (equal to M_{yx}) are given by

$$M_{xx} = \int_{-h/2}^{h/2} \sigma_{xx} z dz = -D \left(\frac{\partial^2 w_b}{\partial x^2} + \nu \frac{\partial^2 w_b}{\partial y^2} \right) \tag{61}$$

$$M_{yy} = \int_{-h/2}^{h/2} \sigma_{xy} z dz = -D \left(\frac{\partial^2 w_b}{\partial y^2} + \nu \frac{\partial^2 w_b}{\partial x^2} \right) \tag{62}$$

$$M_{xy} = \int_{-h/2}^{h/2} \sigma_{xy} z dz = -D(1-\nu) \frac{\partial^2 w_b}{\partial x \partial y} \tag{63}$$

where

$$D = \frac{E h^3}{12\,(1-\nu^2)} \tag{64}$$

is the flexural rigidity of the plate. Writing the equilibrium of forces and moments for the plate, it can be shown that the twisting and bending moments satisfy the following differential equation:

$$\frac{\partial^2 M_{xx}}{\partial x^2} + 2 \frac{\partial^2 M_{xy}}{\partial x \partial y} + \frac{\partial^2 M_{yy}}{\partial y^2} = -q_b \tag{65}$$

Substituting Eqs. (60)–(62) into Eq. (64) gives the following partial differential equation for the deflection w_b:

$$\begin{aligned} \frac{\partial^2}{\partial x^2} \left(-D \left(\frac{\partial^2 w_b}{\partial x^2} + \nu \frac{\partial^2 w_b}{\partial y^2} \right) \right) + 2 \frac{\partial^2}{\partial x \partial y} \left(-D(1-\nu) \frac{\partial^2 w_b}{\partial x \partial y} \right) + \\ \frac{\partial^2}{\partial y^2} \left(-D \left(\frac{\partial^2 w_b}{\partial y^2} + \nu \frac{\partial^2 w_b}{\partial x^2} \right) \right) = -q_b \end{aligned} \tag{66}$$

or as D is assumed to be constant and ν is constant,

$$-D \left(\frac{\partial^4 w_b}{\partial x^4} + 2\nu \frac{\partial^4 w_b}{\partial x^2 y^2} + \frac{\partial^4 w_b}{\partial y^4} \right) - 2D(1-\nu) \frac{\partial^4 w_b}{\partial x^2 y^2} = -q_b \tag{67}$$

that leads to

$$D \left(\frac{\partial^4 w_b}{\partial x^4} + 2 \frac{\partial^4 w_b}{\partial x^2 y^2} + \frac{\partial^4 w_b}{\partial y^4} \right) \equiv D \nabla_x^4 w_b = q_b \tag{68}$$

1.9.2 Plate with constant thickness on a viscous substratum

We consider now that the plate lies on a viscous substratum with density ρ_b, which is the upper mantle density. In this case, we must account for the buoyancy force (which depends on the vertical displacement w_b) that the lithosphere experiences in the underlying viscous substratum. The buoyancy force acts to reduce the exerted force q_b by an amount $\rho_b g w_b$. Then, Eq. (67) writes in the presence of a viscous substratum as [Huybrechts and de Wolde, 1999, Pollard and DeConto, 2012a]

$$D\nabla_{\boldsymbol{x}}^4 w_b + \rho_{\mathrm{b}} g w_b = q_b \tag{69}$$

The load q_b is then defined by

$$q_b = \rho_i g h + \rho_s g h_w - \rho_i g h^{\mathrm{eq}} - \rho_s g h_w^{\mathrm{eq}}\,, \tag{70}$$

where h_w is the ocean column thickness, and h^{eq} and h_w^{eq} are the values of ice thickness and ocean column thickness in equilibrium, respectively, taken from modern observed fields. Equation (68) is solved by a Green's function [Huybrechts and de Wolde, 1999]. The response to a point load P_b ($q_b\times$ area) versus distance from the point load l is then given by

$$w_p(l) = \frac{P_b L_w^2}{2\pi D}\mathrm{kei}\left(\frac{l}{L_w}\right)\,, \tag{71}$$

where kei is a Kelvin function of zeroth order (defined as the imaginary part of a modified Bessel function of the second kind), and $L_w = (D/\rho_b g)^{1/4}$ is the flexural length scale. For any load, the different values of the point loads w_p are summed over all grid cells to yield $w_b(x, y)$.

1.9.3 Plate with spatially-varying thickness

Let us a consider in this section a thin rectangular plate having a spatially-varying thickness $h(x)$. As previous, the plate is assumed to behave as a linear elastic material with constant Young's modulus E and Poisson's ratio ν. The plate is subjected to a transverse load q_b that induces a deflection w_b of the plate. We assume that the above thickness varies gradually and there is no abrupt variation in thickness so that the expressions for the bending and twisting moments derived earlier for plates of constant thickness (60)–(62) also apply with sufficient accuracy to the case of a thin rectangular having a spatially-varying thickness. Please note that in this case, the flexural rigidity D is therefore spatially varying, i.e.,

$$D = D(\boldsymbol{x}) = \frac{Eh(\boldsymbol{x})^3}{12\,(1-\nu^2)} \tag{72}$$

Substituting Eqs. (60)–(62) with the spatially-varying flexural rigidity $D(x)$ into Eq. (64) gives the following partial differential equation for the deflection w_b:

$$\begin{aligned} &D\nabla_x^4 w_b + 2\frac{\partial D}{\partial x}\frac{\partial}{\partial x}\left(\nabla_x^2 w_b\right) + 2\frac{\partial D}{\partial y}\frac{\partial}{\partial y}\left(\nabla_x^2 w_b\right) + \nabla_x^2 D\left(\nabla_x^2 w_b\right) \\ &-(1-\nu)\left(\frac{\partial^2 D}{\partial x^2}\frac{\partial^2 w_b}{\partial y^2} - 2\frac{\partial^2 D}{\partial x \partial y}\frac{\partial^2 w_b}{\partial x \partial y} + \frac{\partial^2 D}{\partial y^2}\frac{\partial^2 w_b}{\partial x^2}\right) + \rho_{\mathrm{b}} g w_b = q_b \end{aligned} \tag{73}$$

In this case, Eq. (72) is solved using numerical methods instead of Green's functions.

1.9.4 Time-dependent bedrock response

The actual rate of change in bedrock elevation is given by a simple relaxation scheme:

$$\frac{\partial b}{\partial t} = -\frac{1}{\tau_w}\left(b - b^{\mathrm{eq}} + w_b\right)\,, \tag{74}$$

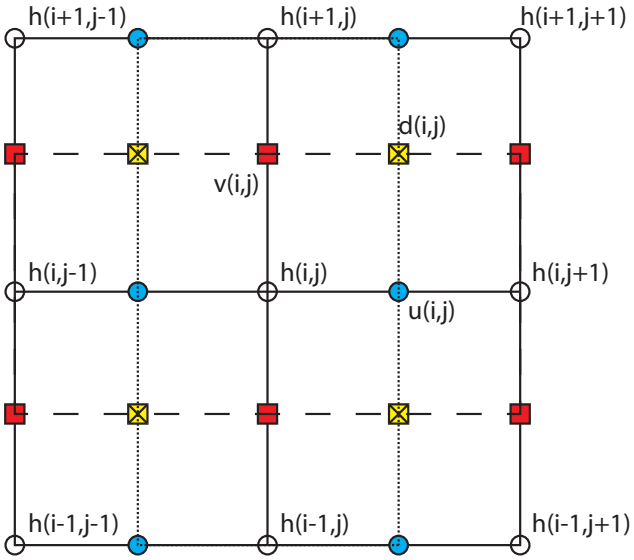

Figure 2: Staggered grids used in the model: the basic grid is the ice-thickness grid (shown in open circles). u and v velocities for the ice shelves (and ice streams) are calculated on two different staggered Arakawa C grids (filled circles and squares, respectively). Diffusion coefficients d in the ice-sheet equation are solved on an Arakawa B grid (crossed squares).

where b is the actual bedrock elevation, b^{eq} is the elevation in equilibrium (taken from modern observed fields), and $\tau_w = 3000$ year [Pollard and DeConto, 2012a]. Also here, we introduced spatially-varying values for τ_w, based on viscosity variations of the upper astenosphere (Coulon et al., in prep).

1.9.5 Geoid changes

Mass changes and redistribution of mass at the surface of the Earth results in changes of the geoid height, hence differences in local sea level that may affect the exact position of the grounding determined from hydrostatic equilibrium. For a unit point mass, the perturbation in the geoid, apart from the deformation of the Earth, due to the point mass is

$$N(\theta) = \frac{a}{M_e}\left(\frac{1}{2\sin(\theta/2)}\right) \tag{75}$$

where θ is the co-latitude of the load point. The angle θ represents the internal angle between the point mass and a given distance along the surface of the Earth with the Earth's centre. This function is then convoluted across the whole domain. Note that only the immediate change in ice volume in geoid height is considered, without taking into account the contribution of changes in the Earth's crust due to mass changes. this is because the geoid change is immediate, while isostatic changes are generally active on longer time scales. Furthermore, Earth rotational effects are neglected. The result influences the position of the grounding line and may retard grounding line retreat due to mass loss of ice sheets.

1.10 Numerical grid and solution

The ice sheet-shelf model uses a finite-difference staggered grid, where horizontal velocities (u, v) are calculated on two separate staggered Arakawa C-grids, as is usual for vector fields [Rommelaere and Ritz, 1996], while diffusion coefficients for the ice-sheet equation d are calculated on an Arakawa B-grid, staggered in both x and y direction, since these are scalar quantities (Fig. 2). The f.ETISh model uses no vertical coordinate, except for the temperature field calculation. Here, the scaled vertical coordinate system consists of 11 irregularly-spaced layers, with a minimum layer thickness of $\Delta\zeta = 0.015$ at the bottom. This way, the number of vertical layers can be greatly reduced, as most of the variability of the vertical temperature profile is situated close to the bed.

The SSA velocity field Eqs. (3–4) is solved as a sparse linear system where both u and v component are solved as once in one matrix $\mathbf{A}$ with size $(2 \times N_x \times N_y)$ by $(2 \times N_x \times N_y)$:

$$\mathbf{A} \cdot \mathbf{u} = \mathbf{b} \tag{76}$$

where N_x, N_y are the number of grid points in the x, y direction, respectively. In order to improve both stability and convergence, u and v velocities are interleaved [Quiquet et al., 2018], so that $\mathbf{u}$ alternates between u and v values for each grid point in the solution matrix.

A similar solution approach is taken for solving the continuity equation for ice thickness [Payne and Dongelmans, 1997], which was favoured over an Alternating Direct Implicit scheme used in several ice-sheet models [Huybrechts, 1992, Pollard and DeConto, 2012a]. To furthermore increase computational stability, upstream differences are employed for SSA velocity gradients in Eq. (8) in combination with an over-implicit Crank-Nicholson scheme [Hindmarsh, 2001, Pattyn, 2006]. This allows for the use of larger time steps than nominally would be the case. The Crank-Nicholson scheme is written, as

$$\frac{H_{t+1} - H_t}{\Delta t} = (1 - \omega)\frac{\partial H}{\partial t}|_t + \omega\frac{\partial H}{\partial t}|_{t+1} \tag{77}$$

where $\partial H/\partial t$ is defined in Eq. (8) and Eq. (10), and where $\omega = 2.5$ for an over-implicit scheme (1 for implicit; 0 for explicit).

For further stability, adaptive time stepping was introduced in a simple way by halving the time step whenever $\partial H/\partial t$ becomes too large. This step involves the solution of the ice thickness equation twice for the halve time step.

The f.ETISh model is implemented in MATLAB®. It takes advantage of inherent matrix computation to optimize the model in terms of calculation time, through omission of all *for*-loops (with exception of the time loop). The bulk of computational time is devoted to the solution of the sparse matrix systems, which are natively optimized in MATLAB® using multi-threading. A preconditioned conjugate gradient method is used for solving the ice sheet/ice shelf continuity equation. The velocity field in the hybrid model is solved using a stabilized bi-conjugate gradients method, which is also preconditioned and further initialized by the velocity field solution from the previous time step. Both numerical solvers are iterative and the preconditioning limits the number of iterations to reach convergence. They are considerably faster compared to the direct solution.

The f.ETISh model is compared to other ice sheet models via a series of benchmarks, such as the EISMINT-I benchmark for isothermal ice-sheet models [Huybrechts et al., 1996, Section 3.1], the EISMINT-II benchmark for thermomechanically-coupled ice sheet models [Payne et al., 2000, Section 3.2], and the MISMIP experiments for marine ice-sheet models

[Pattyn et al., 2012, Section 3.3]. Results show that the f.ETISh model is in close agreement with all of the benchmark experiments.

2 Input, climate forcing and initialization

2.1 Input data sets

For modelling the Antarctic ice sheet, the bedrock topography is either based on BedMachine Antarctica [Morlighem et al., 2019] or alternatively Bedmap2 [Fretwell et al., 2013], from which ice thickness, present-day surface topography and grounding-line position are derived. The data are also used to calculate the standard deviation of the bedrock topography σ_b. Since BedMachine provides a dataset at a high spatial resolution of 400 m, interpolation of data on a coarser grid requires a certain amount of smoothing. Best results are obtained by taking for ice thickness and bedrock elevation the mean value within a square representing the size of the final grid cell. After this smoothing, ice thickness and/or bedrock elevation is corrected to guarantee that grounded ice remains grounded and floating ice remains floated. In order to make sure that the grounding line cannot expend to the edge of the computational domain, bathymetry/bed topography is kept at -4000 m for two grid cells at the domain boundaries.

Surface mass balance and temperatures are obtained from Van Wessem et al. [2014], based on the output of the regional atmospheric climate model RACMO2 for the period 1979–2011 and evaluated using 3234 *in situ* mass balance observations and ice-balance velocities. For geothermal heat flux we employ either a recent update of Fox-Maule et al. [2005] due to Purucker [2013], based on low-resolution magnetic observations acquired by the CHAMP satellite between 2000 and 2010, the seismic-based heat flow dataset due to Shapiro and Ritzwoller [2004] or the more recent seismic-based dataset due to Wiens et al. (in prep.).

2.2 Atmospheric and ocean forcing

Atmospheric forcing is applied in a parametrized way, based on the observed fields of precipitation (accumulation rate) and surface temperature. For a change in background (forcing) temperature ΔT, corresponding fields of precipitation P and atmospheric temperature T_s are defined by [Huybrechts et al., 1998, Pollard and DeConto, 2012a]

$$T_s = T_s^{\rm obs} - \gamma(h_s - h_s^{\rm obs}) + \Delta T\,, \tag{78}$$

$$P = \dot{a}^{\rm obs} \times 2^{(T_s - T_s^{\rm obs})/\delta T}\,, \text{or} \tag{79}$$

$$P = \dot{a}^{\rm obs} \times (1 + 0.053(T_s - T_s^{\rm obs})) \tag{80}$$

where γ = 0.008°C m^{-1} is the lapse rate and δT is 10°C [Pollard and DeConto, 2012a]. The subscript 'obs' in Eq. (77) and Eq. (78) refers to the present-day observed value. Any forcing (increase) in background then leads to an overall increase in surface temperature corrected for elevation changes according to the environmental lapse rate γ. The second parametrization of P is due to Golledge et al. [2015], based on an analysis of CMIP5 models [Frieler et al., 2015]. This leads to a smaller accumulation increase over the interior of ice sheets (and Antarctica in particular) with an increase in background temperature. The parametrizations of T_s and P can easily be replaced by values that stem from GCMs, with appropriate corrections for surface elevation [e.g., de Boer et al., 2015].

Surface melt is parametrized using a positive degree-day model [Huybrechts and de Wolde, 1999]. The total amount of positive degree days (PDD) is obtained as

$$\mathrm{PDD} = \frac{1}{\sigma\sqrt{2\pi}} \int_0^A \left[\int_0^{\overline{T}_s+2.5\sigma} T_s \exp\left(-\frac{\left(T_s - \overline{T}_s\right)^2}{2\sigma^2} \right) \mathrm{d}T_s \right] \mathrm{d}t \,, \tag{81}$$

where σ is taken as 5°C [Reeh, 1989] and $\overline{T}_s$ is the mean annual surface temperature. For numerical efficiency, the expected positive degree function due to Janssens and Huybrechts [2000] is implemented in f.ETISh, which fits an exponential function to Eq. (80). The annual number of positive degree days represents a melt potential, used to melt snow and (superimposed) ice. This is determined by applying a seasonal cycle to the atmospheric temperatures with a double amplitude of 20°C, linearly increasing to 30°C at an elevation of 3000 m, and kept at 30°C at higher elevations [Pollard and DeConto, 2012a]. The PDD melt potential is used to melt snow and (superimposed) ice with degree-day factors of s_f=0.003 and i_f=0.008 m per degree day of ice equivalent, respectively [Huybrechts and de Wolde, 1999]. The liquid water produced by the model (meltwater and rain) will first refreeze in the snowpack and produce superimposed ice. The amount of refreezing depends on the cold content of the upper ice sheet layers, which puts an upper limit on the production of superimposed ice [Huybrechts and de Wolde, 1999], i.e.,

$$R_{fd} = \max\left[\frac{-r_f T_s K}{\kappa \rho_i L}, 0 \right] , \tag{82}$$

where r_f = 2 m. The maximum amount of of superimposed ice is equivalent to the latent heat released to raise the temperature of the uppermost 2 m of the ice sheet surface from the mean annual surface temperature to the melting point [Huybrechts and de Wolde, 1999]. Once this upper limit is reached, any additional snowmelt and/or rainfall is assumed to run off. The amount of PDD available after percolation and refreezing is determined by

$$\mathrm{PDD}_r = \max\left[\mathrm{PDD} - \frac{E_{sm}}{s_f}, 0 \right] , \tag{83}$$

where,

$$E_{sm} = \min\left[P, s_f \times \mathrm{PDD} \right] . \tag{84}$$

The total surface melt rate S then becomes

$$S = i_f \times \mathrm{PDD}_r + \max\left[E_{sm} - R_{fd}, 0 \right] \tag{85}$$

Finally, the surface mass balance is then the sum of the different components, i.e., $\dot{a} = P - S$.

Melting underneath the floating ice shelves is often based on parametrizations that relate sub-shelf melting to ocean temperature and ice-shelf depth [Beckmann and Goosse, 2003, Holland et al., 2008], either in a linear or a quadratic way [Martin et al., 2011, Pollard and DeConto, 2012a, de Boer et al., 2015, DeConto and Pollard, 2016]. This leads to higher melt rates close to the grounding line, as the ice-shelf bottom is the lowest, i.e.,

$$M = \gamma_T \frac{\rho_s c_{po}}{L \rho_i} |T_{oc} - T_{fo}| (T_{oc} - T_{fo}) \,, \tag{86}$$

and where M is the sub-ice-shelf basal melt rate, c_{po} is the specific heat capacity of the ocean, γ_T is the thermal exchange velocity, L is the latent heat of fusion, T_{oc} is the temperature of the ocean underneath the ice shelf, and T_{fo} is the freezing temperature defined by Beckmann and Goosse [2003] as:

$$T_{fo} = \lambda_1 S_o + \lambda_2 + \lambda_3 h_b \,, \tag{87}$$

where S_o is a value for the salinity of the ocean waters. We employ measurements of ocean temperature and salinity defined for each drainage basin of the Antarctic ice sheet based on Schmidtko et al. [2014] (see below for more details).

Alternatively, a linear version of Eq. (85) can be employed, which will also require a different value for γ_T. The latter is in general used as a general tuning parameter for the melt function [Favier et al., 2019].

2.2.1 The PICO ocean-coupler model

Alternatively to the sub-shelf melt parametrization, an ocean-coupling model has been implemented based on PICO (Potsdam Ice-shelf Cavity mOdel; Reese et al. [2018a]). PICO is developed from the ocean box model of Olbers and Hellmer [2010], which is designed to capture the basic overturning circulation in ice shelf cavities which is driven by the "ice pump" mechanism: melting at the ice shelf base near the grounding line reduces salinity and the ambient ocean water becomes buoyant, rising along the ice shelf base towards the calving front. Since the ocean temperatures on the Antarctic continental shelf are generally close to the local freezing point, density variations are primarily controlled by salinity changes. Melting at the ice-shelf base hence reduces the density of ambient water masses, resulting in a haline-driven circulation. Buoyant water rising along the shelf base draws in ocean water at depth, which flows across the continental shelf towards the deep grounding lines of the ice shelves. The warmer these water masses are, the stronger is the melting-induced ice pump. The Olbers and Hellmer [2010] box model describes the relevant physical processes and captures this vertical overturning circulation by defining consecutive boxes following the flow within the ice shelf cavity.

The strength of the overturning flux q is determined from the density difference between the incoming water masses on the continental shelf and the buoyant water masses near the deep grounding lines of the ice shelf. As PICO is implemented in an ice sheet model with characteristic time scales much slower than typical response times of the ocean, we assume steady-state ocean conditions and hence reduce the complexity of the governing equations of the Olbers and Hellmer [2010] model. We assume stable vertical stratification, which motivates neglecting the diffusive heat and salt transport between boxes. Without diffusive transport between the boxes, some of the original ocean boxes from Olbers and Hellmer [2010] become passive and can be incorporated into the governing equations of the set of boxes used in PICO. We explicitly model a single open ocean box which provides the boundary conditions for the boxes adjacent to the ice shelf base following the overturning circulation, as shown in Fig. 3. In order to better resolve the complex melt patterns, PICO adapts the number of boxes based on the evolving geometry of the ice shelf. These simplifying assumptions allow us to analytically solve the system of governing equations [Reese et al., 2018a].

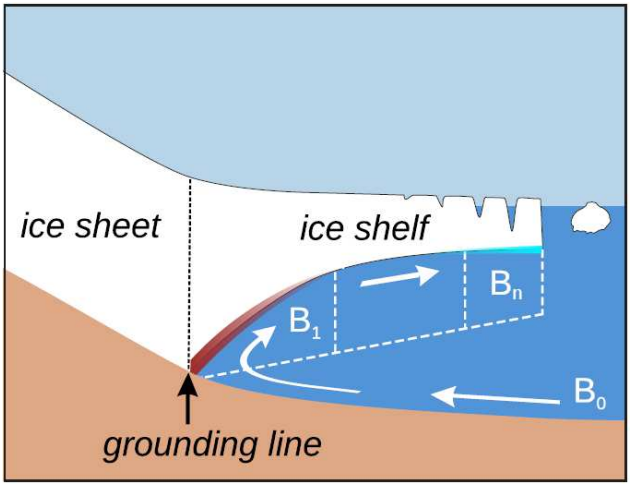

Figure 3: Schematic view of the PICO model. The model mimics the overturning circulation in ice shelf cavities: Ocean water from box B_0 enters the ice shelf cavity at the depth of the sea floor and is advected to the grounding line box B_1. Freshwater influx from melting at the ice shelf base makes the water buoyant, causing it to rise. The cavity is divided into n boxes along the ice shelf base. Generally, the highest melt rates can be found near the grounding line, with lower melt rates or refreezing towards the calving front [Reese et al., 2018a].

In general, PICO solves for the transport of heat and salt between boxes in contact with the base of the ice shelf, starting at the grounding line and ending at the ice front (boxes B_k for $k = \{1, ..., n\}$, where n is typically less than or equal to 5). After simplification and assuming steady-state conditions, the balance of heat and salt in all boxes along the base of the ice shelf can be written as

$$\begin{aligned} q\left(T_{k-1} - T_k\right) - A_k m_k \tfrac{\rho_i}{\rho_s} \tfrac{L}{c_{po}} = 0 \\ q\left(S_{k-1} - S_k\right) - A_k m_k S_k = 0 \end{aligned} \tag{88}$$

Using a simplified formulation of the three-equation melt model by Holland and Jenkins [1999], the transport equations can be solved for salinity S_k and temperature T_k in box Bk and are dependent on the local pressure, the box area A_k, and the temperature T_{k-1} and salinity S_{k-1} of the upstream box $B - k - 1$. The strength of the overturning circulation, q, is calculated once per time step in box B1 from the density difference between the far-field and grounding line water masses:

$$q = C\left(\rho_0 - \rho_1\right) \tag{89}$$

The sub-shelf melt rate in each of the boxes is then determined as

$$m_k(x, y) = -\gamma_T \frac{\rho_s c_{po}}{L \rho_i} \left(\lambda_1 S_k(x, y) + \lambda_2 + \lambda_3 h_b(x, y) - T_k(x, y)\right) \tag{90}$$

where the subscript k refers to the values determined for each box within each ice shelf. Input data for the PICO model are present-day observed ocean temperature and salinity at depth on the continental shelf in front of contemporary ice shelves [Schmidtko et al., 2014]. For the ice sheet to 'feel' these data, the ice sheet is divided up in different drainage basins based on the limits provided by NASA (Zwally, H. Jay, Mario B. Giovinetto, Matthew

A. Beckley, and Jack L. Saba, 2012, Antarctic and Greenland Drainage Systems, GSFC Cryospheric Sciences Laboratory). Mean values of ocean temperature and salinity in front of the ice shelves are then assigned to each basin, so that with retreat of the grounding line, individual ice shelves remain connected to the far-field ocean. These datasets are not calculated within f.ETISh, but should be provided. The PICO model automatically identifies individual ice shelves, divides them up in boxes and calculates ocean properties for each box. Sub-shelf melt rates within each box are determined using the local pressure of the overlying ice [Reese et al., 2018a].

2.2.2 PICOP and plume model

The plume model is a basal melt rate parametrization based on the theory of buoyant meltwater plumes that travel upward along the base of the ice shelf from the grounding line to the location where the plume loses buoyancy. The two-dimensional formulation from Lazeroms et al. [2018] is adapted from the one-dimensional plume model developed by Jenkins [1991] for a plume travelling in direction X in an ocean with ambient temperature T_a and salinity S_a, either provided by PICO (which leads to the PICOP model) or from far-field ocean measurements (which is equivalent to the plume model). The method due to Pelle et al. [2019] has been employed. We begin by defining the grounding line depth, z_{gl}, over the entire ice shelf, as it is necessary to determine where individual plumes originate in order to employ this parametrization. As a first approximation, we solve an advection equation:

$$\begin{cases} v \cdot \nabla z_{\mathrm{gl}} + \epsilon \Delta z_{\mathrm{gl}} = 0 & \text{in } \Omega \\ z_{\mathrm{gl}} = z_{\mathrm{gl0}} & \text{on } \Gamma \end{cases} \tag{91}$$

where z_{gl0} is the grounding line height defined at the grounding line Γ, Ω is the ice shelf, and as a first approximation, v is the modelled, depth-averaged ice velocity. Note that ϵ is a small diffusion coefficient introduced to minimize noise and to provide numerical stability.

Once z_{gl} is defined, we continue by computing both the characteristic freezing point $T_{f,gl}$ and the effective heat exchange coefficient Γ_{TS} as follows:

$$T_{\mathrm{f,gl}} = \lambda_1 S_{\mathrm{a}} + \lambda_2 + \lambda_3 z_{\mathrm{gl}} \tag{92}$$

$$\Gamma_{TS} = \Gamma_T \left(\gamma_1 + \gamma_2 \frac{T_{\mathrm{a}} - T_{\mathrm{f,gl}}}{\lambda_3} \times \frac{E_0 \sin\alpha}{C_{\mathrm{d}}^{1/2} \Gamma_{TS_0} + E_0 \sin\alpha} \right) \tag{93}$$

A geometric scaling factor $g(\alpha)$ and length scale l are defined in order to give the plume model the proper geometry dependence and scaling according to the distance travelled along the plume path. The scaling factor and length scale are computed as follows:

$$g(\alpha) = \left(\frac{\sin\alpha}{C_{\mathrm{d}} + E_0 \sin\alpha} \right)^{1/2} \left(\frac{C_{\mathrm{d}}^{1/2} \Gamma_{TS}}{C_{\mathrm{d}}^{1/2} \Gamma_{TS} + E_0 \sin\alpha} \right)^{1/2} \left(\frac{E_0 \sin\alpha}{C_{\mathrm{d}}^{1/2} \Gamma_{TS} + E_0 \sin\alpha} \right) \tag{94}$$

$$\mu = \frac{T_{\mathrm{a}} - T_{\mathrm{f,gl}}}{\lambda_3} \times \frac{x_0 C_{\mathrm{d}}^{1/2} \Gamma_{TS} + E_0 \sin\alpha}{x_0 \left(C_{\mathrm{d}}^{1/2} \Gamma_{TS} + E_0 \sin\alpha \right)} \tag{95}$$

The dimensionless scale factor x_0 used in the second term of l defines the transition point between melting and refreezing and is constant for all model results. For a complete explanation of the individual terms that make up these two factors, see Sect. 2.2 of Lazeroms et al. [2018]. The length scale is then used in the computation of the dimensionless coordinate, $\hat{X}$:

$$\hat{X} = \frac{z_\mathrm{b} - z_\mathrm{gl}}{l} \tag{96}$$

In order to ensure valid values of $\hat{X}$, we set a lower bound for the ambient ocean temperature: $T_\mathrm{a} \geq \lambda_1 S_\mathrm{a} + \lambda_2$. The melt rate $\dot{m}$ is then calculated as

$$\dot{m} = \hat{M}(\hat{X}) \times M \tag{97}$$

where $\hat{M}(\hat{X})$ is a dimensionless melt curve defined in Lazeroms et al. [2018] and M is defined as

$$M = M_0 \times g(\alpha) \times \left(T_\mathrm{a} - T_\mathrm{f}\left(S_\mathrm{a}, z_\mathrm{gl}\right)\right)^2 \tag{98}$$

2.2.3 Non-local melt-rate parametrization (ISMIP6)

Climate model projections have previously been used to compute ice-shelf basal melt rates in ice-sheet models, but the strategies employed –e.g. ocean input, parametrization, calibration technique, and corrections– have varied widely and are often ad-hoc. Jourdain et al. [2019] propose a methodology for the calculation of circum-Antarctic basal melt rates for floating ice, based on climate models, that is suitable for ISMIP6, the Ice Sheet Model Intercomparison Project for CMIP6 (6th Coupled Model Intercomparison Project). The past and future evolution of ocean temperature and salinity is derived from a climate model by estimating anomalies with respect to the modern day, which are added to an present-day climatology constructed from existing observational datasets. Temperature and salinity are extrapolated to any position potentially occupied by a simulated ice shelf. A simple formulation is proposed for a basal-melt parametrization in ISMIP6, constrained by the observed temperature climatology, with a quadratic dependency on either the non-local or local thermal forcing. Two calibration methods are proposed: (i) based on the mean Antarctic melt rate (MeanAnt) and (ii) based on melt rates near Pine Island's deep grounding line (PIGL).

Melt rates in the common ISMIP6 experiments are derived using a slightly modified version of the non-local quadratic parametrization proposed by Favier et al. [2019]. The parametrization is explicitly defined over regional sectors, rather than for a single ice shelf, and it includes a temperature correction:

$$m(x,y) = \gamma_0 \times \left(\frac{\rho_{sw} c_{pw}}{\rho_i L_f}\right)^2 \times \left(TF\left(x, y, z_\mathrm{draft}\right) + \delta T_\mathrm{sector}\right) \times \left|\langle TF\rangle_{\mathrm{draft}\in\mathrm{sector}} + \delta T_\mathrm{sector}\right| \tag{99}$$

where $TF\left(x, y, z_\mathrm{draft}\right)$ is the thermal forcing at the ice-ocean interface, and $\langle TF\rangle_{\mathrm{draft}\,\in\,\mathrm{sector}}$ the thermal forcing averaged over all the ice-shelves of an entire sector. The uniform coefficient γ_0, with units of velocity, is somewhat similar to the exchange velocity commonly used to calculate ice-ocean heat fluxes. The temperature correction T_sector for each sector is needed to reproduce observation-based melt rates (at the scale of a sector) from observation-based thermal forcing.

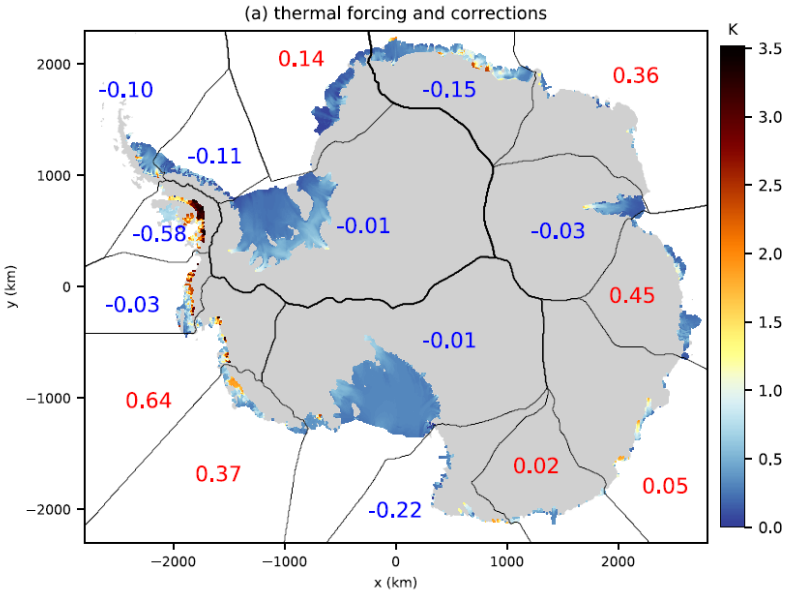

Figure 4: Thermal forcing (shaded) and its corrections (blue/red numbers indicating negative/positive δT) applied to each sector for non-local-MeanAnt with a slope dependency [Figure from Jourdain et al., 2019].

2.3 Initialization

Model initialization to the modern Antarctic ice sheet geometry is based on the method by Pollard and DeConto [2012b] by optimizing basal sliding coefficients in an iterative fashion. It is a two-step approach, where first the model is run forward in time using SIA (preferably) without ice shelves or grounding line flux condition, starting from modern observed bed and ice surface elevations and driven by the observed climatology (surface mass balance and temperature). Full thermomechanical coupling and temperature evolution, isostatic bedrock adjustment, calving and sub-grid ice-shelf pinning is equally considered. Basal sliding coefficients $A_b(x, y)$ are initialized with a constant value ($A_b = 3 \times 10^{-9}$ m a^{-1} Pa^{-2}) for the grounded ice sheet. This is a nominal value for $m = 2$, but a scaling is introduced so that for different exponents of m, the same values and their limits remain valid.

At intervals of Δt_{inv} years, at each grounded ice grid point, the local basal sliding coefficients $A_b(x, y)$ in Eq. (15) are adjusted by a multiplicative factor [Pollard and DeConto, 2012b]:

$$A_b^\star = A_b \times 10^{\Delta z}\,, \tag{100}$$

for $\Delta z \leq \Delta z^0$. Δz is defined as

$$\Delta z = \max\left[-1.5, \min\left(1.5, \frac{h_s - h_s^{\text{obs}}}{h_s^{\text{inv}}}\right)\right]\,, \tag{101}$$

and Δz^0 is its value from the previous iteration step, h_s^{obs} is the observed ice surface elevation and h_s^{inv} is a scaling constant. This means that the optimization of a local point is halted whenever its change Δz is larger than the one of the previous iteration step [Bernales et al., 2017]. During the inversion procedure, basal temperature is still allowed to influence

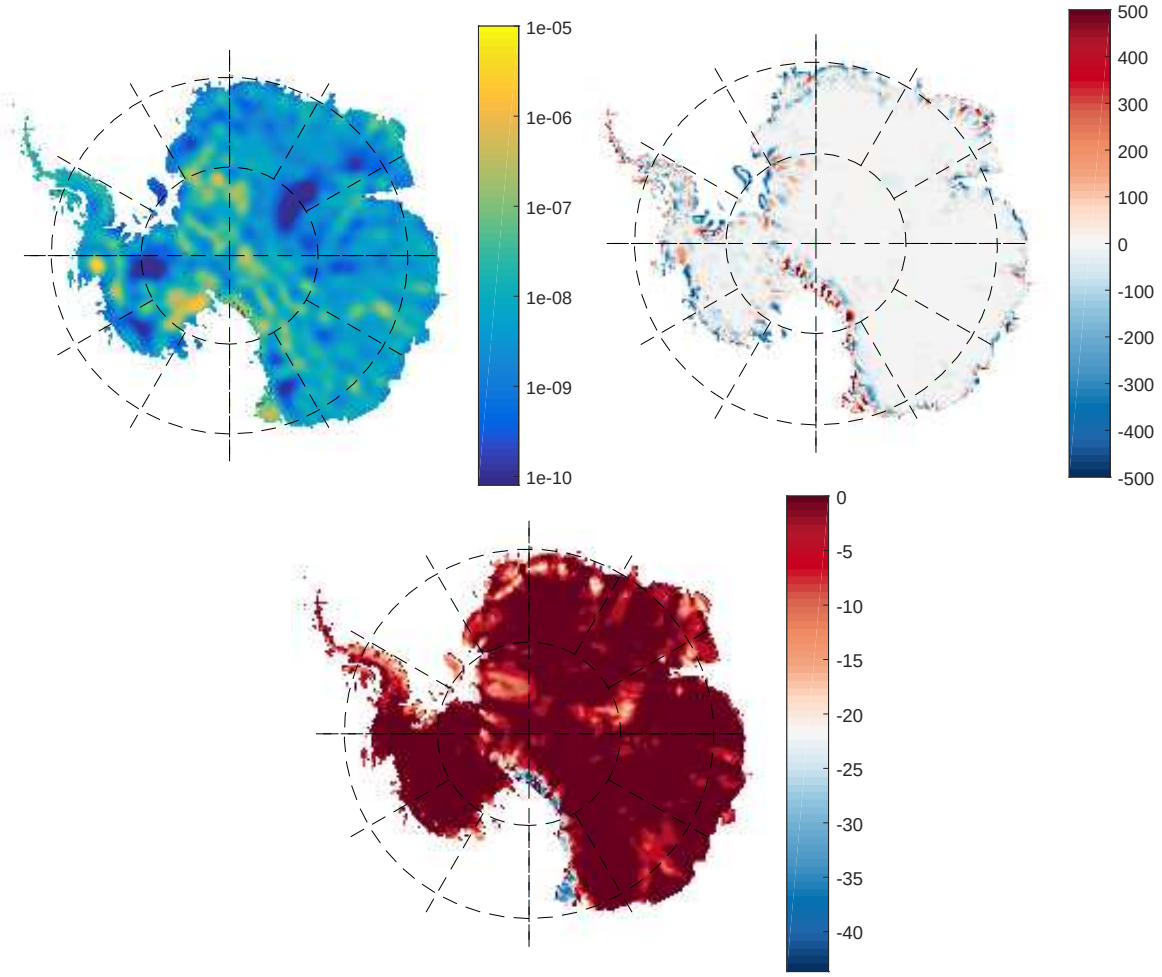

Figure 5: Top left: optimized basal sliding coefficients $A_b^\star(x, y)$ after 80,000 years of integration; Top right: difference between optimized and observed surface elevation for a Weertman sliding law; Bottom: basal temperature relative to pressure melting point. **Update figure**

sliding. Adjusted $A_b^\star(x, y)$ values are limited by defined limit values that take into account dependency on sliding law power coefficients m in Eq. (12). Values for $A_b^\star$ are only updated when $r > 0$ in Eq. (15), so that they are kept unchanged for ice temperatures below a certain limit.

In addition to Pollard and DeConto [2012b] we also introduce a regularization term that essentially smooths high-frequency noise in the basal sliding coefficients by using a Gaussian smoothing filter. The filter is only applied across the grounded domain with the exception of grid cells where the bedrock elevation is higher than 1000 m above present-day sea level and the roughness of the bedrock is above the 99% percentile of the total roughness of the domain. Contrary to Pollard and DeConto [2012b], the revised algorithm only requires about 50 000 years of forward integration to obtain an optimized friction field.

The second step consists of running the model with ice shelves (and groundin line flux condition if pertinent) using the HySSA velocity calculation. In addition to constraining the basal slip coefficients, melet/accretion rates under the floating ice shelves are updated using the method of Bernales et al. [2017].

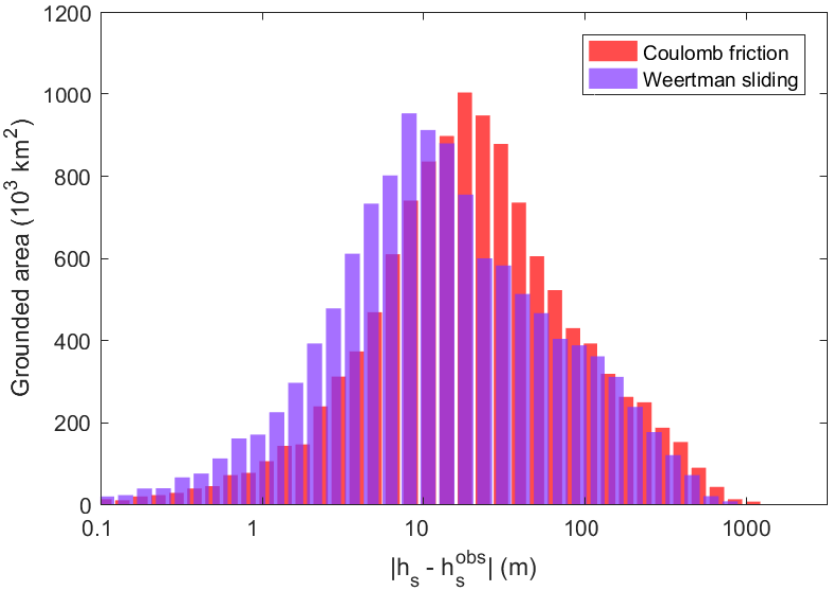

Figure 6: Difference between observed and optimized ice thickness in Fig. 5. **Update figure**

Optimized basal sliding coefficients (Fig. 5) for the Antarctic ice sheet on a spatial resolution of 25 km were obtained after a forward integration of 50,000 years with $h_{\mathrm{inv}} = 500$ and $\Delta t_{\mathrm{inv}} = 200$ year. This results in a small difference (within 10 m) between the observed and the steady-state modelled topographic surface of the interior ice sheet (Fig. 6), which is an improvement compared to Pattyn [2017]. The highest sliding coefficients are found in the marginal areas, especially in the Siple Coast sector, as well as under Pine Island and Thwaites Glaciers. Higher values are also encountered in the centre of the ice sheet, which is also obvious in other studies [Pollard and DeConto, 2012b, Bernales et al., 2016]. These areas also show larger misfits (Fig. 5) and may be attributed to the poor knowledge of bedrock topography, so that uncertainties are translated into a basal friction anomaly. The obtained patterns are in general agreement with the results from Pollard and DeConto [2012a,b], i.e., the largest errors are found around the major mountain ranges (e.g., Transantarctic Mountains), since outlet glaciers protruding through these mountain ranges are not well represented on coarser grid cells. However, this fit has been improved by including bedrock variability in determining basal sliding coefficients A'_b in Eq. (15) to allow for basal sliding of smaller outlet glaciers across mountain ranges.

The basal temperature fields (Fig. 5) for both optimizations are quite similar and in general agreement with basal temperature fields from other Antarctic modelling studies. Differences can easily be attributed to the use of geothermal heat flow datasets, which has the largest impact on basal temperature distribution [Pattyn, 2010].

2.4 Model validation

Modelled velocities form an independent check of the model performance, since the optimized basal sliding coefficients are obtained solely from the observed surface topography. The modelled flow field of the Antarctic ice sheet (Fig. 7) compares well to observations of

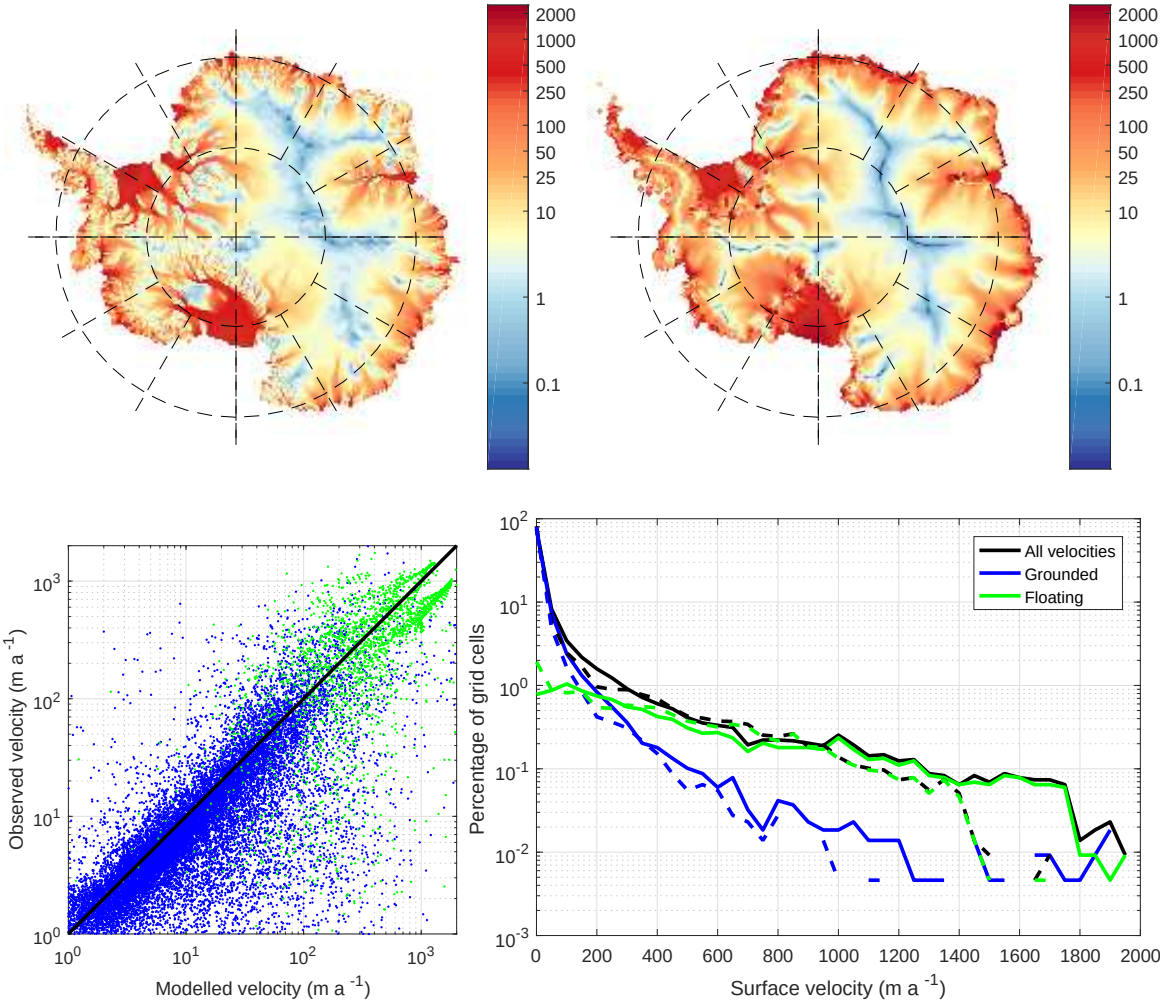

Figure 7: Observed (top left) and modelled (top right) ice sheet surface velocities after optimization; point-by-point scatterplot of modelled and observed [Rignot et al., 2011] ice sheet (blue) and ice shelf (green) velocities (bottom left); histogram of velocity distribution of observed (dashed) and modelled (solid) velocities. Each of the bins contains a velocity range of 50 m a^{-1} (bottom right). **Update figure**

surface velocities due to Rignot et al. [2011], such as the delineation of the different drainage basins and major ice streams discharging into the ice shelves. Some disagreement is found on glaciers discharging through the Transantarctic Mountains in the Ross ice shelf as well as glaciers near the Ellsworth Mountains discharging in the Ronne ice shelf. Those mismatches can be traced back to the difficulty in resolving those feature during the initialization process.

A direct comparison between the present-day velocity field [Rignot et al., 2011] and modelled velocities is shown in Fig. 7. The scatterplot shows a qualitatively good one-to-one fit for both the grounded ice sheet and the floating ice shelves. Quantitative error analysis shows a mean misfit of 20 m a^{-1} with a standard deviation of 265 m a^{-1} for the grounded ice flow, and a mean misfit of 158 m a^{-1} with a standard deviation of 786 m a^{-1} for the floating ice shelves. The histogram comparison demonstrates a good overall fit of observed and modelled velocity magnitudes and the result is in line with other model studies [e.g., Martin et al., 2011].

Exp	Variable	Benchmark	f.ETISh
FM	h_{summit}	3419.90±1.70	3421.82
	q_{midpoint}	789.95±1.83	790.43
	T^b_{summit}	-8.84±1.04	-7.54
MM	h_{summit}	2997.5±7.4	2986.41
	q_{midpoint}	999.24±17.91	994.49
	T^b_{summit}	-13.43±0.75	-11.81

Table 1: Comparison of f.ETISh with the EISMINT-I fixed (FM) and moving margin (MM) experiment benchmark based on an ensemble of 2–3 models [Huybrechts et al., 1996] for the steady-state experiment.

3 Verification experiments

3.1 EISMINT-I benchmark

3.1.1 Fixed-margin experiment

The EISMINT-I benchmark is the first series of ice-sheet model intercomparisons aiming at benchmarking large-scale ice sheet models under idealized and controlled conditions [Huybrechts et al., 1996]. The first (fixed margin) experiment considers a square grid of 1500 × 1500 km with a flat bed at zero elevation. Grid spacing is taken as $\Delta = 50$ km leading to 31 × 31 regularly-spaced grid points. Starting from zero ice thickness, the model is forced with a constant surface mass balance of 0.3 m a^{-1} and surface temperature according to $T_s = 239$ K $+(8 \times 10^{-8}) d^3_{\text{summit}}$, where d_{summit} is defined as $\max(|x - x_{\text{summit}}|, |y - y_{\text{summit}}|)$, expressed in km. Further boundary conditions for the model are zero ice thickness at the edges of the domain and a constant geothermal heat flux of $G = 0.042$ W m^{-2}. The ice temperature is not coupled to the ice flow field and a constant value for the flow parameter of 10^{16} Pa^{-n} a^{-1} is considered.

The f.ETISh model is a 3d Type I model according to the classification scheme in EISMINT-I, i.e., diffusion coefficients for the grounded ice sheet are calculated on a staggered Arakawa-B grid. Table 1 lists the comparison with data from other 3d Type I models. Both ice thickness and flux compare very well within error bounds of the sample range (limited to only 2–3 models in the EISMINT-I benchmark, unfortunately). Also the basal temperature at the divide and along the profile is within the limits given by the EISMINT-I benchmark. Differences can be attributed to the use of the shape functions for the velocity field as well as to the use of a staggered grid for the temperature field, whereby the temperature at the divide and along the profile are interpolated values along the central line.

3.1.2 Moving margin experiment

The moving-margin experiment includes ice ablation, hence the presence of an equilibrium line on the ice sheet. This is obtained by defining the climatic conditions by $\dot{a} = \min\{0.5, h_s(R_{\text{el}} - d_{\text{summit}})\}$ and $T_s = 270 - 0.01h$, where d_{summit} is here defined as the radial distance from the centre (in km), and s and R_{el} are 10^{-2} m a^{-1} km^{-1} and 450 km, respectively [Huybrechts et al., 1996]. The steady-state ice sheet according to this experiment does not reach the edge of the domain, but is circular in shape. Note that, contrary to

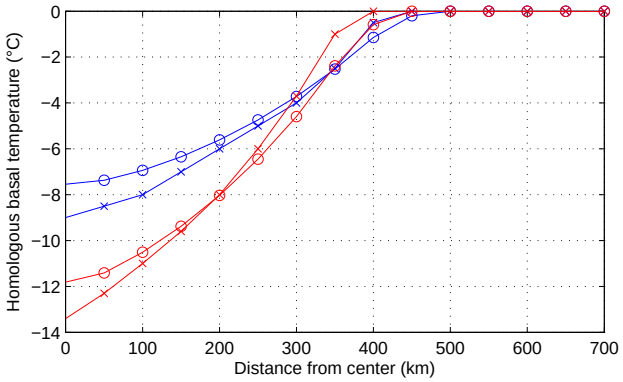

Figure 8: Homologous basal temperatures along the central line according to the EISMINT-I experiment calculated with f.ETISh (circles) and according to the EISMINT-I benchmark (crosses) for the fixed margin (blue) and moving margin (red) experiment.

the fixed margin experiment, surface temperature is a function of surface elevation and not of the geometrical characteristics of the domain. Surface mass balance, however, remains a function of the distance to the centre of the domain.

Basic characteristics of the experiment are listed in Table 1, and simulated values of ice thickness (h_{summit}) and basal temperature at the divide (T^b_{summit}), as well as ice flux between divide and margin are in good agreement with the benchmark. Also the basal temperature profile agrees well with the benchmark and differences can be attributed to the factors listed in Section 3.1.1.

3.1.3 Transient experiment

Temporal changes in ice thickness/volume and basal temperature are analysed with a forcing experiment, where the surface temperature and mass balance perturbations are defined as follows [Huybrechts et al., 1996]:

$$\Delta T = 10 \sin\left(\frac{2\pi t}{T}\right) , \tag{102}$$

$$\Delta \dot{a} = 0.2 \sin\left(\frac{2\pi t}{T}\right) \quad \text{for fixed margin} , \tag{103}$$

$$\Delta R_{\text{el}} = 100 \sin\left(\frac{2\pi t}{T}\right) \quad \text{for moving margin} . \tag{104}$$

The model run starts from the steady-state ice sheet obtained in the previous section and the forcing is applied for a period of 200 ka, with a periodicity of $T = 20$ and 40 ka, respectively. Results are depicted in Fig. 9 for the fixed margin and in Fig. 10 for the moving margin experiment. Table 2 lists the main characteristics of ice thickness and basal temperature amplitude variations, as well as ice thickness at the divide at the end of the experiment (200 ka).

All ice thickness changes (amplitude and phase) as well as the phase in temperature according to the two forcing scenarios are in close agreement with the benchmark. However, amplitude differences for the basal temperatures deviate, but the EISMINT I data sample is

Exp	Variable	Benchmark	f.ETISh
FM 20ka	h_{summit} (200 ka)	3264.8±5.6	3266.02
	Δh_{summit}	563.0±3.7	566.20
	$\Delta T^b_{\text{summit}}$	2.11±0.09	**2.67**
FM 40ka	h_{summit} (200 ka)	3341.7±3.9	3344.51
	Δh_{summit}	619.0±3.2	621.53
	$\Delta T^b_{\text{summit}}$	4.12±0.06	**2.79**
MM 20ka	h_{summit} (200 ka)	2813.5±2.0	2805.19
	Δh_{summit}	528.6±11.3	533.66
	$\Delta T^b_{\text{summit}}$	2.54±0.00	**0.95**
MM 40ka	h_{summit} (200 ka)	2872.5±6.8	2871.85
	Δh_{summit}	591.4±4.6	595.38
	$\Delta T^b_{\text{summit}}$	7.61±0.05	**6.51**

Table 2: Comparison of f.ETISh with the EISMINT-I fixed (FM) and moving margin (MM) experiment benchmark based on an ensemble of 2–3 models [Huybrechts et al., 1996] for the forcing experiments with a sinusoidal signal of 20 and 40 ka, respectively. Bold values are those outside the range given by the benchmark results.

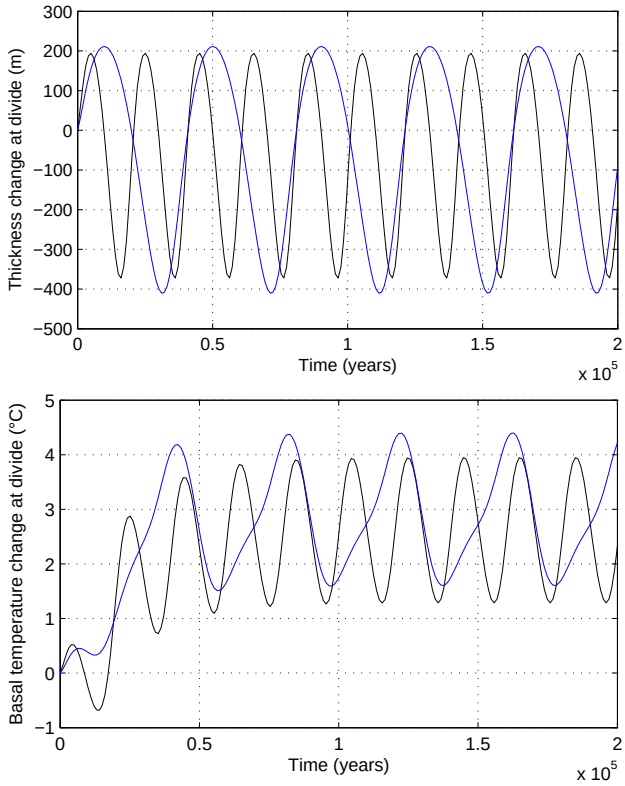

Figure 9: Ice thickness and basal temperature variations for the EISMINT-I fixed margin experiment with a 20 ka (black) and a 40 ka (blue) forcing.

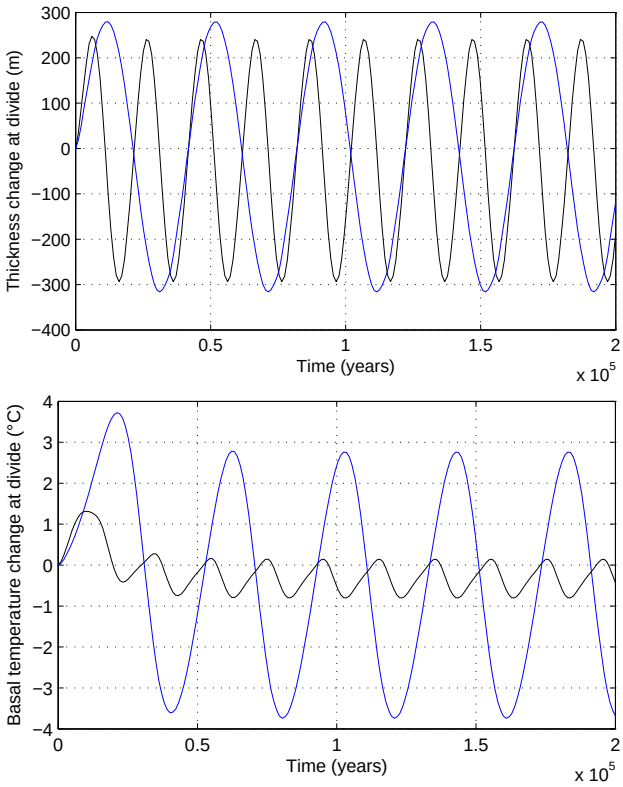

Figure 10: Ice thickness and basal temperature variations for the EISMINT-I moving margin experiment with a 20 ka (black) and a 40 ka (blue) forcing.

rather limited for comparison. The phase of the basal temperature response is in agreement with the benchmark. All other parameters are within the bounds of the benchmark (Table 2).

3.2 EISMINT-II benchmark

The EISMINT-II benchmark [Payne et al., 2000] is based on the moving margin experiment of Huybrechts et al. [1996], but includes thermomechanical coupling of the ice flow to the temperature field. Contrary to the EISMINT-I benchmark, inter-model differences are considerably larger, especially with respect to the area of the ice sheet that reaches pressure melting point at the base. The standard experiment consists of a flat bed of the same size as the EISMINT-I benchmark, but with a spatial resolution of 25 km, leading to 61 $\times$ 61 grid points. The basic experiment [A in Payne et al., 2000] runs the ice sheet in equilibrium starting from zero ice thickness on the domain and with $u_b = 0$. The climatic conditions are defined as:

$$\dot{a} = \min\left\{\dot{a}_{\max}, s\left(R_{\rm el} - d_{\rm summit}\right)\right\} \quad (105)$$

$$T_s = T_{\min} + s_T d_{\rm summit}\,, \quad (106)$$

where $d_{\rm summit}$ is defined as in the moving margin experiment as the radial distance from the centre (in km), s and $R_{\rm el}$ are taken as in the moving margin experiment (10^{-2} m a^{-1} km^{-1} and 450 km, respectively), and $\dot{a}_{\max}$, $T_{\min}$ and s_T are defined as 0.5 m a^{-1}, 238.15K, and 1.67 $\times$ 10^{-2} K km^{-1}, respectively. Contrary to the moving margin experiment, climatic conditions are independent of ice sheet surface elevation, hence the mass-balance elevation feedback is excluded.

Six further experiments were carried out, i.e., experiment B, C, D, F, G and H [in Payne et al., 2000]. They consist of a stepwise change in surface temperature, $T_{\min} = 243.15$K (B), a stepwise change in surface mass balance $\dot{a}_{\max} = 0.25$, $R_{\rm el} = 425$ km (C) and a stepwise shift in equilibrium-line altitude $R_{\rm el} = 425$ km. Experiments B, C and D start from the steady-state solution of A. Experiment F is similar to A, but starting with a value of $T_{\min} = 223.15$K (model run starting without ice). Experiment G incorporates basal slip according to a linear sliding law ($m = 1$ and $A_b = 10^{-3}$ m a^{-1} Pa^{-1}) with a similar setup as A. Finally, experiment H is similar to G, but where sliding is limited to areas that are at pressure melting at the base.

Results for experiments A–H are summarized in Table 3. The majority of parameters are within the bounds of the benchmark, but major differences are related to the basal temperature at the divide. All experiments exhibit a radial pattern in basal temperatures that are at pressure melting point for the outer part of the ice sheet, with a cold spike in the center of the ice sheet. In all experiments, our temperature spike is slightly less cold than the one given by the benchmark. However, despite this difference, the size of the basal area at pressure melting point is in accord with the benchmark. Again, the main reason for this difference is that temperatures in f.ETISh are calculated on a staggered Arakawa-B grid and not exactly at the ice divide. Despite these differences in temperature, ice volume and area coverage are totally in agreement with the benchmark mean.

The emblematic experiments F and H in Payne et al. [2000] displayed an irregular pattern in the basal temperatures of the benchmark for all participating models, leading to cold spikes reaching to the edge of the ice sheet. The pattern was shown to be model-dependent

Exp	Variable	Benchmark	f.ETISh
A	Volume (10^6 km^3)	2.128±0.145	2.133
	Area (10^6 km^2)	1.034±0.086	1.092
	Melt fraction	0.718±0.290	0.703
	H_{summit} (m)	3688.342±96.740	3605.157
	T^b_{summit} (K)	-17.545±2.929	**-11.033**
B	ΔVolume (%)	-2.589±1.002	-3.628
	ΔMelt fraction (%)	11.836±18.669	17.589
	$\Delta H_{\text{summit}}(\%)$	-4.927±1.316	-5.259
	$\Delta T^b_{\text{summit}}(K)$	4.623±0.518	4.115
C	ΔVolume (%)	-28.505±1.204	-27.739
	ΔArea (%)	-19.515±3.554	-21.002
	ΔMelt fraction (%)	-27.806±31.371	-45.160
	$\Delta H_{\text{summit}}(\%)$	-12.928±1.501	-12.764
	$\Delta T^b_{\text{summit}}(K)$	3.707±0.615	3.045
D	ΔVolume (%)	-12.085±1.236	-12.377
	ΔArea (%)	-9.489±3.260	-10.139
	ΔMelt fraction (%)	-1.613±5.745	-4.848
	$\Delta H_{\text{summit}}(\%)$	-2.181±0.532	-2.168
	$\Delta T^b_{\text{summit}}(K)$	-0.188±0.060	**-0.341**
G	Volume (10^6 km^3)	1.589±0.702	1.529
	Area (10^6 km^2)	1.032±0.071	1.088
	Melt fraction	0.352±0.530	0.319
	H_{summit} (m)	2365.206±1468.880	2220.538
	T^b_{summit} (K)	-24.016±7.681	-17.864
H	Volume (10^6 km^3)	1.900±0.461	1.807
	Area (10^6 km^2)	1.032±0.067	**1.807**
	Melt fraction	0.529±0.429	0.496
	H_{summit} (m)	3507.984±394.380	3225.787
	T^b_{summit} (K)	-17.925±2.977	**-12.664**

Table 3: Comparison of f.ETISh with the EISMINT-II experiments [Payne et al., 2000].

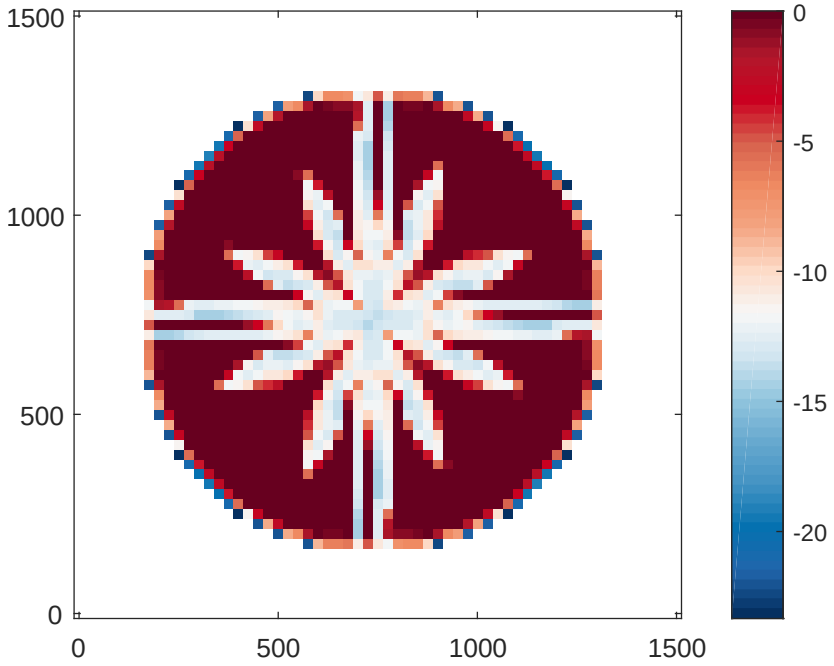

Figure 11: Predicted basal temperatures (corrected for pressure-dependence) according to EISMINT-II experiment H.

and further investigations traced its origin to an interaction between vertical advection (cooling down the base) and strain heating [Hulton and Mineter, 2000]. The pattern was found to be highly dependent on spatial grid resolution due to the lack of membrane stresses in the shallow-ice approximation [Hindmarsh, 2006, 2009]. Also f.ETISh produces a similar patterning for this particular experiment, despite the approximations in the thermomechanical coupling (using a vertically-integrated temperature) and the use of shape functions (Figure 11).

3.3 Modified MISMIP experiments

Experiments to be re-run. The capacity of an ice sheet model to cope with the marine boundary, and more specifically migration of the grounding line, is essential in Antarctic ice-sheet modelling. Since grounding-line dynamics were elucidated mathematically based on boundary layer theory [Schoof, 2007a,b, 2011], two intercomparison exercises were established. The first one tested grounding-line migration and stability on downward sloping beds and instability on retrograde slopes for flow-line models [Pattyn et al., 2012], and the second tested the effect of buttressing for two- and three-dimensional ice-sheet models [Pattyn et al., 2013]. Given that marine ice sheet instability is a crucial feedback process in marine ice sheet behaviour, we performed the flow-line experiments for a plan-view model setup. Ice shelves are included, but without exerting any buttressing strength, i.e. $\tau_{xx} = \tau_f$. The first experiment is an ice sheet on a seaward-sloping bedrock, which in plan view results in a conic bed, defined by [Pattyn et al., 2012]:

$$B = 720 - \frac{778.5}{750} d_{\text{summit}} \,, \tag{107}$$

where d_{summit} (km) is the radial distance from the centre of the domain. The second experiment consists of an overdeepened section in the bedrock profile, hence the presence of a retrograde slope, defined by [Pattyn et al., 2012]:

$$\begin{aligned} B &= 729 - \frac{2184.8}{750^2} d_{\mathrm{summit}}^2 + \frac{1031.72}{750^4} d_{\mathrm{summit}}^4 \\ &\quad - \frac{151.72}{750^6} d_{\mathrm{summit}}^6 \,. \end{aligned} \tag{108}$$

The initial ice sheet is obtained for a constant value of the flow parameter A of 10^{-16} Pa^{-n} a^{-1} and a constant surface mass balance of $\dot{a} = 0.3$ m a^{-1}. A grid-size spacing of $\Delta =$ 50 km is employed. All other parameters are listed in Tables 4–6. Subsequently, the flow-rate parameter A is altered to a new value to obtain a new steady state, where lower/higher values of A leads to grounding-line advance/retreat, respectively. According to theory, a given set of boundary conditions leads to unique steady state grounding-line positions on a downward sloping bedrock, while the grounding line never reaches a steady-state position on an upward-sloping bedrock, which is depicted in Fig. 12. For the overdeepened bed, this leads to hysteresis, i.e., multi-valued grounding-line positions and ice sheet profiles for the same set of boundary conditions (Figs. 12 and 13). The numerical error was estimated by determining the position of each grounding-line grid cell compared to its radial distance from the centre of the ice sheet (both experiments results in radial ice caps). The mean position of the grounding line and the standard deviation corresponding to each steady-state are shown in Fig. 13. Interpolation of the exact position within a grid cell was not considered. All errors are smaller than the nominal grid size of 50 km. The lowest numerical error corresponds to the grounding-line treatment according to the power-law sliding law without the presence of ice shelves ($\sigma \sim 20$ km). Including ice shelves makes the ice sheet more rapidly advance across the unstable section, since ice shelf thickness increases for lower values of A. Associated errors are also larger.

Errors on the advance and retreat grounding-line positions are displayed in the bottom panel of Fig. 13. In all cases, the difference in grounding-line position between advance and retreat is less than 10 km (one-fifth of the spatial resolution of the model). In some cases the error is exactly zero, meaning that the steady state ice sheets (the one obtained during advance compared to the one obtained after retreat) are exactly the same.

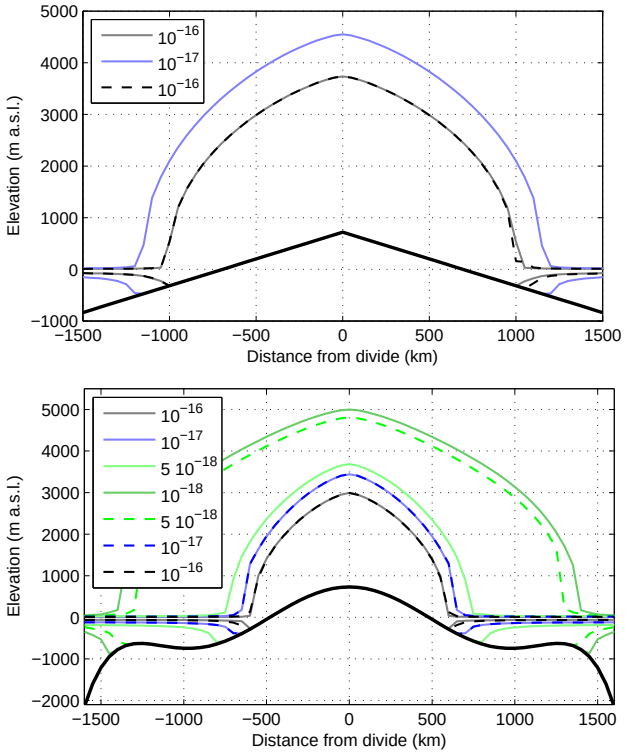

Figure 12: Steady-state ice-sheet/ice-shelf profiles for the MISMIP experiments corresponding to different values of the flow parameter A (Pa^{-n} a^{-1}) along the center-line for the downward-sloping bedrock (upper panel) and the overdeepened bedrock case (lower panel) according to the advance (solid line) and retreat (dashed line) experiments and a grounding-line flux-condition according to Eq. (16).

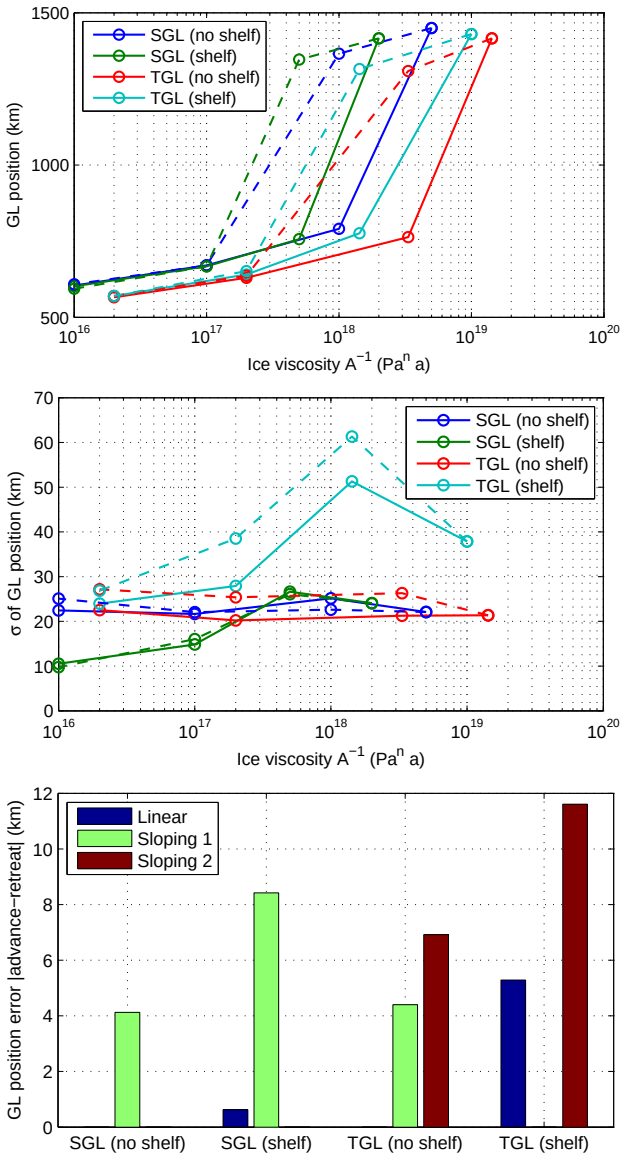

Figure 13: Median (upper panel) and standard deviation (centre panel) of steady-state grounding-line positions according to the MISMIP experiments for a circular ice sheet as a function of the flow parameter A (Pa^{-n} a^{-1}) for the overdeepened bedrock experiment according to different flux conditions at the grounding line and inclusion/exclusion of ice shelves. Solid lines represent advance and dashed lines represent retreat experiments. The lower panel displays the difference in grounding-line position for the steady-state ice sheets obtained during advance with those obtained during retreat (same parameter values) for the linear-sloping bed (Linear) and the overdeepend bed. The latter has two sections with stable steady-state solutions, i.e., a small ice sheet (Sloping 1) and a large one (Sloping 2).

4 Model call

4.1 Requirements

The f.ETISh model is built in MATLAB® and makes use of standard Matlab® toolboxes. Required toolboxes are MATLAB, Signal Processing Toolbox, Image Processing Toolbox, and Statistics and Machine Learning Toolbox. The model runs with versions of MATLAB® R2016b onwards.

4.2 Model run

f.ETISh is based on two MATLAB® script files, i.e., `FetishModel.m` containing the main model code and subroutines and `FetishInputParams.m` containing the main input parameters and constants, excluding parameters that control the model. A further script is needed that creates a MATLAB file with all controlling variables to call `FetishModel.m`. The f.ETISh model is called with the following command line in MATLAB®:

```
FetishModel(infile,outfile,ctr);
```

or

```
FetishModel(infile,outfile,ctr,fc);
```

where `ctr` is a 1×1 `struct` with >40 fields containing values and settings of parameters that control the model run, `fc` is a 1×1 `struct` with 3 fields containing time-dependent forcing control of the model, `infile.mat` is the input file with with either the observed ice sheet geometry or the results of a previous model run. The output file `outfile.mat` is similar to the input file in structure and saves all required matrices to produce a follow-up run. Finally, a variable dump file is automatically created after each model run containing all variables of the model run. This file is named `outfile_toto.mat`. Note that `infile.mat` does not need to exist (it should be defined though). In that case, all initial field values will be set to zero. Also, `fc` is an optional file that by default is set to zero (no forcing).

5 Parameter definition in call: `ctr` and `fc`

The control file is a MATLAB® (.mat) file listing all control parameters necessary to run the model. It can be created with a simple script. Most parameters are set to their default values and should not explicitly be defined. The mandatory parameters are given in the first section. One particularity of the input files is the definition of (x, y) corresponding to (j, i) in the numerical code. In other words, the first element of a matrix corresponds to its vertical position, the second element to its horizontal one. It suffices to transpose input data sets to make the visualization of data fully compliant.

5.1 Mandatory control parameters

`ctr.dt` : time step (years).

`ctr.imax` : number of grid points in the y-direction.

`ctr.jmax` : number of grid points in the x-direction.

`ctr.delta` : grid size (m), equal in both x and y-directions.

`ctr.nsteps` : number of iterations in time, so that `(nsteps - 1)` $\times$ `dt` = total model run time in years.

5.2 General control parameters (optional)

`ctr.runmode` :

- **0** : Run model with graphics that are shown every `ctr.snapshot` (default). A dump file is written at the end of the model run. The name of the dump file is `outfile`_toto.mat;
- **1** : Run model with graphics and output dump is written every `ctr.snapshot`. This allows for restarting the model after failure;
- **2** : As in 0 but run without graphics (especially useful when using batch jobs)
- **3** : As in 1 but run without graphics (especially useful when using batch jobs and securing recovery);

`ctr.plotGL` :

- **1** : Plot grounding line in output graphs (default);
- **0** : No grounding line plotting.

`ctr.restart` :

- **0** : Normal model run (default);
- **1** : Restart from latest dump file (when `ctr.runmode=1` or `ctr.runmode=3`).

`ctr.diagnostic` :

- **0** : Normal model run (default);

1 : Run model without ice-thickness evolution (all other model components run normally.

ctr.inverse :

0 : normal forward model run (default);

1 : optimization of basal sliding coefficients A_s for the grounded ice sheet with fixed grounding line position.

2 : optimization of basal sliding coefficients A_s for the grounded ice sheet and subshelf melt/accretion for floating ice shelves. The parameter `ctr.GroundedMelt` defines whether `MASKo` or `MASK` is used for controlling the grounding line position.

ctr.timeslice :

0 : no extra output (default);

1 : will provide extra output for forcing experiments saved sequentially in a file (`snapshot` times). The variable list is defined by `par.varlist` and consists of a list of 2-d matrices to be saved in each file.

ctr.snapshot : number of snapshots in time dependency and graphical output; for grounding-line monitoring when `ctr.timeslice=1`, snapshot should preferentially be smaller than 250, since it may increase the number of output files dramatically (limit = 999). Default value = 100.

ctr.kmax : number of vertical layers for temperature calculation (default = 11).

ctr.Hinv : Scale factor on iterative optimization of ice thickness [Pollard and DeConto, 2012b]. Default = 500.

ctr.Tinv : Time interval between updates in the optimization scheme [Pollard and DeConto, 2012b]. Default = 200. For basin calculations, the value should be set lower (10 for instance) in order to reduce the run time.

ctr.HinvMelt : Scale factor on iterative optimization of ice thickness for ice shelves [Pollard and DeConto, 2012b]. Default = 100.

ctr.TinvMelt : Time interval between updates in the optimization scheme [Pollard and DeConto, 2012b]. Default = 50.

ctr.upstream :

1 : Upstream differences for ice velocities u, v in advection part of the ice-thickness equation (default). Does not apply to the SIA model.

0 : Central differences

ctr.BetaIter : Number of iterations on β^2 calculation in the nonlinear part of the SSA velocity calculations (default); can be set throughout to `ctr.nsteps`. Default = 5.

ctr.mismip : 1: lateral boundary conditions for the MISMIP+ experiment [Cornford et al., 2020]. These include a symmetric ice divide and ocean condition at the left and right boundaries, respectively; and a symmetry axis at the lateral boundaries. Default = 0.

ctr.basin : 1: Simulation of a singular basin domain. At lateral boundaries either an open ocean prevails or no slip/high viscosity condition for grounded ice outside the simulated basin. Default = 0.

ctr.ItSolv : Iterative solver for both the ice thickness and the SSA/HySSA velocities. Default=1.

ctr.GroundedMelt : Allow for the `MASK` to be defined by hydrostatic equilibrium in the optimization `ctr.inverse` = 2. Default=0.

ctr.radnorm : (default = 50)

ctr.starttime : (default=0)

ctr.stopoptim : (default=0.1)

5.3 Thermodynamical parameters (optional)

ctr.Tcalc :

- **0** : No temperature calculation (default)
- **1** : Calculate temperature field in ice sheet (and ice shelf), isothermal ice sheet ($A =$`Ao`)
- **2** : Calculate temperature field and thermomechanical coupling, , i.e. $A = f(T)$

ctr.Tinit :

- **0** : Initial temperature field read from input file or when not available kept constant at values of surface temperature (default);
- **1** : Initialization of temperature field from semi-analytical steady-state temperature solution;
- **2** : Always use the steady-state semi-analytical solution.

ctr.Ao : Isothermal value of Glen's flow law parameter A (Pa^{-n} a^{-1}); Default = 10^{-16}.

ctr.SlidAdjust :

- **0** : Basal sliding based on coefficients A_s, either constant value or optimized field (default);
- **1** : As above, but basal sliding is also a function of basal temperature (within a range of `par.TrTemp` °C from the local pressure melting point) and bedrock variability `stdB` to allow for sliding in mountainous areas (only when `stdB` exists; this is also invoked in the inversion procedure.

5.4 Ice-dynamical parameters (optional)

ctr.schoof :

0 : no grounding line flux correction (default);

1 : grounding line migration according to Schoof [2007a];

ctr.shelf :

0 : no ice shelves (default);

1 : add ice shelves (requires that ctr.SSA > 0).

ctr.shelftune : Tuning factor for the ice shelf to take into account anisotropy [Ma et al., 2010]. Lower values make ice shelf more viscous. Default = 0.5.

ctr.SSA :

0 : SIA solution for grounded ice sheet (default);

1 : calculation of SSA for grounded ice sheet and ice shelf

2 : calculation of the hybrid HySSA model (SSA+SIA) for the grounded ice sheet.

ctr.m : Power sliding law exponent according to Weertman sliding law (default = 1).

ctr.u0 : Value of u_0 in the regularized Coulomb friction law. Large values (default) indicate Weertman-type sliding. (default=1e12)

ctr.p : Exponent for effective pressure in Weertman sliding law (default = 0).

ctr.Asin : Matrix of size (ctr.imax,ctr.jmax) with coefficients of sliding parameters A_b prior to initialization. Will be overwritten if As is already defined in the infile.

ctr.BedAdj :

0 : no isostatic bedrock adjustment (default);

1 : isostatic adjustment of bedrock (with the modified ELRA model);

2 : local isostatic bed adjustment.

ctr.GeoidCalc :

0 : Local sea level changes not taken into account (default);

1 : Calculate height of the geoid (local sea level) compared to initial state, based on mass changes of the ice sheet.

ctr.subwaterflow :

0 : no subglacial hydrology, i.e., water pressure calculated from depth of the bed below sea level (default);

1 : runs the subglacial water flow model (subglacial hydrology) and calculates effective pressure based on subglacial water thickness;

2 : Porous till water model [Bueler and van Pelt, 2015];

3 : Subglacial hydrology model of Goeller et al. [2013].

`ctr.calving` :

0 : no calving, i.e., ice shelves will extend to the edge of the model domain (default)

1 : Apply ice front calving according to Pollard et al. [2015];

2 : Combination of `calving=1` and `calving=4` to make sure that ice shelves do not extend further than initially

3 : Apply ice front calving according to Pollard and DeConto [2012a];

4 : Calving front kept at observed position.

5 : Calving using LSF function (under development)

`ctr.HydroFrac` :

0 : no hydrofracturing (default)

1 : Apply hydrofracturing according to Pollard et al. [2015];

5.5 Forcing parameters (optional)

`ctr.meltfunc` :

0 : Constant value of sub-shelf melting equal to the value of `ctr.meltfac` for all ice shelves (default);

1 : Melting underneath ice shelves according to the parametrization of Beckmann and Goosse [2003] following Pollard and DeConto [2012a];

2 : idem, but linear [de Boer et al., 2015];

3 : melt based on the PICO ocean-model coupler [Reese et al., 2018a];

4 : melt based on the PICOP model (combined PICO and plume model) [Pelle et al., 2019];

5 : melt based on the plume model [Pelle et al., 2019];

6 : melt as a linear function of ice-shelf thickness [Cornford et al., 2016];

7 : uniform melting according to `ctr.meltfac` for `fc.butfac=1`; in this case `fc.butfac` determines the period for which melting is applied; after invoking the melt scheme, `fc.butfac` is put back to 1 in order to keep buttressing applied;

8 : removal of all ice shelves; supplementary melting can be applied via `ctr.meltfac`

9 : ISMIP6 non-local melt-rate parametrization.

10 : MISMIP+ melt function;

11 : Applying optimized sub-shelf melt/accretion rates to the ice shelves.

ctr.meltfac : Amount of basal melting underneath ice shelves (in m a^{-1} if `ctr.meltfunc=0` for example) or multiplier to sub-shelf melt for `ctr.meltfunc`=1–5; default = 0.

ctr.meltfactor : `fc.DeltaT` fraction of atmospheric forcing to account for ocean temperature change (used when `ctr.meltfunc>0`); can be used as a tuning/ensemble parameter. Default = 0.3.

ctr.slidfac : Multiplier on basal sliding coefficients for perturbation studies; can also be used as a tuning/ensemble parameter. Default = 1.

ctr.gammaT : Effective turbulent temperature exchange velocity (m s^{-1}); can be used as a tuning/ensemble parameter. Default values for different melting schemes are: 3e-5 for PICO/PICOP; 50e-5 for quadratic; 2e-5 for linear.

ctr.M0 : Tuning parameter for the plume/PICOP model. Default values are 5 for Plume; 15 for PICOP.

ctr.MbType : Type of surface mass balance distribution/perturbation **Update needed.**

- **0:** Initial `Mb` distribution
- **1:** $M_b = M_b(0) \times 2^{(T_s - T_s(0))/10}$ and (if PDD exists) surface melt according to PDD model
- **2:** $M_b = M_b(0)[1 + 0.053(T_s - T_s(0))]$
- **3:** EISMINT fixed margin experiment with $M_b = M_b(0) + 0.02\Delta T$
- **4:** EISMINT moving margin experiment
- **5:** EISMINT moving margin experiment with $R_{el} = R_{el} + 10\Delta T$

ctr.TsType = type of surface temperature distribution/perturbation **Update needed.**

- **0:** Initial `Ts` distribution with forcing: $T_s = T_s(0) + \Delta T$
- **1:** Correction for elevation changes using adiabatic lapse rate
- **2:** EISMINT moving margin experiment

ctr.PDDcalc :

- **0** : no calculation of PDD model (default)
- **1** : PDD model

ctr.monthly :

- **0** : (default)
- **1** :

5.6 Time-dependent parameters `fc` (optional)

`fc.DeltaT` : Vector (size of ctr.nsteps) with background temperature forcing (default = 0, no forcing)

`fc.DeltaSL` : Vector (size of ctr.nsteps) with background sea-level forcing (default = 0, no forcing)

`fc.butfac` : Vector (size of ctr.nsteps) with range of full (1) to no (0) buttressing of ice shelves; the vector can also be used to control the timing and duration of sub-shelf melting (see `ctr.meltfunc`). Default = 1.

Update needed.

6 Input and output files

6.1 Input file: `infile`

`infile` is the name of a .mat input file with following (optional) 2d variables: `MASK`, `MASKo`, `H`, `Ho`, `B`, `Bo`, `Bor`, `Bmelt`, `As`, `Asor`, `G`, `stdB`, `Ts`, `Mb`, `To`, `So`, `Db`, `Btau`, `tmp`, `v`, `vx`, `vy`, `lat`, `lon`, `uxssa`, `uyssa`, `Wd`, `Wtil`, `ZB`, `Meltinv`, where

`MASK` : grounded = 1; floating = 0
Note that when `shelf=0` and `schoof=0`, the model domain will be restricted to `MASK=1`

`MASKo` : observed MASK (invariable in time)

`H` : ice thickness (m)

`Ho` : observed ice thickness (m)

`B` : bedrock elevation (m)

`Bo` : observed bedrock elevation (m)

`Bor` : observed bedrock elevation (m), not corrected at the boundaries (= original bathymetry)

`Bmelt` : Subglacial melt underneath the grounded ice sheet (m/a).

`As` : basal sliding coefficient for power-law sliding law.

`Asor` : basal sliding coefficient for power-law sliding law.

`G` : geothermal heat flux (W m^{-2})

`stdB` : Standard deviation of bedrock variability within a grid cell (based on original Bedmap2 or BedMachine data).

`Ts` : Annual mean surface temperature (°C).
Note that this is the unforced value (observed).

`Mb` : Surface mass balance (m a^{-1}).
Note that this is the unforced value (observed; without surface and basal melt, or calving and cliff melting).

`To` : Ocean temperatures on the continental shelf (°C)

`So` : Ocean salinity on the continental shelf (PSU)

`Db` : Flexural rigidity of the lithosphere

`Btau` : Relaxation time of the astenosphere (filled with constant values corresponding to `bedrelax` when `Btau` is not initially defined)

tmp : Englacial temperature field (3d matrix) of previous model run (K) — note that this field is given in Kelvin and **not** in °C.

v : observed surface velocity v

vx : observed surface velocity v in x (on staggered u-grid)

vx : observed surface velocity v in y (on staggered v-grid)

lat : Latitude (degrees)

lon : Longitude (degrees)

uxssa : SSA velocities in x (on staggered u-grid)

uyssa : SSA velocities in y (on staggered v-grid)

Wd : Subglacial water layer thickness (m), set to 0.001 m on the whole domain when subglacial water flow is not calculated explicitly.

Wtil : Thickness of the water column with the subglacial till (m).

ZB : Delineation of drainage basins.

MeltInv : Optimized sub-shelf melt/accretion rate after optimization.

Note that the name of the input file should be given, but the file itself should not necessarily exist. If the file is non-existent, the model will be initialized with zero matrices of `H`, `B`, `As`, `stdB`, `Ts`, `Mb`, and `tmp`. `MASK` will be set to 1 everywhere,and `G` will contain a constant value of geothermal heat flow of G=0.042 W m^{-2}. The extension '.mat' should not be given as part of the name `infile`.

6.2 Output file: `outfile`

`outfile` is the name of a .mat output file (same structure as `input`). This file will contain all necessary matrices to be used as an input file for a subsequent experiment. Nevertheless, all model data and parameters are stored in a file with the name `outfile_toto.mat`. The extension '.mat' should not be given as part of the name `infile`. For `ctr.snapshot=1`, file names starting from `outfile_000.mat` with an increment of 1 will be created where variables listed in `par.varlist` will be saved.

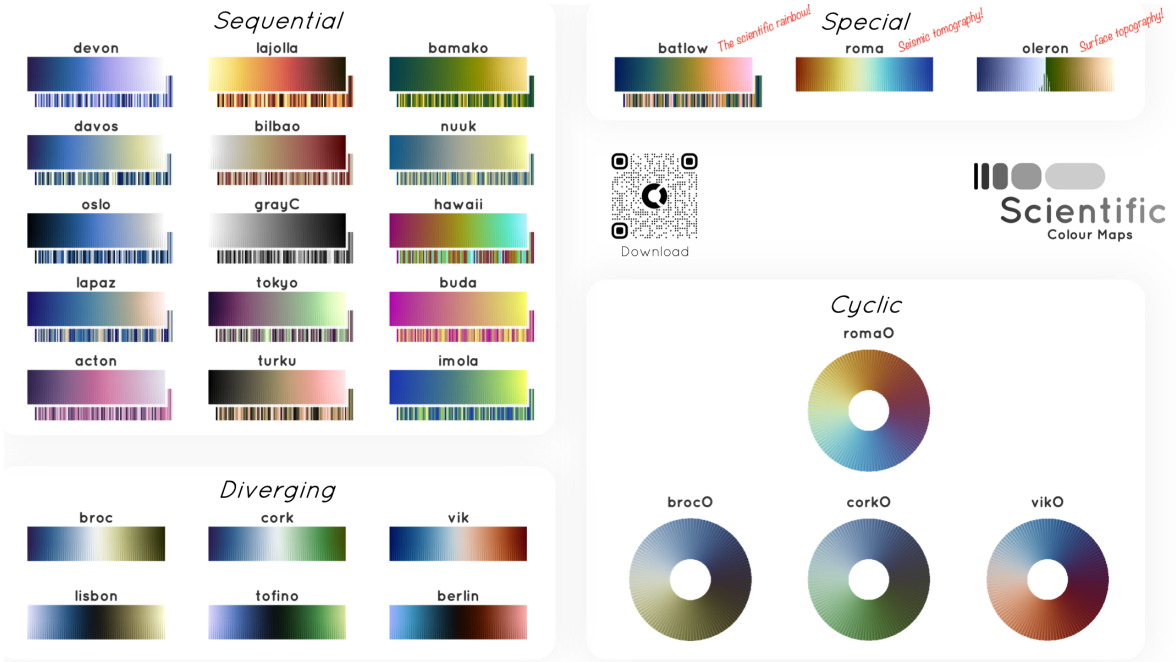

Figure 14: Crameri color scale

7 Physical constants and global model parameters

Model parameters and physical constants are defined in the file `FetishInputParams.m` and are read at the start of the f.ETISh model. These parameters normally remain the same for a series of experiments and define subglacial till rheology, isostasy, thermodynamics and ice properties. The parameters are collected in the `struct` called `par`.

7.1 General control

`par.dcolor = 'vik'`: Crameri color scale for plots of changes in ice thickness; See Figure 14 for all options. A minus sign means reversed scale.

`par.color = '-roma'`: Crameri color scale for plots of velocity; See Figure 14 for all options. A minus sign means reversed scale.

`par.plotH = 0` Plot evolution of $H - H_0$ for each `snapshot`, scale around 0;

1 Plot evolution of H for each `snapshot`

7.2 Numerical control parameters

`par.maxspeed =` 20000: Maximum tolerated flow speed of ice sheet/ice shelf system (m a^{-1})

`par.omega =` 0–2.5: Implicit factor in the Crank-Nicholson scheme for the ice-sheet equation solver: 0=explicit; 1=implicit; 2.5=over-implicit

`par.SSAdifus` :

0 : Pure numerical advection scheme for solving the hybrid and SSA model;

1 : Use diffusion for deformational velocity in `SSA=2`;

2 : idem as 1, but hybrid model is an arithmetic addition of SSA velocities (sliding) and deformational velocities.

par.secperyear = 31556926: number of seconds per year

7.3 Subglacial characteristics

par.u0 = 100: Limit velocity for application of Coulomb friction.

par.phi = 20: Nominal value of the till friction angle (degrees) prior to initialization.

par.PoreFrac = 0.96: Fraction of water pressure to balance ice pressure [Winkelmann et al., 2011]

par.longcoupwater = 5: distance (in number of ice thicknesses over which hydraulic gradient coupling takes place (only for subglacial water model)

par.dirpp_war = [9 8 7 6 5 4 3 2 1]: vector for search directions in subglacial water model (based on Le Brocq et al. [2006])

par.waterviscosity = 1.8e-3/`par.secperyear`: viscosity of subglacial water

par.NeffScale = 5e6: scale factor for Effective Pressure in the porous till model

par.Wdmin = 1e-8: minimum value for `Wd` and `Wtil`

par.Wdmax = 0.015: maximum value for `Wtil`

par.Cdr = 1e-3: background till drainage rate

par.Cc = 0.12: till compressibility [Tulaczyk et al., 2000]

par.e0 = 0.69 reference void ratio at `N0` [Tulaczyk et al., 2000]

par.N0 = 1e3: reference effective pressure [Tulaczyk et al., 2000]

par.sigmat = 0.02: `Ntil` lower bound, as fraction of overburden pressure

7.4 Ice dynamics

par.SuctionCheck :

0 : No safety check (default)

1 : Safety check on ice flux across the grounding line according to Ritz et al. [2015].

par.ShelfPinning :

0 : No sub-shelf pinning;

1 : Sub-shelf pinning of ice shelves based on local bedrock variability `stdB` and water column depth (only when `stdB` exists).

par.g = 9.81: gravitational acceleration

par.rho = 917: ice density

par.rhow = 1028: sea-water density

par.rhom = 3370: lithospheric density

par.n = 3: Glen's flow law exponent

par.visciter = 50: Maximum number of iterations on the nonlinear effective viscosity.

par.Qo = 0.61: Numerical constant in Tsai et al. [2015] boundary condition

7.5 Ocean-ice interaction

par.Latent = 3.35e5: Latent heat of freezing

par.cp0 = 3974: Heat capacity of ocean water

par.Soi = 34.5: ocean salinity (default)

par.Toi = -1.7°C: Ocean temperature (default) [Maris et al., 2014]

par.SeaIceThickness = 0.1: Thickness of the sea-ice layer uniformely on the ocean domain (m); used to control stress transfer from the modelled domain edges to the ice shelves.

par.ArcOcean :

0 : Not used;

1 : Calculates the radial opening of ice shelves to open ocean. Used for optimizing basal melt in ice shelves [DeConto and Pollard, 2016].

7.6 PICO and plume/PICOP ocean-model coupler

par.nbox = 5: Maximum number of ocean boxes in PICO model

par.alphao = 7.5e-5: Thermal expansion coefficient in EOS [1] ($°C^{-1}$)

par.betao = 7.7e-4: Salt contraction coefficient in EOS (PSU^{-1})

par.rhoref = 1033: Reference density in EOS (kg m^{-3})

par.C = 1e6: Overturning strength of ocean circulation underneath ice shelf (m^3 s^{-1})

par.lambda1 = -0.0573: Salinity coefficient of freezing equation (°C PSU^{-1})

[1] EOS: equations of state

par.lambda2 = 0.0832: Constant coefficient of freezing equation (°C)

par.lambda3 = 7.61e-4: Pressure coefficient (as a function of HB of freezing equation (°C m^{-1})

par.gamma1 = 0.545: Heat exchange parameter

par.gamma2 = 3.5e-5: Heat exchange parameter

par.CdGamT = 1.1e-3: Turbulent heat exchange coefficient

par.CdGamTS0 = 6e-4: Heat exchange parameter

par.Eo = 3.6e-2: Entrainment coefficient

par.Cd = 2.5e-3: Drag coefficient

par.x0 = 0.56: Dimensionless scaling factor

par.pcof = coefficients for the 11th-degree polynomial describing the melt-refreezing function in Lazeroms et al. [2018].

7.7 Isostasy

par.FlexRigid = 1e25: Flexural rigidity of the lithosphere (Pa m^3); its value is defined by

$$D_b = \frac{E h_e^3}{12(1-\nu^2)}$$

where E is Young's modulus (100 GPa), ν is Poisson's ratio (0.25), and h_e is the effective elastic lithosphere thickness [Chen et al., 2017]

par.bedrelax = 3000: Relaxation time of the asthenosphere (year) as nominal value (used when Btau is not defined).

par.flexdist = 600e3: Flexural distance of the lithosphere (m)

par.nuB = 0.25: Poisson coefficient in the full derivation of lithospheric deformation.

7.8 Sea-level fingerprints

par.Re = 6.3781e6: Radius of the Earth

par.Me = 5.972e24: Mass of the Earth

par.Aoc = 3.618e14: Global ocean surface

par.geoidist = 5000e3: size of the convolution filter over wich fingerprinting is calculated (m)

par.rhof = 1000: fresh water density

par.rhoL = 2830: mean lithosphere density

par.SLref = 0: reference sea level

7.9 Model initialization

par.VelInverse : This parameter is only used for initialization purposes (inverse=1)

- **0** : Ice shelf velocities either calculated with ice shelf model (shelf = 1) or set to the flux at the grounding line (shelf = 0);
- **1** : Use Rignot et al. [2011] velocities for calculating the buttressing factor Θ in shelves. In this case velocities in the ice shelf are not calculated (shelf = 0). **Recent experiments have shown that it is better to set schoof=0 for the initialization, which makes this parameter obsolete.**

par.SmoothInv :

- **0** : no regularization in the optimization
- **1** : Use low-pass filter on optimized field of A_s as regularization term in optimization

par.SmoothSpan = 150: Size of low-pass filter (in km)

par.invmin = 1.e-10 (for $m = 2$): Minimum value of A_s in optimization scheme. AsScale is employed for scaling with other values of m

par.invmax = 1.e-5 (for $m = 2$): Maximum value of A_s in optimization scheme. AsScale is employed for scaling with other values of m

par.AsFroz = 1e-11 (for $m = 2$): Minimum value of A_s corresponding to frozen bed conditions (should be different from zero to avoid division by zero); AsScale is employed for scaling with other values of m

par.AsScale = $(1e5)^{2-m}$: scaling factor for other values of m different from 2

7.10 Thermodynamics

par.T0 = 273.15 K: absolute temperature

par.K = 2.1: thermal conductivity

par.kdif = 1.1487e-6: $k = K/(\rho c_p)$, where $c_p = 2009$

par.pmp = 8.66e-4: Clausius Clapeyron dependence of melt on pressure; taken as a function of ice thickness H [Payne et al., 2000]

par.atune = 1: tuning factor in Arrhenius equation (for ice sheet; scales with tuning factor for ice shelf)

par.a1 = 3.985e-13 $\times$ par.secperyear: factor in Arrhenius equation [Payne et al., 2000]

par.a2 = 1.916e3 $\times$ par.secperyear: factor in Arrhenius equation [Payne et al., 2000]

par.Q1 = 6e4: factor in Arrhenius equation [Payne et al., 2000]

par.Q2 = 13.9e4: factor in Arrhenius equation [Payne et al., 2000]

par.R = 8.314: Gas constant

par.udfrac = 0.25: fraction of deformational velocity in heat dissipation for initialization of the temperature field with semi-analytical solution (`Tinit=1`).

par.intT = 10: Temperature calculation every `intT` iterations.

par.TrTemp = -5: Basal temperature for which ice is frozen to bed (-5°C).

par.QL1 = 78.2e3: factor in Arrhenius equation [Ritz, 1992]

par.QL2 = 95.45e3: factor in Arrhenius equation [Ritz, 1992]

par.aL1 = 1.66e-16: factor in Arrhenius equation [Ritz, 1992]

par.aL2 = 2e-16: factor in Arrhenius equation [Ritz, 1992]

7.11 Positive-Degree Day (PDD) scheme

par.snowfac = 0.003: PDD factor for melting snow

par.icefac = 0.008: PDD factor for melting ice

par.refreeze = 2: Maximum depth of refreezing of percolating meltwater (m)

par.Tlapse = -0.008: rate of atmospheric temperature change with height

par.Tsigma = 5: Standard deviation of daily temperature variation

par.PDDsteps = 12: number of integration steps (minimum 12 = 1 month)

8 Main model variables

8.1 Spatially varying variables

Spatially-varying parameters are matrices of size `imax` by `jmax`. All variables are written out at the end of the model run in the file `output_toto.mat`. The x and y-grids correspond to the Arakawa C grid, while the d-grid corresponds to the Arakawa B grid.

A = Glen's flow factor (temperature dependent)

Ak = PICO: mean area of ice shelf box

As = Initial or optimized sliding parameters A_s for the power-law sliding law

As0 = Values of A_s at the start of the model run

Asf = Corrected values of A_s for dependence on temperature and bedrock variability; these values are used in the sliding law

Ax = Glen's flow factor on the staggered x-grid

Axy = Glen's flow factor on the staggered d-grid

Ay = Glen's flow factor on the staggered y-grid

B = Bedrock elevation B (m)

B0 = Bedrock elevation B at the start of the model run (m)

beta2 = Basal friction parameter β^2

betax = Basal friction parameter β on staggered x-grid

betay = Basal friction parameter β on staggered y-grid

Bk = PICO: ice shelf box number

bload = Ice sheat load on the lithosphere

Bm = Bedrock elevation on staggered d-grid

Bmx = Bedrock elevation on staggered x-grid

Bmy = Bedrock elevation on staggered y-grid

Bo = Bedrock elevation B from original dataset (Bedmap2/BedMachine) (m)

Bn = Bedrock elevation B on time step $t + 1$

CMB = Calving rates in the mass balance (m a^{-1})

d = Diffusion coefficients of ice sheet equation on staggered d-grid. These contain sliding and deformation for the SIA model and only deformation for the Hybrid model (SSA+SIA).

Db = Spatially varying (can be constant) flexural rigidity of the lithosphere

Db0 = Spatially varying (can be constant) flexural rigidity of the lithosphere divided in `Bclass` classes

dHdt = Ice sheet imbalance $\partial H/\partial t$ (m a^{-1})

dMelt = Ice shelf melt rate: $\min(M\Delta t, H)$

div = ice flow divergence $(\partial u/\partial x + \partial v/\partial y)$

dudx = Ice flow stretching rate in the x direction $(\partial u/\partial x)$

dvdy = Ice flow stretching rate in the y direction $(\partial v/\partial y)$

Wd = Subglacial water depth (m); initialized with 1e-8.

eta = effective viscosity in SSA

fg = Correction factor for subgrid pinning points in ice shelves

flux = Ice flux on H-grid (m^3 a^{-1})

FluxWater = Subglacial water flux in subglacial hydrology

FMB = Vertical cliff melting (m a^{-1})

G = Geothermal heat flux (W m^{-2})

glMASK = Complete mask for ice sheet-ice shelf-ocean system

- **1:** Grounded ice sheet
- **2:** Last grounded grid point (grounding line)
- **3:** First floating grid point
- **4:** Ice shelf
- **5:** Calving front (last floating grid point, may replace the first floating grid point in absence of ice shelf)
- **6:** Open ocean (covered by `SeaIceThickness`)

glMASKx = Complete mask for ice sheet-ice shelf-ocean system on staggered x-grid

glMASKy = Complete mask for ice sheet-ice shelf-ocean system on staggered y-grid

gradm = square of the surface gradients $(\nabla h_s)^2$ on staggered d-grid

gradmx = square of the surface gradients $(\nabla h_s)^2$ on staggered x-grid

gradmy = square of the surface gradients $(\nabla h_s)^2$ on staggered y-grid

H = ice thickness (m)

H0 = ice thickness at the start of the model run

HAF = Height above floatation (positive for grounded ice; negative for floating ice)

HAFm = Height above floatation on staggered d-grid

HAFmx = Height above floatation on staggered x-grid

HAFmy = Height above floatation on staggered y-grid

HB = lower ice boundary; for grounded ice $h_b = b$

HB0 = lower ice boundary at the start of the model run

HBo = Same as HB0 but for the original data set (Bedmap2/BedMachine)

he = Edge ice thickness (for calving; m)

Hm = ice thickness (m) on staggered d-grid

Hmx = ice thickness (m) on staggered x-grid

Hmy = ice thickness (m) on staggered y-grid

Hn = ice thickness (m) on time step $t + 1$

Ho = ice thickness (m) for the original dataset (Bedmap2/BedMachine)

load0 = Initial ice load at the start of the model run

mflux = Integrated ice flux in time on H-grid (m^3)

MASK = Grounded-non-grounded mask; 1 for grounded ice sheet; 0 otherwise; Note that when `shelf=0` and `schoof=0`, the model domain will be restricted to `MASK=1`

MASK0 = Mask at the start of the model run

MASKinv = Mask for inversion (adds first floating grid point to grounded grid)

MASKm = Mask on staggered d-grid

MASKmx = Mask for hybrid/SSA model on staggered x-grid

MASKmy = Mask on hybrid/SSA model staggered y-grid

MASKo = `MASK` for the original dataset (Bedmap2/BedMachine). Note that `MASK=3` refers to the ice shelves

Mb = Surface mass balance (including surface accumulation, ablation, surface melt determined from PDD model, sub-ice shelf melt and calving)

Mb0 = Surface mass balance (accumulation/ablation) at start of the model run

Mbend = Surface mass balance `Mb` at the end of the model run (including all losses, i.e. surface melting with PDD model, sub-shelf melting and calving); At the end of the model run `Mb0` is copied on `Mb`

Mbm = Surface mass balance (accumulation/ablation) on staggered d-grid

Melt = Sub-ice shelf melting rate (m a^{-1})

MeltTot = Total integrated sub-ice shelf melt over time (m)

ncorx = Weighing factor in application of flux condition at grounding line (on staggered x-grid)

ncory = Weighing factor in application of flux condition at grounding line (on staggered y-grid)

Neff = Effective pressure at the base of the ice sheet (Pa)

P = Weight of ice/ocean on the lithosphere (Pa m^2)

PDD = Number of positive degree days (degree days)

pwv = Subglacial water pressure (Pa)

r = Fraction of subglacial sliding/freezing as a function of basal temperature and bedrock variability, so that: $A_{sf} = (1 - r)As_{Froz} + A_s r$

S0 = Surface elevation (m) at the start of the model run

ShelfN = PICO: ice shelf number

shMASK = PICO: ice shelf mask (1 for floating ice)

signx = Flow direction in x (positive/negative)

signy = flow direction in y (positive/negative)

SLR = Height of sea level (m)

Smelt = Surface melt rate from PDD model (m a^{-1})

sn = Surface elevation (m)

sn0 = Surface elevation (m) from original dataset (Bedmap2/BedMachine)

So = Ocean salinity (PSU)

stdB = Standard deviation of bedrock variability in each grid cell, based on original Bedmap2/BedMachine data

tanphi = Tangent of the till friction angle ($\tan\phi$), optimized in the inversion procedure

taudx = Driving stress on staggered d grid

taudx = Driving stress on staggered x grid

taudy = Driving stress on staggered y grid

Tb = Basal temperature (°C)

Thetax = Buttressing factor Θ in x direction on the staggered x grid

Thetay = Buttressing factor Θ in y direction on the staggered y grid

Tmean = Mean column temperature for thermomechanical coupling (°C)

tmp = 3d englacial temperature field (`imax` $\times$ `jmax` $\times$ `kmax`; in Kelvin)

To = Ocean temperature (°C)

Ts = Surface temperature (°C)

Ts0 = Surface temperature (°C) at the start of the model run

Tsend = Surface temperature (°C) at the end of the model run; At the end of the model run `Ts0` is copied on `Ts`

Tsm = Surface temperature (°C) on staggered d-grid

Txx = Longitudinal normal stress deviator in x direction

Tyy = Longitudinal normal stress deviator in y direction

u = vertical mean horizontal velocity (m a^{-1}), $u = u_s + u_d$ on staggered d-grid

ud = vertical mean deformation al velocity (m a^{-1}) on staggered d grid

ub = sliding velocity (m a^{-1}) on staggered d-grid

ux = vertical mean horizontal velocity in x direction (m a^{-1}) on staggered x-grid

uxssa = sliding/ice shelf velocity in x direction (m a^{-1}) on staggered x-grid

uxsch = Flux-adjusted grounding-line velocity in x direction (m a^{-1}) on staggered x-grid

uy = vertical mean horizontal velocity in y direction (m a^{-1}) on staggered y-grid

uyssa = sliding/ice shelf velocity in y direction (m a^{-1}) on staggered y-grid

uysch = Flux-adjusted grounding-line velocity in y direction (m a^{-1}) on staggered y-grid

v = Observed surface velocity from Rignot et al. [2011] on staggered d-grid

VAF0 = Volume above floatation at start of the model run

VAFi = Volume above floatation

vx = Observed surface velocity in x direction from Rignot et al. [2011] on staggered x-grid

vy = Observed surface velocity in y direction from Rignot et al. [2011] on staggered y grid

Wd = Subglacial water layer depth (m)

Wtil = Height of subglacial water in porous till (m)

X = Horizontal x coordinates (km)

Y = Horizontal y coordinates (km)

8.2 Time-dependent variables

The following series of variables are produced (or provided) at every time step.

butfac = Buttressing factor for grounding line control (0–1); default = 1

DeltaSL = Background sea level (for paleoclimatic simulations)

DeltaT = Background temperature change

InvVol = Ice-sheet elevation change during optimization (`inverse = 1`)

time = Time (a)

Ag = Grounded ice sheet area (m^2)

Af = Floating ice shelf area (m^2)

IVg = Grounded ice sheet volume (m^3)

IVf = Floating ice shelf volume (m^3)

glflux = Total grounding-line ice flux ($m^3\ a^{-1}$)

SLC = Sea-level contribution (different from VAF)

VAF = Contribution to sea level rise (m), based on the volume above floatation (positive = ice loss)

8.3 Snapshot variables

The following series of variables are produced `snapshot` times to form each a 3d matrix. They are only created when `forcing = 1`

EVB = Bedrock elevation in time (m)

EVbeta2 = Basal friction in SSA and HySSA model

EVflux = Ice flux integrated in time ($m^3\ a^{-1}$)

EVH = Ice thickness in time (m)

EVmask = `MASK` in time (0/1)

EVMelt = `Melt` in time ($m\ a^{-1}$)

EVUx = `ux` in time ($m\ a^{-1}$)

EVUy = `uy` in time ($m\ a^{-1}$)

EVT = Basal temperature corrected for pressure melting point in time (°C)

9 Script examples

9.1 EISMINT experiment

Below is an example script for running the EISMINT standard model run for a fixed margin ice sheet on a square flat topography. The script initializes all necessary input parameters for the model call and creates the input file for this particular experiment descriped in Huybrechts et al. [1996].

```
% EISMINT fixed margin experiment with f.ETISh 1.7
% Basic experiments as outlined in Pattyn 2017

function TestFetish

clear; close all;

ctr.imax=31;
ctr.jmax=31;
ctr.delta=50.e3;
ctr.nsteps=2001;
ctr.snapshot=10;
ctr.dt=50.;
ctr.Tcalc=1;

Li=(ctr.imax-1)*ctr.delta/1e3;
Lj=(ctr.jmax-1)*ctr.delta/1e3;
[X,Y] = meshgrid(0:ctr.delta/1e3:Li,0:ctr.delta/1e3:Lj);
dist=max(abs(X-Lj/2.),abs(Y-Li/2.));
Ts=239.+8e-8*dist.^3.-273.15;
Mb=zeros(ctr.imax,ctr.jmax)+0.3;
save('EISMINT1','Mb','Ts');

FetishModel('EISMINT1','eismint01',ctr);

end
```

9.2 Running simulations on the Antarctic ice sheet

To be inserted.

9.3 Data visualization

Description of mytex and myevol to be inserted.

References

A. Beckmann and H. Goosse. A parameterization of ice shelf-ocean interaction for climate models. *Ocean Modelling*, 5(2):157 – 170, 2003. ISSN 1463-5003. doi: 10.1016/S1463-5003(02)00019-7.

S. Berger, L. Favier, R. Drews, J.-J. Derwael, and F. Pattyn. The control of an uncharted pinning point on the flow of an antarctic ice shelf. *Journal of Glaciology*, 62(231):37–45, Feb 2016. doi: 10.1017/jog.2016.7.

J. Bernales, I. Rogozhina, R. Greve, and M. Thomas. Comparison of hybrid schemes for the combination of shallow approximations in numerical simulations of the antarctic ice sheet. *The Cryosphere Discussions*, 2016:1–32, 2016. doi: 10.5194/tc-2016-117.

J. Bernales, I. Rogozhina, R. Greve, and M. Thomas. Comparison of hybrid schemes for the combination of shallow approximations in numerical simulations of the antarctic ice sheet. *The Cryosphere*, 11(1):247–265, 2017. doi: 10.5194/tc-11-247-2017. URL https://www.the-cryosphere.net/11/247/2017/.

M. Bougamont, P. Christoffersen, A. L. Hubbard, A. A. Fitzpatrick, S. H. Doyle, and S. P. Carter. Sensitive response of the greenland ice sheet to surface melt drainage over a soft bed. *Nature Communications*, 5(1):5052, 2014. ISSN 2041-1723. doi: 10.1038/ncomms6052. URL https://doi.org/10.1038/ncomms6052.

E. Bueler and J. Brown. Shallow shelf approximation as a "sliding law" in a thermomechanically coupled ice sheet model. *Journal of Geophysical Research: Earth Surface*, 114(F3), 2009. ISSN 2156-2202. doi: 10.1029/2008JF001179. F03008.

E. Bueler and W. van Pelt. Mass-conserving subglacial hydrology in the parallel ice sheet model version 0.6. *Geoscientific Model Development*, 8(6):1613–1635, 2015. doi: 10.5194/gmd-8-1613-2015.

B. Chen, C. Haeger, M. K. Kaban, and A. G. Petrunin. Variations of the effective elastic thickness reveal tectonic fragmentation of the antarctic lithosphere. *Tectonophysics*, 2017. doi: http://dx.doi.org/10.1016/j.tecto.2017.06.012.

S. L. Cornford, D. F. Martin, V. Lee, A. J. Payne, and E. G. Ng. Adaptive mesh refinement versus subgrid friction interpolation in simulations of antarctic ice dynamics. *Annals of Glaciology*, 57(73):1–9, 2016. doi: 10.1017/aog.2016.13.

S. L. Cornford, H. Seroussi, X. S. Asay-Davis, G. H. Gudmundsson, R. Arthern, C. Borstad, J. Christmann, T. Dias dos Santos, J. Feldmann, D. Goldberg, M. J. Hoffman, A. Humbert, T. Kleiner, G. Leguy, W. H. Lipscomb, N. Merino, G. Durand, M. Morlighem, D. Pollard, M. Rückamp, C. R. Williams, and H. Yu. Results of the third marine ice sheet model intercomparison project (mismip+). *The Cryosphere*, 14(7):2283–2301, 2020. doi: 10.5194/tc-14-2283-2020. URL https://tc.copernicus.org/articles/14/2283/2020/.

V. Coulon, K. Bulthuis, P. L. Whitehouse, S. Sun, K. Haubner, L. Zipf, and F. Pattyn. Contrasting response of west and east antarctic ice sheets to glacial isostatic adjustment. *Journal of Geophysical Research: Earth Surface*, 126(7):e2020JF006003, 2021.

doi: https://doi.org/10.1029/2020JF006003. URL https://agupubs.onlinelibrary.wiley.com/doi/abs/10.1029/2020JF006003. e2020JF006003 2020JF006003.

B. de Boer, A. M. Dolan, J. Bernales, E. Gasson, H. Goelzer, N. R. Golledge, J. Sutter, P. Huybrechts, G. Lohmann, I. Rogozhina, A. Abe-Ouchi, F. Saito, and R. S. W. van de Wal. Simulating the antarctic ice sheet in the late-pliocene warm period: Plismip-ant, an ice-sheet model intercomparison project. *The Cryosphere*, 9(3):881–903, 2015. doi: 10.5194/tc-9-881-2015.

R. M. DeConto and D. Pollard. Contribution of Antarctica to past and future sea-level rise. *Nature*, 531:591–597, 2016. doi: 10.1038/nature17145.

G. Durand and F. Pattyn. Reducing uncertainties in projections of antarctic ice mass loss. *The Cryosphere*, 9(6):2043–2055, 2015. doi: 10.5194/tc-9-2043-2015.

G. Durand, O. Gagliardini, T. Zwinger, E. Le Meur, and R. C. Hindmarsh. Full stokes modeling of marine ice sheets: influence of the grid size. *Annals of Glaciology*, 50(52): 109–114, 2009. ISSN 0260-3055. doi: doi:10.3189/172756409789624283.

L. Favier, F. Pattyn, S. Berger, and R. Drews. Dynamic influence of pinning points on marine ice-sheet stability: a numerical study in dronning maud land, east antarctica. *The Cryosphere*, 10(6):2623–2635, 2016. doi: 10.5194/tc-10-2623-2016.

L. Favier, N. C. Jourdain, A. Jenkins, N. Merino, G. Durand, O. Gagliardini, F. Gillet-Chaulet, and P. Mathiot. Assessment of sub-shelf melting parameterisations using the ocean–ice-sheet coupled model nemo(v3.6)–elmer/ice(v8.3). *Geoscientific Model Development*, 12(6):2255–2283, 2019. doi: 10.5194/gmd-12-2255-2019. URL https://www.geosci-model-dev.net/12/2255/2019/.

G. E. Flowers. Modelling water flow under glaciers and ice sheets. *Proceedings of the Royal Society of London A: Mathematical, Physical and Engineering Sciences*, 471(2176), 2015. ISSN 1364-5021. doi: 10.1098/rspa.2014.0907.

C. Fox-Maule, M. E. Purucker, N. Olsen, and K. Mosegaard. Heat flux anomalies in Antarctica revealed by satellite magnetic data. *Science*, 309:464–467, 2005.

P. Fretwell, H. D. Pritchard, D. G. Vaughan, J. L. Bamber, N. E. Barrand, R. Bell, C. Bianchi, R. G. Bingham, D. D. Blankenship, G. Casassa, G. Catania, D. Callens, H. Conway, A. J. Cook, H. F. J. Corr, D. Damaske, V. Damm, F. Ferraccioli, R. Forsberg, S. Fujita, Y. Gim, P. Gogineni, J. A. Griggs, R. C. A. Hindmarsh, P. Holmlund, J. W. Holt, R. W. Jacobel, A. Jenkins, W. Jokat, T. Jordan, E. C. King, J. Kohler, W. Krabill, M. Riger-Kusk, K. A. Langley, G. Leitchenkov, C. Leuschen, B. P. Luyendyk, K. Matsuoka, J. Mouginot, F. O. Nitsche, Y. Nogi, O. A. Nost, S. V. Popov, E. Rignot, D. M. Rippin, A. Rivera, J. Roberts, N. Ross, M. J. Siegert, A. M. Smith, D. Steinhage, M. Studinger, B. Sun, B. K. Tinto, B. C. Welch, D. Wilson, D. A. Young, C. Xiangbin, and A. Zirizzotti. Bedmap2: improved ice bed, surface and thickness datasets for antarctica. *The Cryosphere*, 7:375–393, 2013.

K. Frieler, P. U. Clark, F. He, C. Buizert, R. Reese, S. R. M. Ligtenberg, M. R. van den Broeke, R. Winkelmann, and A. Levermann. Consistent evidence of increasing antarctic accumulation with warming. *Nature Climate Change*, 5:348 EP –, Mar 2015. URL https://doi.org/10.1038/nclimate2574.

O. Gagliardini, D. Cohen, P. Raback, and T. Zwinger. Finite-element modeling of subglacial cavities and related friction law. *J. Geophys. Res.*, 112(F2):n/a–n/a, 2007. doi: 10.1029/2006JF000576.

N. Gandy, L. J. Gregoire, J. C. Ely, S. L. Cornford, C. D. Clark, and D. M. Hodgson. Exploring the ingredients required to successfully model the placement, generation, and evolution of ice streams in the british-irish ice sheet. *Quaternary Science Reviews*, 223:105915, 2019. ISSN 0277-3791. doi: https://doi.org/10.1016/j.quascirev.2019.105915. URL http://www.sciencedirect.com/science/article/pii/S0277379119304962.

R. M. Gladstone, A. J. Payne, and S. L. Cornford. Parameterising the grounding line in ice sheet models. *The Cryosphere*, 4:605–619, 2010. doi: 10.5194/tc-4-605-2010.

S. Goeller, M. Thoma, K. Grosfeld, and H. Miller. A balanced water layer concept for subglacial hydrology in large-scale ice sheet models. *The Cryosphere*, 7(4):1095–1106, 2013. doi: 10.5194/tc-7-1095-2013. URL https://www.the-cryosphere.net/7/1095/2013/.

N. R. Golledge, D. E. Kowalewski, T. R. Naish, R. H. Levy, C. J. Fogwill, and E. G. W. Gasson. The multi-millennial antarctic commitment to future sea-level rise. *Nature*, 526:421–425, 2015.

G. H. Gudmundsson, J. Krug, G. Durand, L. Favier, and O. Gagliardini. The stability of grounding lines on retrograde slopes. *The Cryosphere Discuss.*, 6:2597–2619, 2012. doi: 10.5194/tcd-6-2597-2012.

C. Helanow, N. R. Iverson, J. B. Woodard, and L. K. Zoet. A slip law for hard-bedded glaciers derived from observed bed topography. *Science Advances*, 7(20), 2021. doi: 10.1126/sciadv.abe7798. URL https://advances.sciencemag.org/content/7/20/eabe7798.

R. C. A. Hindmarsh. On the numerical computation of temperature in an ice sheet. *J. Glaciol.*, 45(151):568–574, 1999.

R. C. A. Hindmarsh. Notes on basic glaciological computational methods and algorithms. In B. Straughan, R. Greve, H. Ehrentraut, and Y. Wang, editors, *Continuum Mechanics and Applications in Geophysics and the Environment*, pages 222–249. Springer Verlag, Berlin, 2001.

R. C. A. Hindmarsh. Stress gradient damping of thermoviscous ice flow instabilities. *Journal of Geophysical Research: Solid Earth*, 111(B12), 2006. ISSN 2156-2202. doi: 10.1029/2005JB004019. B12409.

R. C. A. Hindmarsh. Consistent generation of ice-streams via thermo-viscous instabilities modulated by membrane stresses. *Geophysical Research Letters*, 36(6), 2009. ISSN 1944-8007. doi: 10.1029/2008GL036877. L06502.

D. M. Holland and A. Jenkins. Modeling thermodynamic ice-ocean interactions at the base of an ice shelf. *J. Phys. Oceanogr.*, 29(8):1787–1800, 1999.

P. R. Holland, A. Jenkins, and D. M. Holland. The response of ice shelf basal melting to variations in ocean temperature. *Journal of Climate*, 21(11), 2008.

N. R. J. Hulton and M. J. Mineter. Modelling self-organization in ice streams. *Annals of Glaciology*, 30(1):127–136, 2000. doi: doi:10.3189/172756400781820561.

K. Hutter. *Theoretical Glaciology*. Dordrecht, Kluwer Academic Publishers, 1983.

P. Huybrechts. The Antarctic ice sheet and environmental change: a three-dimensional modelling study. *Berichte für Polarforschung*, 99:1–241, 1992.

P. Huybrechts and J. de Wolde. The dynamic response of the greenland and antarctic ice sheets to multiple-century climatic warming. *Journal of Climate*, 12(8):2169–2188, 1999.

P. Huybrechts, A. Payne, and The EISMINT Intercomparison Group. The EISMINT benchmarks for testing ice–sheet models. *Ann. Glaciol.*, 23:1–12, 1996.

P. Huybrechts, A. Abe-Ouchi, I. Marsiat, F. Pattyn, A. Payne, C. Ritz, and V. Rommelaere. *Report of the Third EISMINT Workshop on Model Intercomparison*. European Science Foundation (Strasbourg), 1998.

I. Janssens and P. Huybrechts. The treatment of meltwater retention in mass-balance parameterisations of the greenland ice sheet. *Annals of Glaciology*, 31:133–140, 2000.

A. Jenkins. A one-dimensional model of ice shelf-ocean interaction. *Journal of Geophysical Research: Oceans*, 96(C11):20671–20677, 1991. doi: 10.1029/91JC01842. URL https://agupubs.onlinelibrary.wiley.com/doi/abs/10.1029/91JC01842.

I. Joughin, B. E. Smith, and C. G. Schoof. Regularized coulomb friction laws for ice sheet sliding: Application to pine island glacier, antarctica. *Geophysical Research Letters*, 46 (9):4764–4771, 2019. doi: https://doi.org/10.1029/2019GL082526.

N. C. Jourdain, X. Asay-Davis, T. Hattermann, F. Straneo, H. Seroussi, C. M. Little, and S. Nowicki. A protocol for calculating basal melt rates in the ismip6 antarctic ice sheet projections. *The Cryosphere Discussions*, 2019:1–33, 2019. doi: 10.5194/tc-2019-277. URL https://www.the-cryosphere-discuss.net/tc-2019-277/.

R. F. Katz and M. G. Worster. Stability of ice-sheet grounding lines. *Proceedings of the Royal Society of London A: Mathematical, Physical and Engineering Sciences*, pages n/a–n/a, 2010. ISSN 1364-5021. doi: 10.1098/rspa.2009.0434.

W. M. J. Lazeroms, A. Jenkins, G. H. Gudmundsson, and R. S. W. van de Wal. Modelling present-day basal melt rates for antarctic ice shelves using a parametrization of buoyant meltwater plumes. *The Cryosphere*, 12(1):49–70, 2018. doi: 10.5194/tc-12-49-2018. URL https://www.the-cryosphere.net/12/49/2018/.

A. Le Brocq, A. Payne, M. Siegert, and R. Alley. A subglacial water-flow model for west antarctica. *Journal of Glaciology*, 55(193):879–888, 2009. doi: 10.3189/002214309790152564.

A. M. Le Brocq, A. J. Payne, and M. J. Siegert. West Antarctic balance calculations: Impact of flux-routing algorithm, smoothing algorithm and topography. *Computers and Geosciences*, 32:1780–1795, 2006.

A. Levermann, T. Albrecht, R. Winkelmann, M. A. Martin, M. Haseloff, and I. Joughin. Kinematic first-order calving law implies potential for abrupt ice-shelf retreat. *The Cryosphere*, 6(2):273–286, 2012. doi: 10.5194/tc-6-273-2012.

L. Lliboutry. A critical review of analytical approximate solutions for steady state velocities and temperatures in cold ice-sheets. *Zeitschrift für Gletscherkunde und Glazialgeologie*, 35(2):135–148, 1979.

M. Lüthi, M. Funk, A. Iken, S. Gogineni, and M. Truffer. Mechanisms of fast flow in jakobshavn isbræ, west greenland: Part iii. measurements of ice deformation, temperature and cross-borehole conductivity in boreholes to the bedrock. *Journal of Glaciology*, 48 (162):369–385, 2002. doi: 10.3189/172756502781831322.

Y. Ma, O. Gagliardini, C. Ritz, F. Gillet-Chaulet, G. Durand, and M. Montagnat. Enhancement factors for grounded ice and ice shelves inferred from an anisotropic ice-flow model. *Journal of Glaciology*, 56:805–812, Dec. 2010. doi: 10.3189/002214310794457209.

D. R. MacAyeal. Large-scale ice flow over a viscous basal sediment: Theory and application to Ice Stream B, Antarctica. *J. Geophys. Res*, 94(B4):4071–4087, 1989.

M. N. A. Maris, B. de Boer, S. R. M. Ligtenberg, M. Crucifix, W. J. van de Berg, and J. Oerlemans. Modelling the evolution of the antarctic ice sheet since the last interglacial. *The Cryosphere*, 8(4):1347–1360, 2014. doi: 10.5194/tc-8-1347-2014.

M. A. Martin, R. Winkelmann, M. Haseloff, T. Albrecht, E. Bueler, C. Khroulev, and A. Levermann. The potsdam parallel ice sheet model (pism-pik) part 2: Dynamic equilibrium simulation of the antarctic ice sheet. *The Cryosphere*, 5(3):727–740, 2011. doi: 10.5194/tc-5-727-2011.

L. Morland. Unconfined ice-shelf flow. In C. J. van der Veen and J. Oerlemans, editors, *Dynamics of the West Antarctica Ice Sheet*, pages 99–116. Kluwer Acad., Dordrecht, Netherlands, 1987.

M. Morlighem, E. Rignot, T. Binder, D. Blankenship, R. Drews, G. Eagles, O. Eisen, F. Ferraccioli, R. Forsberg, P. Fretwell, V. Goel, J. S. Greenbaum, H. Gudmundsson, J. Guo, V. Helm, C. Hofstede, I. Howat, A. Humbert, W. Jokat, N. B. Karlsson, W. S. Lee, K. Matsuoka, R. Millan, J. Mouginot, J. Paden, F. Pattyn, J. Roberts, S. Rosier, A. Ruppel, H. Seroussi, E. C. Smith, D. Steinhage, B. Sun, M. R. v. d. Broeke, T. D. v. Ommen, M. v. Wessem, and D. A. Young. Deep glacial troughs and stabilizing ridges unveiled beneath the margins of the antarctic ice sheet. *Nature Geoscience*, 2019. ISSN 1752-0908. doi: 10.1038/s41561-019-0510-8. URL `https://doi.org/10.1038/s41561-019-0510-8`.

D. Olbers and H. Hellmer. A box model of circulation and melting in ice shelf caverns. *Ocean Dynamics*, 60(1):141–153, Feb 2010. ISSN 1616-7228. doi: 10.1007/s10236-009-0252-z.

F. Pattyn. Grantism: An exceltm model for greenland and antarctic ice-sheet response to climate changes. *Comput. Geosci.*, 32(3):316–325, Apr. 2006. ISSN 0098-3004. doi: 10.1016/j.cageo.2005.06.020.

F. Pattyn. Antarctic subglacial conditions inferred from a hybrid ice sheet/ice stream model. *Earth Planet. Sci. Lett.*, 295:451–461, 2010.

F. Pattyn. Sea-level response to melting of Antarctic ice shelves on multi-centennial timescales with the fast Elementary Thermomechanical Ice Sheet model (f.ETISh v1.0). *The Cryosphere*, 11:1851–1878, 2017. doi: 10.5194/tc-11-1851-2017.

F. Pattyn and G. Durand. Why marine ice sheet model predictions may diverge in estimating future sea level rise. *Geophysical Research Letters*, 40(16):4316–4320, 2013. ISSN 1944-8007. doi: 10.1002/grl.50824.

F. Pattyn, S. De Brabander, and A. Huyghe. Basal and thermal control mechanisms of the Ragnhild glaciers, East Antarctica. *Ann. Glaciol.*, 40:225–231, 2005.

F. Pattyn, A. Huyghe, S. De Brabander, and B. De Smedt. Role of transition zones in marine ice sheet dynamics. *Journal of Geophysical Research: Earth Surface*, 111(F2):n/a–n/a, 2006. ISSN 2156-2202. doi: 10.1029/2005JF000394. F02004.

F. Pattyn, C. Schoof, L. Perichon, R. C. A. Hindmarsh, E. Bueler, B. de Fleurian, G. Durand, O. Gagliardini, R. Gladstone, D. Goldberg, G. H. Gudmundsson, P. Huybrechts, V. Lee, F. M. Nick, A. J. Payne, D. Pollard, O. Rybak, F. Saito, and A. Vieli. Results of the marine ice sheet model intercomparison project, mismip. *The Cryosphere*, 6(3):573–588, 2012. doi: 10.5194/tc-6-573-2012.

F. Pattyn, L. Perichon, G. Durand, L. Favier, O. Gagliardini, R. C. Hindmarsh, T. Zwinger, T. Albrecht, S. Cornford, D. Docquier, J. J. Fürst, D. Goldberg, G. H. Gudmundsson, A. Humbert, M. Hütten, P. Huybrechts, G. Jouvet, T. Kleiner, E. Larour, D. Martin, M. Morlighem, A. J. Payne, D. Pollard, M. Rückamp, O. Rybak, H. Seroussi, M. Thoma, and N. Wilkens. Grounding-line migration in plan-view marine ice-sheet models: results of the ice2sea mismip3d intercomparison. *Journal of Glaciology*, 59(215):410–422, 2013. doi: 10.3189/2013JoG12J129.

A. J. Payne and P. W. Dongelmans. Self-organisation in the thermomechanical flow of ice sheets. *J. Geophys. Res.*, 102(B6):12219–12234, 1997.

A. J. Payne, P. Huybrechts, A. Abe-Ouchi, R. Calov, J. L. Fastook, R. Greve, S. J. Marshall, I. Marsiat, C. Ritz, L. Tarasov, and M. Thomassen. Results from the EISMINT model intercomparsion: the effects of thermomechanical coupling. *J. Glaciol.*, 46(153):227–238, 2000.

T. Pelle, M. Morlighem, and J. H. Bondzio. Brief communication: Picop, a new ocean melt parameterization under ice shelves combining pico and a plume model. *The Cryosphere*, 13(3):1043–1049, 2019. doi: 10.5194/tc-13-1043-2019. URL `https://www.the-cryosphere.net/13/1043/2019/`.

D. Pollard and R. M. DeConto. Modelling West Antarctic ice sheet growth and collapse through the past five million years. *Nature*, 458:329–332, 2009. doi: 10.1038/nature07809.

D. Pollard and R. M. DeConto. Description of a hybrid ice sheet-shelf model, and application to Antarctica. *Geosci. Model Dev.*, 5:1273–1295, 2012a. doi: 10.5194/gmd-5-1273-2012.

D. Pollard and R. M. DeConto. A simple inverse method for the distribution of basal sliding coefficients under ice sheets, applied to antarctica. *The Cryosphere*, 6(5):953–971, 2012b. doi: 10.5194/tc-6-953-2012.

D. Pollard, R. M. DeConto, and R. B. Alley. Potential antarctic ice sheet retreat driven by hydrofracturing and ice cliff failure. *Earth and Planetary Science Letters*, 412:112 – 121, 2015.

M. Purucker. *Geothermal heat flux data set based on low resolution observations collected by the CHAMP satellite between 2000 and 2010, and produced from the MF-6 model following the technique described in Fox Maule et al. (2005).* http://websrv.cs.umt.edu/isis/index.php, 2013.

A. Quiquet, C. Dumas, C. Ritz, V. Peyaud, and D. M. Roche. The grisli ice sheet model (version 2.0): calibration and validation for multi-millennial changes of the antarctic ice sheet. *Geoscientific Model Development Discussions*, 2018:1–35, 2018. doi: 10.5194/gmd-2018-105. URL `https://www.geosci-model-dev-discuss.net/gmd-2018-105/`.

N. Reeh. Parameterization of melt rate and surface temperature on the greenland ice sheet. *Polarforschung*, 59(3):113–128, 1989.

R. Reese, T. Albrecht, M. Mengel, X. Asay-Davis, and R. Winkelmann. Antarctic subshelf melt rates via pico. *The Cryosphere*, 12(6):1969–1985, 2018a. doi: 10.5194/tc-12-1969-2018.

R. Reese, R. Winkelmann, and G. H. Gudmundsson. Grounding-line flux formula applied as a flux condition in numerical simulations fails for buttressed antarctic ice streams. *The Cryosphere*, 12(10):3229–3242, 2018b. doi: 10.5194/tc-12-3229-2018. URL `https://www.the-cryosphere.net/12/3229/2018/`.

E. Rignot, J. Mouginot, and B. Scheuchl. Ice flow of the antarctic ice sheet. *Science*, 333 (6048):1427–1430, 2011.

C. Ritz. Time dependent boundary conditions for calculation of temperature fields in ice sheets. *IAHS Publ.*, 170:207–216, 1987.

C. Ritz. *Un Modèle Thermo-Mèchanique d'Evolution pour le Bassin Glaciaire Antarctique Vostok-Glacier Byrd: Sensibilité aux Valeurs des Paramètres Mal Connus*. PhD Thesis, Univ. J. Fourier, 1992.

C. Ritz, d. G. D. T. L. Edwards a, A. J. Payne, V. Peyaud, and R. C. A. Hindmarsh. Potential sea-level rise from Antarctic ice-sheet instability constrained by observations. *Nature*, 528:115–118, 2015. doi: 10.1038/nature16147.

V. Rommelaere and C. Ritz. A thermomechanical model of ice-shelf flow. *Annals of Glaciology*, 23:13–20, 1996.

S. Schmidtko, K. J. Heywood, A. F. Thompson, and S. Aoki. Multidecadal warming of antarctic waters. *Science*, 346(6214):1227–1231, 2014. ISSN 0036-8075. doi: 10.1126/science.1256117.

C. Schoof. The effect of cavitation on glacier sliding. *Proc. R. Soc. Lond. A*, 461:609–627, 2005. doi: 10.1098/rspa.2004.1350.

C. Schoof. Ice sheet grounding line dynamics: Steady states, stability, and hysteresis. *Journal of Geophysical Research: Earth Surface*, 112(F3):n/a–n/a, 2007a. ISSN 2156-2202. doi: 10.1029/2006JF000664. F03S28.

C. Schoof. Marine ice sheet dynamics. Part I. The case of rapid sliding. *J. Fluid Mech.*, 573:27–55, 2007b.

C. Schoof. Marine ice sheet dynamics. Part 2. A Stokes flow contact problem. *J. Fluid Mech.*, 679:122–155, 2011.

N. M. Shapiro and M. H. Ritzwoller. Inferring surface heat flux distributions guided by a global seismic model: Particular application to Antarctica. *Earth and Planetary Science Letters*, 223:213–224, 2004.

G. Stokes. On the theories of internal friction of fluids in motion. *Trans. Cambridge Philos. Soc.*, 8:287–305, 1845.

V. C. Tsai, A. L. Stewart, and A. F. Thompson. Marine ice-sheet profiles and stability under coulomb basal conditions. *Journal of Glaciology*, 61(226):205–215, 2015. doi: doi:10.3189/2015JoG14J221.

S. M. Tulaczyk, B. Kamb, and H. F. Engelhardt. Basal mechanics of Ice Stream B, West Antarctica. I. till mechanics. *J. Geophys. Res.*, 105(B1):463–481, 2000.

N. van der Wel, P. Christoffersen, and M. Bougamont. The influence of subglacial hydrology on the flow of kamb ice stream, west antarctica. *Journal of Geophysical Research: Earth Surface*, 118(1):97–110, 2013. doi: 10.1029/2012JF002570. URL `https://agupubs.onlinelibrary.wiley.com/doi/abs/10.1029/2012JF002570`.

W. J. Van Pelt and J. Oerlemans. Numerical simulations of cyclic behaviour in the parallel ice sheet model (pism). *Journal of Glaciology*, 58(208):347–360, 2012. doi: 10.3189/2012JoG11J217.

J. Van Wessem, C. Reijmer, M. Morlighem, J. Mouginot, E. Rignot, B. Medley, I. Joughin, B. Wouters, M. Depoorter, J. Bamber, J. Lenaerts, W. De Van Berg, M. Van Den Broeke, and E. Van Meijgaard. Improved representation of east antarctic surface mass balance in a regional atmospheric climate model. *Journal of Glaciology*, 60(222):761–770, 2014. ISSN 0022-1430. doi: doi:10.3189/2014JoG14J051.

J. Weertman. Effect of a basal water layer on the dimensions of ice sheets. *Journal of Glaciology*, 6(44):191–207, 1966. doi: 10.3189/S0022143000019213.

R. Winkelmann, M. A. Martin, M. Haseloff, T. Albrecht, E. Bueler, C. Khroulev, and A. Levermann. The Potsdam Parallel Ice Sheet Model (PISM-PIK) Part 1: Model description. *The Cryosphere*, 5:715–726, 2011.

L. K. Zoet and N. R. Iverson. A slip law for glaciers on deformable beds. *Science*, 368 (6486):76–78, 2020. ISSN 0036-8075. doi: 10.1126/science.aaz1183. URL `https://science.sciencemag.org/content/368/6486/76`.

A Variables and constants

Symbol	Description	Units	Value
$\dot{a}$	Surface mass balance (SMB)	m a^{-1}	
A	Glen's flow law factor	Pa^{-n} a^{-1}	
A_b, A'_b	Basal sliding factor in power-law sliding	Pa^{-m} m a^{-1}	
A_{froz}	Basal sliding factor for frozen conditions	Pa^{-m} m a^{-1}	
b	Bedrock elevation	m	
$\dot{b}$	Basal melt rate (grounded ice)	m a^{-1}	
b_f	Buttressing factor		0–1
c_p	Specific heat of ice	J kg^{-1} K^{-1}	2009
c_{po}	Specific heat of seawater	J kg^{-1} K^{-1}	3974
C	Overturning strength	m^6 s^{-1} kg^{-1}	1×10^6
C_c	Till compressibility		
C_d	Drag coefficient		2.5×10^{-3}
$C_d^{1/2}\Gamma_T$	Turbulent heat exchange coefficient		6×10^{-4}
$C_d^{1/2}\Gamma_{TS_0}$	Heat exchange parameter		1.1×10^{-3}
C_r	Calving rate	m a^{-1}	
C_t	Till drainage rate	m a^{-1}	
c_0	Till cohesion	Pa	0
d	Diffusion coefficient grounded ice sheet	m^2 a^{-1}	
d_w	Subglacial water layer thickness	m	
D	Flexural rigidity of lithosphere	N m	10^{25}
e, e_0	Sediment void ratio and reference ratio		
E_0	Entrainment coefficient		3.6×10^{-2}
E_f	Adjustment factor in Arrhenius equation		0.1–1
f_g	Fractional area of shelf grid contact with bed		0–1
g	Gravitational acceleration	m s^{-2}	9.81
G	Geothermal heat flux	W m^{-2}	
h	Ice thickness	m	
h_b	Bottom of ice sheet/ice shelf	m	
h_e	Subgrid ice thickness on ice shelf edge	m	
h_g	Interpolated ice thickness at grounding line	m	
h_s	Ice sheet surface	m	
h_w	Water column thickness under ice shelf	m	
K	Thermal conductivity	J m^{-1} s^{-1} K^{-1}	2.1
L	Latent heat of fusion	J kg^{-1}	3.35×10^5
L_w	Flexural length scale of the lithosphere		
m	Exponent in basal sliding law		1–3
M	Basal melting rate under ice shelves/ice sheet	m a^{-1}	
M_0	Melt rate parameter	m a^{-1} °C^{-1}	10
n	Glen's flow law exponent		3
n_x, n_y	Outward pointing normal vectors in x and y		
N	Effective basal pressure	Pa	

Table 4: Model symbols, units and nominal values

Symbol	Description	Units	Value
P	Precipitation rate (accumulation)	m a^{-1}	
p	Exponent of the effective pressure		0–1
p_r	Power of velocity shape function		
p_o	Ice overburden pressure	Pa	
p_w	Subglacial water pressure	Pa	
P_w	Fraction of subglacial water pressure		0–1
P_b	Point load on bedrock		
q	Exponent in Coulomb friction law		0–1
q_b	Bedrock load	Pa	
q_g	Ice flux at the grounding line	m^2 a^{-1}	
Q_o	Numerical coefficient in Tsai et al. [2015]		0.61
r	Scaling factor in sliding law		0–1
R	Gas constant	J kg^{-1} mol^{-1}	8.314
S	Surface melt rate	m a^{-1}	
S_o	Ocean salinity	psu	35
T	Mean ice column temperature	K	
T_{fo}	Ocean freezing temperature	K	271.03
T_m	Pressure melting temperature	K	
T_{oc}	Ocean temperature	°C	
T_r	Temperature at which basal sliding starts	°C	
T_s	Surface temperature	K	
$T^\star$	Homologous temperature	K	
ΔT	Background temperature forcing	°C	
δT	Scaling factor in mass balance forcing	°C	10
u	Horizontal ice velocities in x direction	m a^{-1}	
u_b	Basal velocity in x direction	m a^{-1}	
u_g	Velocity at the grounding line [e.g., Schoof, 2007a]	m a^{-1}	
u_0	Limit velocity in Coulomb friction law	m a^{-1}	100
v	Horizontal ice velocities in y direction	m a^{-1}	
v_b	Basal velocity in y direction	m a^{-1}	
$\vec{v}$	Vertical mean horizontal velocity	m a^{-1}	
$\vec{v}_b$	Horizontal basal velocity	m a^{-1}	
$\vec{v}_d$	Horizontal deformational velocity	m a^{-1}	
W	Saturated till layer thickness	m	
$W_{\max}$	Maximum saturated till layer thickness	m	2
w	Vertical ice velocity	m a^{-1}	
w_b	Lithospheric deflection		
w_c	Weighting factor in calving law		0–1
w_p	Response to point load on bedrock		
x, y	Orthogonal horizontal coordinates	m	
x_0	Dimensionless scaling factor		0.56
z	Vertical elevation	m	
z_{sl}	Sea level elevation	m	0

Table 5: Model symbols, units and nominal values (continued)

Symbol	Description	Units	Value
β^2	Basal friction coefficient		
γ	Atmospheric lapse rate	°C m^{-1}	0.008
γ_T	Thermal exchange velocity	m s^{-1} K^{-1}	
δ	Fraction of ice overburden pressure		0.02
Δ	Grid cell size, equal in x and y directions	m	
$\dot{\varepsilon}_0$	Minimum strain rate in effective viscosity	a^{-1}	10^{-20}
η	Effective viscosity	Pa a	
κ	Thermal diffusivity	m^2 s^{-1}	1.1487×10^{-6}
λ_1	Freezing point–salinity coefficient	K psu^{-1}	-5.73 $\times 10^{-2}$
λ_2	Freezing point offset	K	8.32 $\times 10^{-2}$
λ_3	Freezing point–depth coefficient	K m^{-1}	7.61 $\times 10^{-4}$
ν	Poisson ratio of the lithosphere		0.25
μ	Water viscosity	Pa s	1.8 $\times 10^{-3}$
ρ_b	Upper mantle density	kg m^{-3}	3370
ρ_i	Ice density	kg m^{-3}	917
ρ_s	Ocean water density	kg m^{-3}	1027
ρ_w	Water density	kg m^{-3}	1000
ω	Crank-Nicholson implicit factor		2.5
ϕ	Till friction angle	deg	
Φ	Hydraulic potential	Pa	
Φ_d	Deformational heating		
Φ_0	Limit on hydraulic potential	Pa	10^5
σ_b	Standard deviation of bedrock variability		
Θ	Buttressing at grounding line		$[0, 1]$
θ	Ice temperature	K	
θ_b	Basal temperature	K	
θ_b^s	Basal temperature of the ice shelf	K	
τ_b	Basal drag	Pa	
τ_c	Coulomb stress	Pa	
τ_d	Driving stress	Pa	
τ_f	Free-water tensile stress	Pa	
τ_{xx}, τ_{yy}	Longitudinal stress in x and y	Pa	
τ_w	Relaxation time for lithospheric response	a	3000
ζ	Scaled vertical coordinate		$[0, 1]$

Table 6: Model symbols, units and nominal values (continued)

B Version history since *f.ETISh v1.0*

- Weighting factor on grounding line flux condition that does not allow the GL flux to be used when bed is shallow or above sea level (ncorx and ncory)
- Initialization: regularization only applied for marine basins (according to weighting factor in Schoof flux - unrelated)
- Optimization of PDD model
- Implementation of PICO ocean box model for melting under ice shelves
- Inclusion of ocean temperature To and salinity So as boundary conditions (input data set)
- Use of effective lithosphere thickness to derive spatially varying flexural rigidity of lithosphere in bedrock deformation module
- Changes in configuration of options in MbFunc and TsFunc
- Addition of 'restart' to allow the model to restart from a previous dumpfile 'toto'
- Removal of grounding line wedge 'GLwedge'
- Inclusion of vertical cliff melting (FMB) following Pollard and DeConto [2012a]
- Less output graphics (only two graphs are shown during/at end of model run)
- New time-dependent parameters, such as ice volume, grounded ice area, floating ice area, float ice volume, etc.
- Bed adjustment invoked every intT iterations (as temperature).
- Recoding of sparse matrices of SSA velocity field according to Rommelaere and Ritz; improvement on iterative scheme for nonlinear term.
- Renaming of some variables that may be confused with existing Matlab routines.
- PICO model called every intT iterations; interpolated melt calculated inbetween calls
- Add copy of Bedmap2/BedMachine bed and ice thickness (Bo and Ho) as reference for multiple initialization steps. Corrected that MB-elevation feedback and optimization uses this reference surface (Bo+Ho) instead of surface from previous input (important for paleo runs)
- Correction on 'ocean'/'sea ice' viscosity eta; model now requires a thin layer of sea ice (not ice thickness zero) to function
- Inclusion of Pollard (2015) calving law and hydrofracturing using surface melt defined from PDD model. In absence of hydrofracturing, CMB only applied at calving front.
- Further optimization of grounding line flux and ice thickness solver to speed up model runs using upstream differences for SSA and an over-implicit Crank-Nicholson scheme

- Subglacial hydrology implemented based on a Le Brocq/Alley approach
- Calculation of subglacial melt underneath grounded ice sheet
- Spatial variations in flexural rigidity (based on effective lithosphere thickness) and spatial variations in relaxation time based on upper mantle viscosity. Kelvin functions are defined for different Db classes for computational efficiency
- Implementation of PICOP model (combined box and plume model for sub-shelf melting) and plume model
- Addition of SLC due to bedrock adjustment (Heiko method - Vio)
- Major bug in restart corrected (Vio)
- Inclusion of sea-level fingerprinting based on self-gravitation - defines local sea level instead of global sea level
- New parameter 'diagnostic' to run model without ice-thickness evolution
- Homogenized use of parameters in different melt function and melt models
- Generalization of sliding and friction laws with introduction of effective pressure in Weertman sliding law
- Subglacial till model (Bueler and Van Pelt, 2015)
- New call of FetishModel with control file, input and output file
- Glacial-isostatic adjustment: full derivation of non-local effective lithosphere thickness
- Local sea level (geoid) implementation
- Implementation of starttime + output of initial conditions (nsteps should preferably be nsteps+1)
- Default ctr values do not need to be defined in run file
- Implementation of Crameri color scheme instead of Brewermap
- No linearization in beta2 (now function of u instead of taud)
- Renaming of different velocities (u, ub, ud) and their vectors (ux,uy; udx,udy; ubx,uby), SSA velocity (uxssa,uyssa), Schoof-corrected velocity (uxsch,uysch), the latter used for solving H
- Choice between advection/diffusion solving for SSA=2 via par.SSAdiffus
- Thermomechanical coupling based on Lliboutry (1976) and Ritz (1992)
- Expansion of default values originally in FetishInputParams
- Corrections on geodynamics

- Application on MISMIP+ and MISMIP3d geometry: ctr.mismip=1
- Application to single or mutiple basins of an ice sheet: ctr.basin=1
- Corrections on velocity field (upstream differences)
- Major correction on ctr.schoof based on Pollard and DeConto (2020)

C GNU GENERAL PUBLIC LICENSE

Version 3, 29 June 2007

Preamble

The GNU General Public License is a free, copyleft license for software and other kinds of works.

The licenses for most software and other practical works are designed to take away your freedom to share and change the works. By contrast, the GNU General Public License is intended to guarantee your freedom to share and change all versions of a program–to make sure it remains free software for all its users. We, the Free Software Foundation, use the GNU General Public License for most of our software; it applies also to any other work released this way by its authors. You can apply it to your programs, too.

When we speak of free software, we are referring to freedom, not price. Our General Public Licenses are designed to make sure that you have the freedom to distribute copies of free software (and charge for them if you wish), that you receive source code or can get it if you want it, that you can change the software or use pieces of it in new free programs, and that you know you can do these things.

To protect your rights, we need to prevent others from denying you these rights or asking you to surrender the rights. Therefore, you have certain responsibilities if you distribute copies of the software, or if you modify it: responsibilities to respect the freedom of others.

For example, if you distribute copies of such a program, whether gratis or for a fee, you must pass on to the recipients the same freedoms that you received. You must make sure that they, too, receive or can get the source code. And you must show them these terms so they know their rights.

Developers that use the GNU GPL protect your rights with two steps: (1) assert copyright on the software, and (2) offer you this License giving you legal permission to copy, distribute and/or modify it.

For the developers' and authors' protection, the GPL clearly explains that there is no warranty for this free software. For both users' and authors' sake, the GPL requires that modified versions be marked as changed, so that their problems will not be attributed erroneously to authors of previous versions.

Some devices are designed to deny users access to install or run modified versions of the software inside them, although the manufacturer can do so. This is fundamentally incompatible with the aim of protecting users' freedom to change the software. The systematic pattern of such abuse occurs in the area of products for individuals to use, which is precisely where it is most unacceptable. Therefore, we have designed this version of the GPL to prohibit the practice for those products. If such problems arise substantially in other domains, we stand ready to extend this provision to those domains in future versions of the GPL, as needed to protect the freedom of users.

Finally, every program is threatened constantly by software patents. States should not allow patents to restrict development and use of software on general-purpose computers, but in those that do, we wish to avoid the special danger that patents applied to

a free program could make it effectively proprietary. To prevent this, the GPL assures that patents cannot be used to render the program non-free.

The precise terms and conditions for copying, distribution and modification follow.

TERMS AND CONDITIONS

0. Definitions.

"This License" refers to version 3 of the GNU General Public License.

"Copyright" also means copyright-like laws that apply to other kinds of works, such as semiconductor masks.

"The Program" refers to any copyrightable work licensed under this License. Each licensee is addressed as "you". "Licensees" and "recipients" may be individuals or organizations.

To "modify" a work means to copy from or adapt all or part of the work in a fashion requiring copyright permission, other than the making of an exact copy. The resulting work is called a "modified version" of the earlier work or a work "based on" the earlier work.

A "covered work" means either the unmodified Program or a work based on the Program.

To "propagate" a work means to do anything with it that, without permission, would make you directly or secondarily liable for infringement under applicable copyright law, except executing it on a computer or modifying a private copy. Propagation includes copying, distribution (with or without modification), making available to the public, and in some countries other activities as well.

To "convey" a work means any kind of propagation that enables other parties to make or receive copies. Mere interaction with a user through a computer network, with no transfer of a copy, is not conveying.

An interactive user interface displays "Appropriate Legal Notices" to the extent that it includes a convenient and prominently visible feature that (1) displays an appropriate copyright notice, and (2) tells the user that there is no warranty for the work (except to the extent that warranties are provided), that licensees may convey the work under this License, and how to view a copy of this License. If the interface presents a list of user commands or options, such as a menu, a prominent item in the list meets this criterion.

1. Source Code.

The "source code" for a work means the preferred form of the work for making modifications to it. "Object code" means any non-source form of a work.

A "Standard Interface" means an interface that either is an official standard defined by a recognized standards body, or, in the case of interfaces specified for a particular programming language, one that is widely used among developers working in that language.

The "System Libraries" of an executable work include anything, other than the work as a whole, that (a) is included in the normal form of packaging a Major Component, but which is not part of that Major Component, and (b) serves only to enable use of the

work with that Major Component, or to implement a Standard Interface for which an implementation is available to the public in source code form. A "Major Component", in this context, means a major essential component (kernel, window system, and so on) of the specific operating system (if any) on which the executable work runs, or a compiler used to produce the work, or an object code interpreter used to run it.

The "Corresponding Source" for a work in object code form means all the source code needed to generate, install, and (for an executable work) run the object code and to modify the work, including scripts to control those activities. However, it does not include the work's System Libraries, or general-purpose tools or generally available free programs which are used unmodified in performing those activities but which are not part of the work. For example, Corresponding Source includes interface definition files associated with source files for the work, and the source code for shared libraries and dynamically linked subprograms that the work is specifically designed to require, such as by intimate data communication or control flow between those subprograms and other parts of the work.

The Corresponding Source need not include anything that users can regenerate automatically from other parts of the Corresponding Source.

The Corresponding Source for a work in source code form is that same work.

2. Basic Permissions.

   All rights granted under this License are granted for the term of copyright on the Program, and are irrevocable provided the stated conditions are met. This License explicitly affirms your unlimited permission to run the unmodified Program. The output from running a covered work is covered by this License only if the output, given its content, constitutes a covered work. This License acknowledges your rights of fair use or other equivalent, as provided by copyright law.

   You may make, run and propagate covered works that you do not convey, without conditions so long as your license otherwise remains in force. You may convey covered works to others for the sole purpose of having them make modifications exclusively for you, or provide you with facilities for running those works, provided that you comply with the terms of this License in conveying all material for which you do not control copyright. Those thus making or running the covered works for you must do so exclusively on your behalf, under your direction and control, on terms that prohibit them from making any copies of your copyrighted material outside their relationship with you.

   Conveying under any other circumstances is permitted solely under the conditions stated below. Sublicensing is not allowed; section 10 makes it unnecessary.

3. Protecting Users' Legal Rights From Anti-Circumvention Law.

   No covered work shall be deemed part of an effective technological measure under any applicable law fulfilling obligations under article 11 of the WIPO copyright treaty adopted on 20 December 1996, or similar laws prohibiting or restricting circumvention of such measures.

   When you convey a covered work, you waive any legal power to forbid circumvention of technological measures to the extent such circumvention is effected by exercising

rights under this License with respect to the covered work, and you disclaim any intention to limit operation or modification of the work as a means of enforcing, against the work's users, your or third parties' legal rights to forbid circumvention of technological measures.

4. Conveying Verbatim Copies.

   You may convey verbatim copies of the Program's source code as you receive it, in any medium, provided that you conspicuously and appropriately publish on each copy an appropriate copyright notice; keep intact all notices stating that this License and any non-permissive terms added in accord with section 7 apply to the code; keep intact all notices of the absence of any warranty; and give all recipients a copy of this License along with the Program.

   You may charge any price or no price for each copy that you convey, and you may offer support or warranty protection for a fee.

5. Conveying Modified Source Versions.

   You may convey a work based on the Program, or the modifications to produce it from the Program, in the form of source code under the terms of section 4, provided that you also meet all of these conditions:

   (a) The work must carry prominent notices stating that you modified it, and giving a relevant date.

   (b) The work must carry prominent notices stating that it is released under this License and any conditions added under section 7. This requirement modifies the requirement in section 4 to "keep intact all notices".

   (c) You must license the entire work, as a whole, under this License to anyone who comes into possession of a copy. This License will therefore apply, along with any applicable section 7 additional terms, to the whole of the work, and all its parts, regardless of how they are packaged. This License gives no permission to license the work in any other way, but it does not invalidate such permission if you have separately received it.

   (d) If the work has interactive user interfaces, each must display Appropriate Legal Notices; however, if the Program has interactive interfaces that do not display Appropriate Legal Notices, your work need not make them do so.

   A compilation of a covered work with other separate and independent works, which are not by their nature extensions of the covered work, and which are not combined with it such as to form a larger program, in or on a volume of a storage or distribution medium, is called an "aggregate" if the compilation and its resulting copyright are not used to limit the access or legal rights of the compilation's users beyond what the individual works permit. Inclusion of a covered work in an aggregate does not cause this License to apply to the other parts of the aggregate.

6. Conveying Non-Source Forms.

   You may convey a covered work in object code form under the terms of sections 4 and 5, provided that you also convey the machine-readable Corresponding Source under the terms of this License, in one of these ways:

(a) Convey the object code in, or embodied in, a physical product (including a physical distribution medium), accompanied by the Corresponding Source fixed on a durable physical medium customarily used for software interchange.

(b) Convey the object code in, or embodied in, a physical product (including a physical distribution medium), accompanied by a written offer, valid for at least three years and valid for as long as you offer spare parts or customer support for that product model, to give anyone who possesses the object code either (1) a copy of the Corresponding Source for all the software in the product that is covered by this License, on a durable physical medium customarily used for software interchange, for a price no more than your reasonable cost of physically performing this conveying of source, or (2) access to copy the Corresponding Source from a network server at no charge.

(c) Convey individual copies of the object code with a copy of the written offer to provide the Corresponding Source. This alternative is allowed only occasionally and noncommercially, and only if you received the object code with such an offer, in accord with subsection 6b.

(d) Convey the object code by offering access from a designated place (gratis or for a charge), and offer equivalent access to the Corresponding Source in the same way through the same place at no further charge. You need not require recipients to copy the Corresponding Source along with the object code. If the place to copy the object code is a network server, the Corresponding Source may be on a different server (operated by you or a third party) that supports equivalent copying facilities, provided you maintain clear directions next to the object code saying where to find the Corresponding Source. Regardless of what server hosts the Corresponding Source, you remain obligated to ensure that it is available for as long as needed to satisfy these requirements.

(e) Convey the object code using peer-to-peer transmission, provided you inform other peers where the object code and Corresponding Source of the work are being offered to the general public at no charge under subsection 6d.

A separable portion of the object code, whose source code is excluded from the Corresponding Source as a System Library, need not be included in conveying the object code work.

A "User Product" is either (1) a "consumer product", which means any tangible personal property which is normally used for personal, family, or household purposes, or (2) anything designed or sold for incorporation into a dwelling. In determining whether a product is a consumer product, doubtful cases shall be resolved in favor of coverage. For a particular product received by a particular user, "normally used" refers to a typical or common use of that class of product, regardless of the status of the particular user or of the way in which the particular user actually uses, or expects or is expected to use, the product. A product is a consumer product regardless of whether the product has substantial commercial, industrial or non-consumer uses, unless such uses represent the only significant mode of use of the product.

"Installation Information" for a User Product means any methods, procedures, authorization keys, or other information required to install and execute modified versions

of a covered work in that User Product from a modified version of its Corresponding Source. The information must suffice to ensure that the continued functioning of the modified object code is in no case prevented or interfered with solely because modification has been made.

If you convey an object code work under this section in, or with, or specifically for use in, a User Product, and the conveying occurs as part of a transaction in which the right of possession and use of the User Product is transferred to the recipient in perpetuity or for a fixed term (regardless of how the transaction is characterized), the Corresponding Source conveyed under this section must be accompanied by the Installation Information. But this requirement does not apply if neither you nor any third party retains the ability to install modified object code on the User Product (for example, the work has been installed in ROM).

The requirement to provide Installation Information does not include a requirement to continue to provide support service, warranty, or updates for a work that has been modified or installed by the recipient, or for the User Product in which it has been modified or installed. Access to a network may be denied when the modification itself materially and adversely affects the operation of the network or violates the rules and protocols for communication across the network.

Corresponding Source conveyed, and Installation Information provided, in accord with this section must be in a format that is publicly documented (and with an implementation available to the public in source code form), and must require no special password or key for unpacking, reading or copying.

7. Additional Terms.

"Additional permissions" are terms that supplement the terms of this License by making exceptions from one or more of its conditions. Additional permissions that are applicable to the entire Program shall be treated as though they were included in this License, to the extent that they are valid under applicable law. If additional permissions apply only to part of the Program, that part may be used separately under those permissions, but the entire Program remains governed by this License without regard to the additional permissions.

When you convey a copy of a covered work, you may at your option remove any additional permissions from that copy, or from any part of it. (Additional permissions may be written to require their own removal in certain cases when you modify the work.) You may place additional permissions on material, added by you to a covered work, for which you have or can give appropriate copyright permission.

Notwithstanding any other provision of this License, for material you add to a covered work, you may (if authorized by the copyright holders of that material) supplement the terms of this License with terms:

(a) Disclaiming warranty or limiting liability differently from the terms of sections 15 and 16 of this License; or

(b) Requiring preservation of specified reasonable legal notices or author attributions in that material or in the Appropriate Legal Notices displayed by works containing it; or

(c) Prohibiting misrepresentation of the origin of that material, or requiring that modified versions of such material be marked in reasonable ways as different from the original version; or

(d) Limiting the use for publicity purposes of names of licensors or authors of the material; or

(e) Declining to grant rights under trademark law for use of some trade names, trademarks, or service marks; or

(f) Requiring indemnification of licensors and authors of that material by anyone who conveys the material (or modified versions of it) with contractual assumptions of liability to the recipient, for any liability that these contractual assumptions directly impose on those licensors and authors.

All other non-permissive additional terms are considered "further restrictions" within the meaning of section 10. If the Program as you received it, or any part of it, contains a notice stating that it is governed by this License along with a term that is a further restriction, you may remove that term. If a license document contains a further restriction but permits relicensing or conveying under this License, you may add to a covered work material governed by the terms of that license document, provided that the further restriction does not survive such relicensing or conveying.

If you add terms to a covered work in accord with this section, you must place, in the relevant source files, a statement of the additional terms that apply to those files, or a notice indicating where to find the applicable terms.

Additional terms, permissive or non-permissive, may be stated in the form of a separately written license, or stated as exceptions; the above requirements apply either way.

8. Termination.

You may not propagate or modify a covered work except as expressly provided under this License. Any attempt otherwise to propagate or modify it is void, and will automatically terminate your rights under this License (including any patent licenses granted under the third paragraph of section 11).

However, if you cease all violation of this License, then your license from a particular copyright holder is reinstated (a) provisionally, unless and until the copyright holder explicitly and finally terminates your license, and (b) permanently, if the copyright holder fails to notify you of the violation by some reasonable means prior to 60 days after the cessation.

Moreover, your license from a particular copyright holder is reinstated permanently if the copyright holder notifies you of the violation by some reasonable means, this is the first time you have received notice of violation of this License (for any work) from that copyright holder, and you cure the violation prior to 30 days after your receipt of the notice.

Termination of your rights under this section does not terminate the licenses of parties who have received copies or rights from you under this License. If your rights have been terminated and not permanently reinstated, you do not qualify to receive new licenses for the same material under section 10.

9. Acceptance Not Required for Having Copies.

   You are not required to accept this License in order to receive or run a copy of the Program. Ancillary propagation of a covered work occurring solely as a consequence of using peer-to-peer transmission to receive a copy likewise does not require acceptance. However, nothing other than this License grants you permission to propagate or modify any covered work. These actions infringe copyright if you do not accept this License. Therefore, by modifying or propagating a covered work, you indicate your acceptance of this License to do so.

10. Automatic Licensing of Downstream Recipients.

    Each time you convey a covered work, the recipient automatically receives a license from the original licensors, to run, modify and propagate that work, subject to this License. You are not responsible for enforcing compliance by third parties with this License.

    An "entity transaction" is a transaction transferring control of an organization, or substantially all assets of one, or subdividing an organization, or merging organizations. If propagation of a covered work results from an entity transaction, each party to that transaction who receives a copy of the work also receives whatever licenses to the work the party's predecessor in interest had or could give under the previous paragraph, plus a right to possession of the Corresponding Source of the work from the predecessor in interest, if the predecessor has it or can get it with reasonable efforts.

    You may not impose any further restrictions on the exercise of the rights granted or affirmed under this License. For example, you may not impose a license fee, royalty, or other charge for exercise of rights granted under this License, and you may not initiate litigation (including a cross-claim or counterclaim in a lawsuit) alleging that any patent claim is infringed by making, using, selling, offering for sale, or importing the Program or any portion of it.

11. Patents.

    A "contributor" is a copyright holder who authorizes use under this License of the Program or a work on which the Program is based. The work thus licensed is called the contributor's "contributor version".

    A contributor's "essential patent claims" are all patent claims owned or controlled by the contributor, whether already acquired or hereafter acquired, that would be infringed by some manner, permitted by this License, of making, using, or selling its contributor version, but do not include claims that would be infringed only as a consequence of further modification of the contributor version. For purposes of this definition, "control" includes the right to grant patent sublicenses in a manner consistent with the requirements of this License.

    Each contributor grants you a non-exclusive, worldwide, royalty-free patent license under the contributor's essential patent claims, to make, use, sell, offer for sale, import and otherwise run, modify and propagate the contents of its contributor version.

    In the following three paragraphs, a "patent license" is any express agreement or commitment, however denominated, not to enforce a patent (such as an express permission to practice a patent or covenant not to sue for patent infringement). To "grant" such

a patent license to a party means to make such an agreement or commitment not to enforce a patent against the party.

If you convey a covered work, knowingly relying on a patent license, and the Corresponding Source of the work is not available for anyone to copy, free of charge and under the terms of this License, through a publicly available network server or other readily accessible means, then you must either (1) cause the Corresponding Source to be so available, or (2) arrange to deprive yourself of the benefit of the patent license for this particular work, or (3) arrange, in a manner consistent with the requirements of this License, to extend the patent license to downstream recipients. "Knowingly relying" means you have actual knowledge that, but for the patent license, your conveying the covered work in a country, or your recipient's use of the covered work in a country, would infringe one or more identifiable patents in that country that you have reason to believe are valid.

If, pursuant to or in connection with a single transaction or arrangement, you convey, or propagate by procuring conveyance of, a covered work, and grant a patent license to some of the parties receiving the covered work authorizing them to use, propagate, modify or convey a specific copy of the covered work, then the patent license you grant is automatically extended to all recipients of the covered work and works based on it.

A patent license is "discriminatory" if it does not include within the scope of its coverage, prohibits the exercise of, or is conditioned on the non-exercise of one or more of the rights that are specifically granted under this License. You may not convey a covered work if you are a party to an arrangement with a third party that is in the business of distributing software, under which you make payment to the third party based on the extent of your activity of conveying the work, and under which the third party grants, to any of the parties who would receive the covered work from you, a discriminatory patent license (a) in connection with copies of the covered work conveyed by you (or copies made from those copies), or (b) primarily for and in connection with specific products or compilations that contain the covered work, unless you entered into that arrangement, or that patent license was granted, prior to 28 March 2007.

Nothing in this License shall be construed as excluding or limiting any implied license or other defenses to infringement that may otherwise be available to you under applicable patent law.

12. No Surrender of Others' Freedom.

    If conditions are imposed on you (whether by court order, agreement or otherwise) that contradict the conditions of this License, they do not excuse you from the conditions of this License. If you cannot convey a covered work so as to satisfy simultaneously your obligations under this License and any other pertinent obligations, then as a consequence you may not convey it at all. For example, if you agree to terms that obligate you to collect a royalty for further conveying from those to whom you convey the Program, the only way you could satisfy both those terms and this License would be to refrain entirely from conveying the Program.

13. Use with the GNU Affero General Public License.

    Notwithstanding any other provision of this License, you have permission to link or combine any covered work with a work licensed under version 3 of the GNU Affero

General Public License into a single combined work, and to convey the resulting work. The terms of this License will continue to apply to the part which is the covered work, but the special requirements of the GNU Affero General Public License, section 13, concerning interaction through a network will apply to the combination as such.

14. Revised Versions of this License.

    The Free Software Foundation may publish revised and/or new versions of the GNU General Public License from time to time. Such new versions will be similar in spirit to the present version, but may differ in detail to address new problems or concerns.

    Each version is given a distinguishing version number. If the Program specifies that a certain numbered version of the GNU General Public License "or any later version" applies to it, you have the option of following the terms and conditions either of that numbered version or of any later version published by the Free Software Foundation. If the Program does not specify a version number of the GNU General Public License, you may choose any version ever published by the Free Software Foundation.

    If the Program specifies that a proxy can decide which future versions of the GNU General Public License can be used, that proxy's public statement of acceptance of a version permanently authorizes you to choose that version for the Program.

    Later license versions may give you additional or different permissions. However, no additional obligations are imposed on any author or copyright holder as a result of your choosing to follow a later version.

15. Disclaimer of Warranty.

    THERE IS NO WARRANTY FOR THE PROGRAM, TO THE EXTENT PERMITTED BY APPLICABLE LAW. EXCEPT WHEN OTHERWISE STATED IN WRITING THE COPYRIGHT HOLDERS AND/OR OTHER PARTIES PROVIDE THE PROGRAM "AS IS" WITHOUT WARRANTY OF ANY KIND, EITHER EXPRESSED OR IMPLIED, INCLUDING, BUT NOT LIMITED TO, THE IMPLIED WARRANTIES OF MERCHANTABILITY AND FITNESS FOR A PARTICULAR PURPOSE. THE ENTIRE RISK AS TO THE QUALITY AND PERFORMANCE OF THE PROGRAM IS WITH YOU. SHOULD THE PROGRAM PROVE DEFECTIVE, YOU ASSUME THE COST OF ALL NECESSARY SERVICING, REPAIR OR CORRECTION.

16. Limitation of Liability.

    IN NO EVENT UNLESS REQUIRED BY APPLICABLE LAW OR AGREED TO IN WRITING WILL ANY COPYRIGHT HOLDER, OR ANY OTHER PARTY WHO MODIFIES AND/OR CONVEYS THE PROGRAM AS PERMITTED ABOVE, BE LIABLE TO YOU FOR DAMAGES, INCLUDING ANY GENERAL, SPECIAL, INCIDENTAL OR CONSEQUENTIAL DAMAGES ARISING OUT OF THE USE OR INABILITY TO USE THE PROGRAM (INCLUDING BUT NOT LIMITED TO LOSS OF DATA OR DATA BEING RENDERED INACCURATE OR LOSSES SUSTAINED BY YOU OR THIRD PARTIES OR A FAILURE OF THE PROGRAM TO OPERATE WITH ANY OTHER PROGRAMS), EVEN IF SUCH HOLDER OR OTHER PARTY HAS BEEN ADVISED OF THE POSSIBILITY OF SUCH DAMAGES.

17. Interpretation of Sections 15 and 16.

    If the disclaimer of warranty and limitation of liability provided above cannot be given local legal effect according to their terms, reviewing courts shall apply local law that most closely approximates an absolute waiver of all civil liability in connection with the Program, unless a warranty or assumption of liability accompanies a copy of the Program in return for a fee.

END OF TERMS AND CONDITIONS

How to Apply These Terms to Your New Programs

If you develop a new program, and you want it to be of the greatest possible use to the public, the best way to achieve this is to make it free software which everyone can redistribute and change under these terms.

To do so, attach the following notices to the program. It is safest to attach them to the start of each source file to most effectively state the exclusion of warranty; and each file should have at least the "copyright" line and a pointer to where the full notice is found.

```
<one line to give the program's name and a brief idea of what it does.>

Copyright (C) <textyear>  <name of author>

This program is free software: you can redistribute it and/or modify
it under the terms of the GNU General Public License as published by
the Free Software Foundation, either version 3 of the License, or
(at your option) any later version.

This program is distributed in the hope that it will be useful, but
WITHOUT ANY WARRANTY; without even the implied warranty of
MERCHANTABILITY or FITNESS FOR A PARTICULAR PURPOSE.  See the GNU
General Public License for more details.

You should have received a copy of the GNU General Public License
along with this program.  If not, see <https://www.gnu.org/licenses/>.
```

Also add information on how to contact you by electronic and paper mail.

If the program does terminal interaction, make it output a short notice like this when it starts in an interactive mode:

```
<program>  Copyright $\copyright$ \the\year\ Frank Pattyn

This program comes with ABSOLUTELY NO WARRANTY; for details type
'show w'. This is free software, and you are welcome to redistribute
it under certain conditions; type 'show c' for details.
```

The hypothetical commands `show w` and `show c` should show the appropriate parts of the General Public License. Of course, your program's commands might be different; for a GUI interface, you would use an "about box".

You should also get your employer (if you work as a programmer) or school, if any, to sign a "copyright disclaimer" for the program, if necessary. For more information on this, and how to apply and follow the GNU GPL, see https://www.gnu.org/licenses/.

The GNU General Public License does not permit incorporating your program into proprietary programs. If your program is a subroutine library, you may consider it more useful to permit linking proprietary applications with the library. If this is what you want to do, use the GNU Lesser General Public License instead of this License. But first, please read https://www.gnu.org/licenses/why-not-lgpl.html.